Frontal Polymerization in Fiber Reinforced Polymers:

Influence of varying fibre volume fraction and varying geometry

Anup Bhagali Nataraja

TUDelft

Frontal Polymerization in Fiber Reinforced Polymers:

Influence of varying fibre volume fraction and varying geometry

by

Anup Bhagali Nataraja

in partial fulfilment of the requirements for the degree of

Master of Science
in Aerospace Engineering

at the Delft University of Technology.

TUDelft

Preface

This thesis presents the research that was conducted at the Faculty of Aerospace Engineering at TU Delft, marking the end of my journey as a master's student. The process of researching and writing this thesis has been a challenging, yet immensely rewarding experience, one that would not have been possible without the guidance and support of numerous individuals.

First and foremost, I would like to express my profound gratitude to my family, who have been a constant source of support and encouragement throughout my academic journey. Their unwavering belief in me has helped me to overcome challenges and to achieve my goals.

Next, I would like to express my sincere gratitude to my supervisors, Dr. Bariş Çağlar and Jeroen Staal, for their invaluable guidance, support, and encouragement throughout this research project. I am particularly thankful for their patience in both failures and successes. Their expertise and insights have been invaluable in shaping this thesis.

I would like to extend special thanks to the staff at DASML, Victor Horbowiec, Johan Boender, Dave Ruijtenbeek, Durga Mainal, and Alexander Uithol, for their guidance in the lab. Their support has greatly enhanced the quality of this work.

I would like to offer my special thanks to Onur Yüksel for his valuable guidance throughout my thesis. I extremely grateful for his willingness to help, even during odd hours. It was a genuine privilege to work with and learn from him.

Lastly, I'd like to thank all my friends with whom I made great memories. They have been a constant source of joy and motivation throughout this period. I will always cherish them.

I hope this thesis contributes to the body of knowledge in the field of frontal polymerization and provides a useful resource for future researchers.

Anup Bhagali Nataraja
Delft, April 2023

Abstract

Frontal polymerization (FP) has emerged as a promising alternative to traditional bulk curing methods in recent years for manufacturing high-performance fibre-reinforced polymer (FRP) composites. The energy utilized in this self-propagating curing strategy is solely derived from the exothermic enthalpy of polymerization, making it potentially more efficient than traditional curing methods, which are extremely energy-intensive and therefore unsustainable. Research in the field of FP has been primarily focused on studying the effectiveness of the FP formulations, particularly the relationship between the monomer types and initiator concentrations on front properties. However, the research on the use of FP for manufacturing FRPs has been limited to flat rectangular plates. Therefore, this research aims to investigate the behaviour of the propagating fronts in composites with varying fibre volume fractions (V_f) within the sample and varying geometries to assess the feasibility of using FP in structures that more closely resemble real-life applications. Several test setups were explored to determine the best method for maintaining the heat balance required to sustain a propagating front. Through these trials, a stainless steel-based closed mould test setup with Teflon sheets was conceptualized and manufactured, consistently allowing for the manufacturing of composite samples with a V_f below 36%. The influence of changing V_fs on the behaviour of the front was studied, and the results were quantified using temperature data captured via thermocouples placed at strategic locations. Through a series of experiments, a critical length was established that allowed the propagation of the front from the low V_f region to the high V_f region. When the length of the low V_f region with respect to the high V_f region was smaller than the critical length, the front was seen to quench at the interface. This phenomenon was attributed to the physical reduction in the volume of the resin, which implied a reduction in the generated heat through polymerization. This led to fronts with lower peak temperatures, which upon reaching the interface would quickly fall below the threshold temperature required to sustain the front due to the higher rate of heat loss resulting from the higher fibre content. This study was followed by the manufacturing of L-shaped composite samples with uniform V_f, which showed the propagation of the front in complex geometry. Finally, the V_f was varied within the L-shaped samples, and the behaviour of the front showed similarities to the rectangular samples with varied V_f, leading to the conclusion of the presence of a critical length irrespective of geometry. These findings effectively contribute to the knowledge base necessary for implementing FP as a curing strategy for FRPs. The results obtained from this study can inform the design of manufacturing processes and setups tailored for the use of FP, potentially leading to more efficient and sustainable manufacturing practices.

Contents

List of Figures

List of Tables

Nomenclature

ABBREVIATION	STANDS FOR
$A_{textile}$	Areal weight
AIBN	azobisisobutyronitrile
BADGE	Bisphenol A diglycidylether resin
BPO	dibenzoyl peroxide
CFRP	Carbin Fiber Reinforced polymer
CE	3,4-epoxycyclohexylmethyl- 3',4'-epoxy cyclohexane carboxylate
CHDGE	cyclohexanedimethanol diglycidylether
DMTA	Dynamic mechanical thermal analysis
DSC	Differential Scanning Calorimetry
DETA	diethylenetriamine
EOM	3-ethyloxetan-3-yl) methanol
FP	Frontal Polymerization
FRPs	Fibre Reinforced polymers
FRPCs	Fibre Reinforced Polymer Matrix Composite
FTIR	Fourier Transform Infrared Spectroscopy
GFRP	Glass fiber reinforced polymer
HDGE	1,6-hexanediol diglycidyl ether
HDDGE	1,6-hexanediol diglycidylether
HOPH-SbF$_6$	[4-(2-hydroxytetradecyl)oxy]-phenyl iodonium-SbF6
IOC-8 SbF$_6$	[[(4-(octyloxy)phenyl] phenyl iodonium-SbF6
LCM	Liquid composite moulding
NPDGE	Neopentyl glycol diglycidyl ether
PAG	Photo acid generator
PDMS	Polydimethylsiloxane
PTFE	Polytetrafluoroethylene
PVC	Polyvinyl chloride
PLA	Polylactic acid
RTM	Resin Transfer Moulding
RICP	Radical Induced Cationic Polymerization
RICFP	Radical induced cationic frontal polymerization
RTI	Radical thermal initiator
RTV	Room Temperature Vulcanizing
ρ_{fabric}	Fibre density
T_g	Glass transition temperature
T_m	Melting temperature
TPED	benzopinacol
TREN	Tris(2-aminoethyl) amine
UV	Ultra Violet
VARTM	Vacuum assited resin transfer moulding
V_f	Fiber volume fraction
V_{f_t}	Theoretical fiber volume fraction
V_{f_a}	Actual fiber volume fraction
V_v	Void volume fraction

<div align="right">

1

</div>

<div align="right">

Introduction

</div>

1.1. Background and Motivation

The aviation industry's rapid growth, along with rising fuel costs and its significant environmental impact, has placed tremendous pressure on aircraft manufacturers to deliver low-cost, fuel-efficient and lighter aircraft [1]. This requirement has led to rapid innovation in the key technology fields, including the increasing use of high-performance structural materials for building load-carrying components of an aircraft. One such high-performance material being used today is the fibre-reinforced polymer (FRP) composites [2].

FRPs are heterogeneous mixtures of two separate phases at the micro-scale: the reinforcement, in the form of a fibrous structure, and the matrix (binder), which holds these fibres together. The reinforcement and the matrix phase have a distinct interface between them, allowing each of the individual constituents to retain their physical and chemical characteristics. The reinforcement phase, which naturally possesses high strengths and stiffness, generally acts as the primary load-carrying member, while they are held in the desired location and orientation by the matrix phase. In addition to protecting the fibres from environmental damage, the matrix also acts as the medium for load transfer between the fibres [3] [4].

The manufacturing process of composite parts involves incorporating a large number of reinforcement fibres into a thin layer of matrix, to form a lamina or ply [4]. The thickness of a single lamina can range from 0.1 to 1 mm. When several lamina layers are stacked together and consolidated to the desired thickness, they form a laminate, which is a composite part. By varying the stacking sequence of each lamina and, in turn, the direction of fibre orientation, the resulting physical and mechanical properties of the FRPs can be tuned [4].

Initially developed to meet the demands of the aerospace industry, FRPs, in particular, carbon fibre-reinforced polymers (CFRP) and glass fibre-reinforced polymers (GFRP), have now found extensive usage in fields ranging from sports to the automotive sector. FRPs are attractive for aerospace applications because of their excellent strength and stiffness-to-density ratios [2].

The use of composites in commercial aircraft became an attractive proposition due to reduced airframe weights, resulting in better fuel economy and lower operational costs. The first significant use of composites in commercial aircraft began with the Airbus A300 and A310 series, where the rudders and the vertical tail fins were made of composites. In the latter case, only 100 parts were used in the composite fin, as opposed to the 2000 parts used in the metal fin, resulting in a reduction in weight and production costs. Following these successes and the subsequent development of high-performance composites, they were increasingly used in secondary and primary load-carrying structures of aircraft. Today's state-of-the-art commercial aircraft, such as the Boeing 787, consists of up to 50% composite materials by weight, offering up to 20% weight savings [2].

Traditional manufacturing methods of fibre-reinforced polymer composites and high-performance composites typically involve curing in large autoclaves or ovens, which requires significant initial investments. The components are subjected to complex, long cycles of temperature and pressure to prevent non-uniform curing and the formation of residual stresses. These long cycles are energy-intensive, with some reasonable estimates suggesting that the curing process for the carbon fibre/epoxy fuselage of the Boeing 787 requires 350 gigajoules of energy over an eight-hour period, resulting in an estimated 80 tons of carbon dioxide emissions[5]. Given the growing concern about climate change, there is increasing pressure on the industry to seek more sustainable alternatives and reduce its environmental footprint. One such promising alternative is the use of frontal polymerization (FP) as a substituent for autoclave-based bulk curing.

1.2. Overview of the Research Topic

FP is a polymerization technique that involves converting monomers into useful polymers through a propagating reaction wavefront. It was first discovered by Chechilo and Enikolopyan in 1972 [6], who studied the polymerization of methyl methacrylate in a highly pressurized system, while investigating the effect of initiator type and concentration on the front velocity [7]. Later, Pojman et al.[7] demonstrated that fronts can form at ambient pressures in a solution of thermal free radical initiators in different neat monomers which polymerize and have a melting point higher than the front temperature. This led to the realization that thermal-based FP could be an excellent substitute for bulk curing of polymers due to the reduced external energy requirements of FP. Since then, extensive work has been carried out to develop the theory of FP, and a significant breakthrough came with the use of FP in epoxy curing [8].

The possibility of using FP to manufacture fibre-reinforced thermosetting polymer-matrix composites with epoxy monomers as the matrix phase was demonstrated through the use of the radically induced cationic frontal polymerization (RICFP) method [9]. Building on this achievement, Sangermano et al. [10][11] used the RICFP method and successfully fabricated epoxy-based CFRP and GFRP plates.

Frontal polymerization promises to be a rapid and energy-efficient method of curing composites, utilizing the enthalpy of polymerization alone to convert the monomers into a useful polymer. This has allowed for an exponential increase in the curing speed compared to oven-based curing while reducing the environmental footprint, making FP an attractive method for sustainably curing large composite parts [12]. However, for frontal polymerization to be considered a viable alternative to the oven/autoclave-based curing utilized today, the curing of composite parts using this technique has to be reliable, reproducible and consistent. Unfortunately, with the current state of research, large gaps still exist in our understanding of the behaviour of the front as it propagates through the reinforcement phase in the FRPs.

1.3. Aim and Relevance

The aim of this research is to study and understand frontal polymerization in fibre-reinforced polymers. The scope of this research is limited to studying the behaviour of the propagating front in composite parts with varying fibre volume fractions (V_f) within the sample and varying geometries. This area of research has been chosen because the composite parts and products used in aerospace applications are complex structures with varying shapes and thicknesses. Therefore, to truly utilize FP in manufacturing aerospace-grade composite parts and to contribute to making the aviation industry more sustainable and environmentally friendly, this study is timely and relevant.

1.4. Overview of the Report

A summary of what to expect in the report is included in this section. This thesis report will first provide a detailed overview of frontal polymerization. The report will start with a literature review in chapter 2, which includes a general introduction to frontal polymerization in section 2.1 and an overview of the chemistry of the frontal polymerization system used for the epoxy monomers in section 2.2. The working mechanism of the RICFP method will be explained in section 2.3, followed by the summary of the current state-of-the-art in the manufacturing of epoxy-based composites using the RICFP method. Section 2.4 will discuss the physical phenomena of heat transfer governing a frontal system, as well as the factors that need to be taken into consideration in order to implement FP in the manufacturing of FRPs.

Following the literature review, chapter 3 of the report will identify the research gap and define the scope of the research. Section 3.1 will present the reach questions formulated based on the identified scope, while section 3.2 will present the relevant hypothesis to support the research questions. Finally, section 3.3 will define the overall objective of the thesis and present the sub-goals followed to achieve the objective.

Chapter 4 of the report will present the methodology followed to achieve the objective. Section 4.1 and 4.2 will present the steps followed to mix the FP formulation and cast silicone moulds, respectively. Before studying the behaviour of the propagating front, a test setup was required that would allow the consistent and repeatable manufacturing of composite parts. Therefore, three different mould test setups were tested, and the tests involved the manufacturing of composite samples using all the setups. The test setups and the manufacturing methods used to produce composite samples have been presented in section 4.3. To determine the quality of the samples, void content was studied by observing the cross-section of the samples under a microscope, presented in section 4.4. Following these steps, the influence of varying V_f s and geometries on the behaviour was studied, and the methodologies used have been presented in section 4.5 and 4.6, respectively.

Chapter 5 of the report presents the results of the experiments performed and provides a discussion on the observed results. Section 5.1 discusses the results of the characterization of the FP formulation carried out through the differential scanning calorimetry (DSC) technique. The results of the composite samples manufactured through the various test setups are presented in section 5.2. Following these, the results of the composite samples with varied V_f cured via FP have been presented in section 5.3. The quantification of the front propagating through the sample with varied V_f was done through the incorporation of thermocouples across the layup, and the results of these have been presented in section 5.4. Finally, the results from the manufacturing of L-shaped samples cured via FP have been presented in section 5.5.

The thesis report draws various conclusions from the results obtained, which have been presented in chapter 6. Finally, the report ends by presenting some recommendations (chapter 7) for future researchers in this field.

2

Frontal Polymerization

This chapter will give the reader a comprehensive understanding of the state of the art in frontal polymerization used as a potential curing technique in manufacturing composite parts.

2.1. Introduction to Frontal Polymerization

Frontal polymerization, as shown in Figure 2.1, is a curing strategy that involves a self-propagating reaction wavefront to convert monomers into fully cured polymers. The polymerization reaction proceeds via a localized reaction zone that propagates through a combination of thermal diffusion and the released enthalpy of polymerisation. By using the exothermic enthalpy of polymerization alone, frontal polymerization reduces the external energy required to convert the monomers into useful polymers. This reduction in external energy requirements has the potential to significantly reduce the cost and environmental impact of curing composite parts.

Robertson et al. [13] demonstrated that employing this manufacturing process can greatly improve the efficiency of manufacturing composite parts. Their study showed that with precise control of the polymerization kinetics at both elevated and ambient temperatures, a high degree of stable monomers can be converted to a fully cured polymer within seconds, reducing the energy required for curing compared to conventional curing methods.

Frontal polymerization in its most primitive form involves a solution of a monomer and a latent initiator. The initiator can be activated through heat, similar to a conventional curing process, for the polymerization of the monomer [9]. The conversion of the monomers into a polymer is exothermic, and the heat released is further used to drive the reaction to completion. This auto-activation process, depending on the initiator concentration, allows for high degrees of monomer conversion, as reported by Pojman et al [7]. The choice of monomer and initiator determines the speed at which the front travels through the reactant medium and the maximum achievable temperature [14][15][16]. Frontal polymerization has been demonstrated as a suitable method for synthesizing functionally graded polymers [17][18], hydrogels [16], nanocomposites [19], fibre-reinforced polymer matrix composites [20] and sensory materials [21][22].
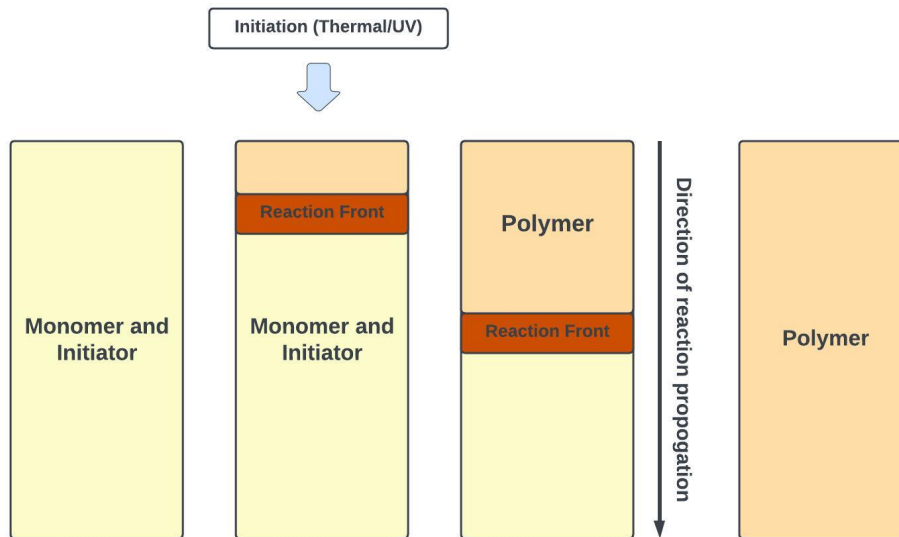
Figure 2.1: A schematic diagram representing the frontal polymerization process

2.2. Frontal Cationic Polymerization

Several different polymerization mechanisms facilitate the frontal processes. In this thesis, composite samples were manufactured using the epoxy monomer as the matrix phase. The reaction mechanism utilized for converting epoxy monomers into a polymer chain is called chain-growth ring-opening polymerization. Two types of chain growth polymerization mechanisms are commonly used in commercial applications: (1) poly-addition reaction and (2) cationic ring-opening polymerization.

The first mechanism, referred to as polyaddition polymerization, involves a growing chain with a cationic centre at the chain ends. Monomer chains are added through the S_N1 and S_N2 mechanisms, as depicted in Figure 2.2. Industrially, Polyaddition polymerization is extensively used to manufacture amine-cured epoxy composites.
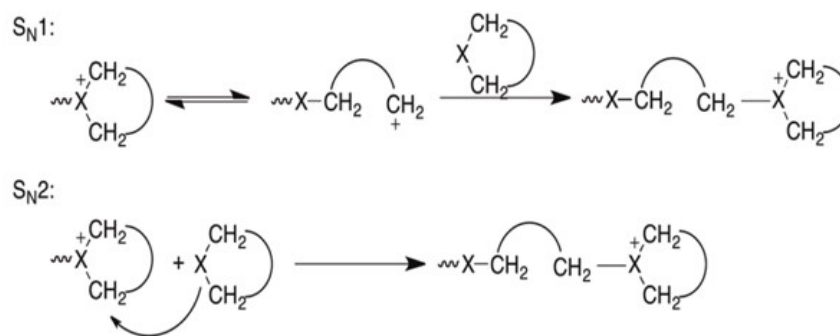
Figure 2.2: Cationic ring opening polymerization based on polyaddition of monomers via S_N1 and S_N2 mechanisms of active chain ends. [23]

The second chain propagation mechanism, known as the cationic ring-opening reaction mechanism, involves an activated monomer that carries the cationic centre. The growth of the polymer chain occurs through the electrophilic attack of the activated monomer on the chain end. A schematic for this method has been shown in Figure 2.3.
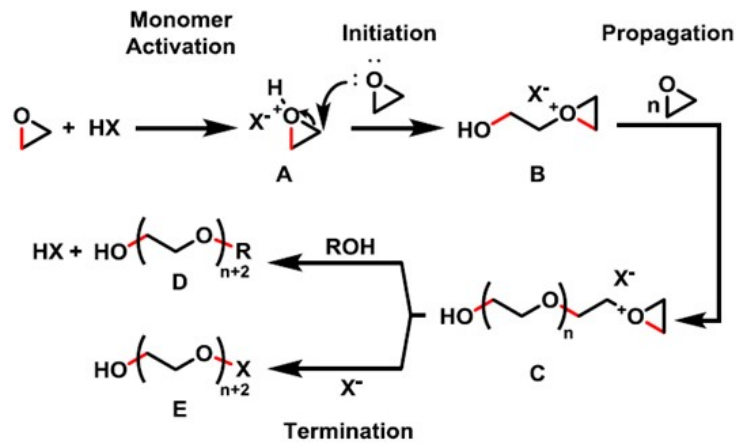
Figure 2.3: Cationic ring opening polymerization via an activated monomer [14]

The primary initiators used in frontal epoxy ring-opening polymerization include amine-boron trifluoride adducts [24][25], crosslinking polyamines [26] [27] and photoacid generators (PAGs) [9] [10] [28] [29] [24]. While the mode of chain propagation with these initiators remains the same as the general mechanism described in Figure 2.3, there are several differences in terms of monomer activation and initiation.

Amine-boron trifluoride-initiated FP occurs in the presence of moisture-rich surroundings. These initiators readily react with water to form a transient solvent-separated species ([RNH$_3$][BF$_3$OH]). The catatonic amine initiates the polymerization process, while the anionic species decomposes via disproportionation reactions into boric acid [14][30]. Polymerization via amine-boron trifluoride initiators is presented in Figure 2.4.

Figure 2.4: Polymerization via amine boron trifluoride initiators [14]

Polyamine initiators such as diethylenetriamine [DETA], tris(2-aminoethyl) amine [TREN] are used to make highly crosslinked epoxy copolymers. As depicted in Figure 2.5, monomer activation occurs through complexation with an amine [14]. High concentrations are used in this type of polymerization, followed by a copolymerization event that forms a reactive ring-opening nucleophile. Therefore, frontal systems initiated via polyamines form epoxy anime copolymers [31].
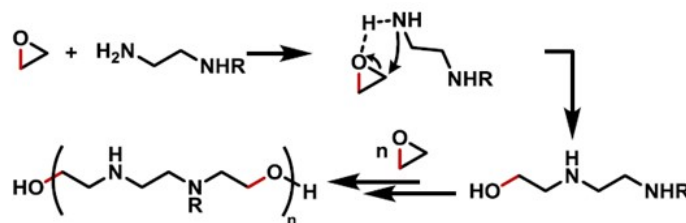
Figure 2.5: Polymerization via polyamine [14]

Finally, Figure 2.6 shows the schematic for cationic polymerization via PAGs. As summarized in the review by Suslick et al.[14], until 2020, iodonium reagents were the only PAG initiator used for cationic frontal polymerization. Photoexcitation of diaryliodonium salts via UV light leads to the formation of an excited state, which relaxes either through homolytic or heterolytic Ar–I scission [32]. Radicals generated through homolytic scission abstract hydrogen from C–H bonds, generating an acid HX. Alternatively, in heterolytic scission, a single electron is transferred from the aryl radical to the monoaryl iodonium, generating ArI and aryl cations [33]. These act as potent electrophiles that interact with C-H bonds from HX.
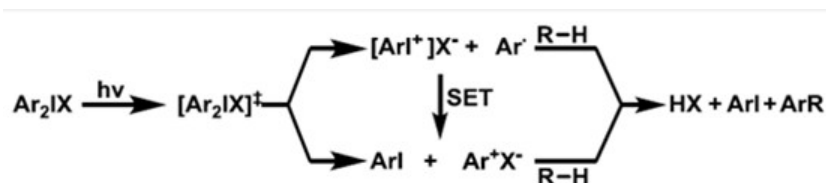
Figure 2.6: Polymerization via PAG [14]

The use of just PAGs for frontal processes is limited by the depth of light penetration through a large volume of monomers. This is because a photo gradient is formed through the material as a certain percentage of the incoming photons are diffracted or absorbed by the initiators in the formulation. Initiator molecules on the surface receive more photons than those deeper in the material, resulting in non-uniform initiation and propagation. As a result, the surface undergoes a higher degree of polymerization than the deeper layers. Crivello et al.[34] demonstrated that uniform polymerization occurs only in thin films of $2mm$ or less. To overcome this challenge, PAGs are used in conjugation with a thermal radical source, leading to cationic FP known as radically induced cationic frontal polymerization (RICFP).

2.3. Radically Induced Cationic Frontal Polymerization

Epoxy resin is by far the most common monomer type that finds a wide range of commercial applications in industries such as sports, automotive, marine and aviation [10][9]. As alluded to in section 2.2, there are two methods available for the curing of epoxy monomers. The first curing method is called thermal bulk curing, which involves the polyaddition of amine or anhydrides and requires subjecting the monomer to high temperatures cycles for extended periods. Thermal bulk curing is inherently disadvantaged due to its rather high energy requirements and its inability to provide equal quality in curing all areas. Highly reactive epoxy formulations also have a short pot life, which reduces the processing window, which means that the operator must mix the formulation right before usage [9][28].

Photo-polymerization by cationic ring-opening of the epoxy group is the alternative method available for bulk curing of the monomer. This method is a suitable energy-efficient way of curing epoxy resin, but it has been limited to thin layers due to the low penetration depth of UV light. Additionally, the difficulty of using UV light increases with the addition of opaque fillers, such as carbon fibres.

As described in section 2.2, cationic photo-polymerization utilizes a cationic photo-initiator known as PAG. When excited with UV light, the PAG is cleaved, forming a carbocation that initiates polymerization either by itself or by abstracting protons. The PAG can be cleaved either by UV light or a suitable radical through a redox reaction. This method of decomposing PAG through radicals is called radical-induced cationic polymerization(RICP) [35][36][37]. While RICP on its own would only be a viable method of curing thin layers, but when combined with FP it becomes a far-reaching technique that allows for rapid bulk curing of parts with any thickness. This technique is appropriately named Radical induced cationic frontal polymerization (RICFP) [29][9][28].

RICFP systems rely on three active components: the PAG, the radical thermal initiator(RTI) and the monomer that need to be cured. RICFP allows for two possible initiation routes due to the presence of PAG and RTI. FP can be started through both thermal and UV initiation. Regardless of the initiation method, the RICFP mechanism remains the same.

As shown in Figure 2.7, when irradiated with UV light (1), the PAG is cleaved to form a cation (2). This cation then abstracts a proton from the monomer or the solvent, leading to the formation of a superacid (3). This superacid initiates the ring-opening reaction of the monomers, which is exothermic and generates heat (4). The heat then decomposes the RTI, producing reactive radicals (5) that cleave the PAG to form a new superacid (2). If the same process were initiated through heat/thermal energy, then the cycle would start from the decomposition of RTI to form reactive radicals (5-2-3-4-5), while the rest of the cycle would remain the same.
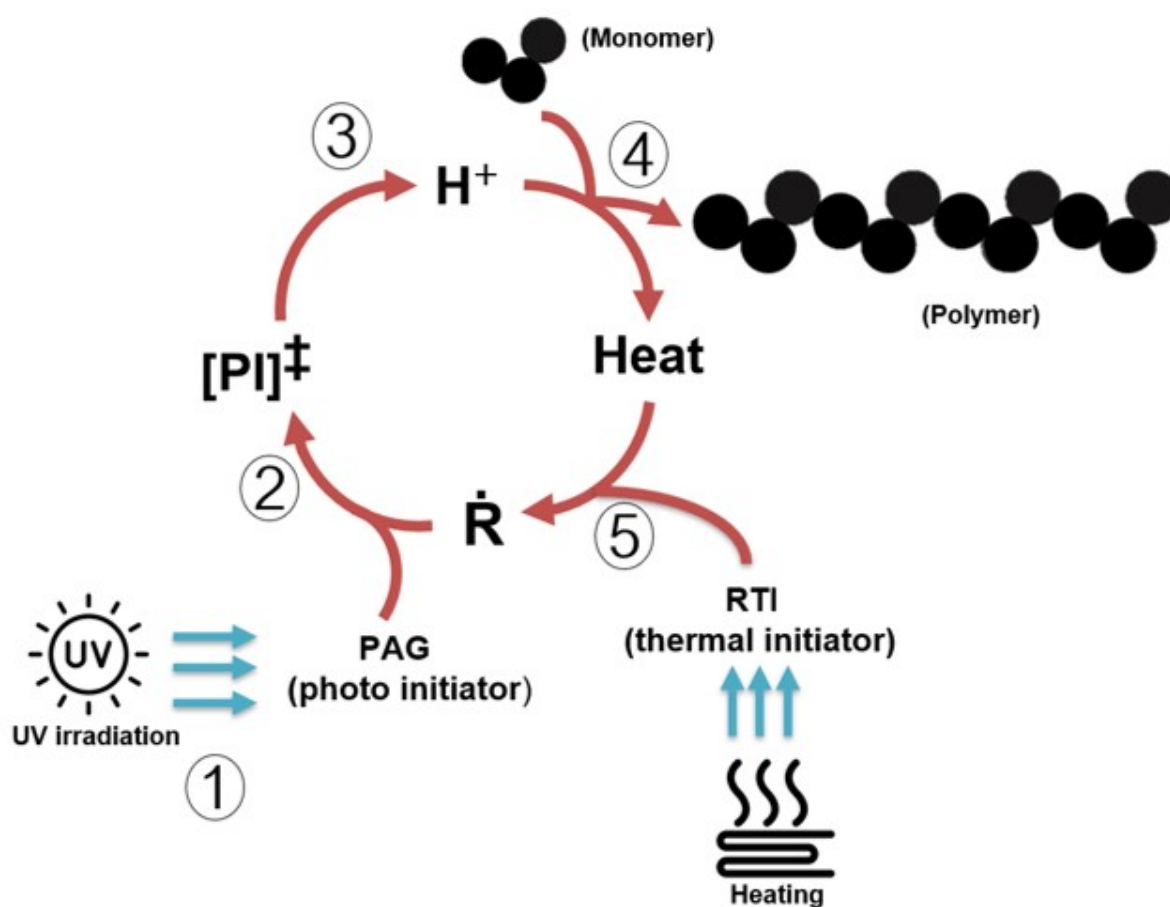
Figure 2.7: RICFP flow diagram

The first successful demonstration of RICFP was conducted by Mariani et al. [29]. They showed the viability of RICFP for bulk curing of thick samples of an epoxy monomer. Later, Bomze et al.[9] extended this work and successfully demonstrated the frontal polymerization of bisphenol A diglycidylether resin (BADGE), a commonly used epoxy monomer. RICFP was shown to be a technique that allows for the curing of monomer formulations in hard-to-reach places, which are not easily accessible with traditional curing methods. This research group demonstrated the initiation and sustenance of a front by using a formulation containing a combination of carbon-centred labile compound (high-temperature radical initiators [38]) as RTI with diaryliodonium salt as PAG. In the subsequent work, Bomze et al.[28] showed the high storage stability of the RICFP formulation (high pot life) with the ability to influence front properties, such as front speed and front temperature, through the variation of initiator concentration.

The success of the RICFP technique in creating neat monomer samples led to its natural extension for the manufacturing of composites, which was first attempted by Sangermano et al.[10]. This research group demonstrated the use of RICFP for manufacturing GFRP composites with BADGE as the epoxy monomer. Sangermano et al.[11] then investigated the preparation of epoxy-carbon fibre composite through UV-induced RICFP. In both cases, they compared the mechanical properties of composites cured through FP with those cured thermally and found that both carbon fibre and glass fibre composites exhibit excellent thermo-mechanical properties. Dung Tran et al.[39] further investigated the effect of fillers on FP while simultaneously demonstrating the effectiveness of FP when combined with an existing resin infusion technique, such as vacuum-assisted resin transfer moulding (VARTM). Lastly, Dung Tran et al.[40] demonstrated the possibility of manufacturing Prepregs capable of undergoing FP.

As mentioned previously, RICFP systems comprise three active components, and the choice of these components seems to fundamentally dictate the physical properties of any frontal system. Several successful frontal formulations have been developed using iodonium [41], sulfonium[33], bismuthonium [42] and pyrylium [42] based PAG architecture as photoinitiators. Similarly, several different thermal radical initiators, such as dibenzoyl peroxide (BPO), azobis(isobutyronitrile) (AIBN) [35], and C-C labile compounds like benzopinacol (TPED) [35] based FP formulations, have been demonstrated.

Several studies have noted the effect of initiator concentration on the front properties. For example, Mariani et al.[29] demonstrated frontal formulations with stable fronts. This study showed UV-triggered polymerization of CE (3,4-epoxy cyclohexylmethyl- 3',4'-epoxycyclohexanecarboxylate) in the presence of HOPH-SbF$_6$ ([4-(2-hydroxytetradecyl)oxy]-phenyl iodonium-SbF6) or IOC-8 SbF$_6$ ([[4-(octyloxy)phenyl] phenyl iodonium-SbF6) as PAG salts with BPO as the thermal initiator. The concentration of PAG and RTI was observed to affect the front velocity and temperature. At low PAG concentration (1 to 3mol % iodonium), sustainable fronts were observed. At these concentrations, the front exhibited a front velocity of 3.2 $cmmin^{-1}$ and a maximum temperature of 250 $°C$. However, at high PAG concentrations, the front velocity increased ($\approx 5cmmin^{-1}$) and the maximum front temperature decreased to 232 $°C$. In contrast, front velocity and maximum temperature were observed to increase linearly with RTI concentrations. Bomze et al.[28] also performed similar studies with the epoxy resin bisphenol-A diglycidyl ether (BADGE) in combination with IOC-8 SbF$_6$ and TPED as the RTI. The results of this study are best summarized in the bar graph shown in Figure 2.8. Front velocities show an increasing trend with an increase in the concentration of each initiator, with a steeper increase observed at higher PAG concentrations.
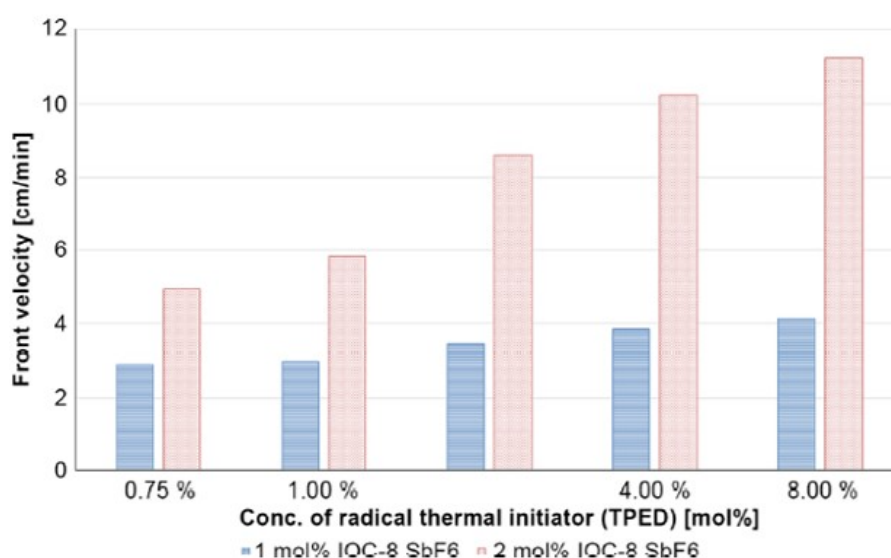
Figure 2.8: Comparison of front velocities with the variation in concentration of RTI and PAG [28]

Similarly, Figure 2.9 summarizes the dependence of maximum front temperature on the concentration of RTI and PAG. The maximum temperature is observed for 1 mol % RTI, and as the concentration of RTI increases, the maximum temperature is observed to decrease. A similar decreasing trend is observed for PAG concentrations [28]. In conclusion, these results suggest that within a certain range, higher initiator concentrations allow for faster and hotter fronts.
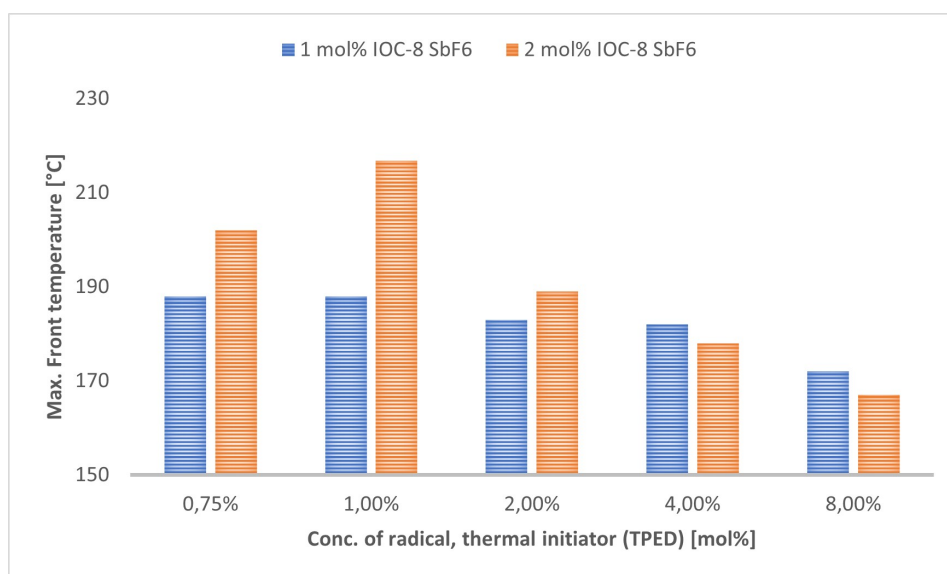
Figure 2.9: Comparison of maximum front temperatures with the variation in concentration of RTI and PAG [28]

According to Suslick et al.[14], frontal formulations developed so far involve cyclic ethers, some of which are depicted in Figure 2.10. Additionally, Bomez et al.[9] conducted a comparative study to investigate the impact of the monomer type on front properties. The study involved frontal formulations created using a neat mixture of bis(epoxy) monomers with TPED and IOC-8 SbF$_6$. The observed front properties are summarized in Table 2.1.
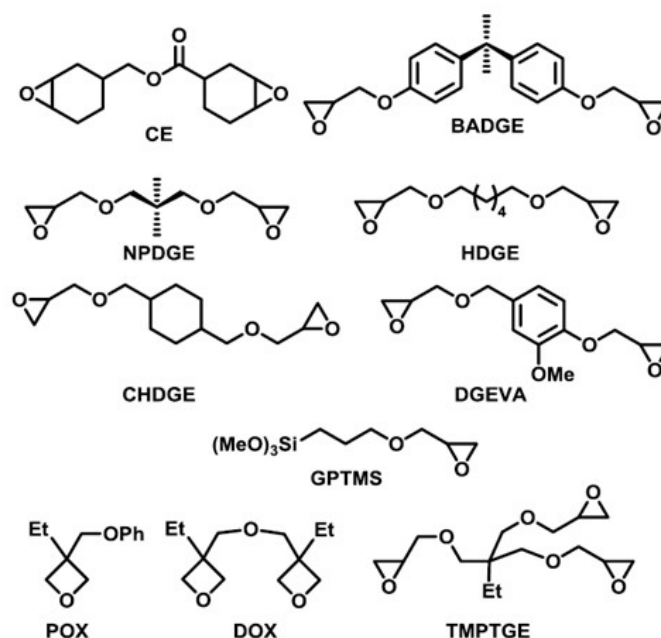
Figure 2.10: Commonly used monomers in RICFP formulations [14]

Table 2.1: Frontal properties of bis(epoxy) monomers under UV-ignited conditions

Monomer	MW($gmol^{-1}$)	T_{max}(°C)	V_f($cmmin^{-1}$)	t_{ignite}(s)
CE	252	176	26.2	31
BADGE	340	173	2.7	38
NPDGE	216	169	19.9	10
HDGE	230	181	28.6	12
CHDGE	256	140	37.9	23

The formulations exhibited stable fronts after UV irradiation for a fixed duration. It was observed that while there was some variation in ignition time, the formulations could be repeatedly ignited within the same time frame. The study showed no apparent relationship between the ignition time and front velocity. For instance, CE had more than twice the ignition time of HDGE, yet it had a faster front. Similarly, there was no clear correlation between the maximum front temperature and the front velocity. Among all the monomers tested, CHDGE and HDGE provide the fastest fronts, despite having a temperature difference (ΔT_{max}) of 41°C. The study also noted bubble formation in all of the monomers except BADGE. These bubbles resulted from the evaporation or boiling of small molecules caused by the decomposition of monomers or initiators. Consequently, most RICFP formulations employ BADGE monomer as it supports stable and robust fronts[9].

As previously mentioned, Sangermano et al.[10] demonstrated the manufacturing of GFRP through the RICFP process. The composite samples were manufactured using a RICFP formulation that contained BADGE epoxy monomer paired with TPED (1,1,2,2-tetraphenyl-1,2-ethanediol) as the RTI and IOC-8 SbF$_6$ cationic photoinitiator ((p-octyloxyphenyl) phenyl iodonium hexafluoroantimonate) as the PAG. The GFRP composites consisted of two fabric layers, each weighing $0.9g$, deposited into a silicone mould with orientations of 0° and 90°, with a sample dimension of 4.0 × 5,5 cm, and $20g$ of the epoxy formulation was added. The cross-linking was UV initiated, and $10s$ of irradiation was required to initiate a moving front. For comparison, GFRP samples containing two fabric layers with 0° and 90° orientation were thermally cured in the presence of an amine hardener at 80°C for $5hours$. Both these samples were then characterized by dynamic mechanical thermal analysis (DMTA) and tensile tests. The summary of the observed properties is presented in Table 2.2.

Table 2.2: Properties of the glass fibres reinforced epoxy composites obtained by UV or thermal curing [10]

Sample	T_g(° C)	Tensile strength$(MPa)^2$	Tensile Modulus E$(GPa)^3$
UV cured	105	367±14	23.5 ±1.3
Thermally cured	95	345±23	21.8 ± 2.8

The samples cured using the RICFP method showed a higher glass transition temperature (T_g), which was attributed to the difference in the polymer networks. The use of amine hardeners reduced the flexibility of the epoxy network, while the network in a RICFP sample is purely formed of repeating epoxy units. Moreover, the RICFP method allows for higher curing temperatures, which can lead to a higher degree of epoxy conversion. The tensile tests showed that composites cured using the RICFP method exhibited slightly higher mechanical performance, likely due to their higher T_g[10].

Sangermano et al. [11] conducted a similar study to demonstrate the feasibility of manufacturing CFRP composites cured via UV-initiated RICFP. This composite used carbon fabric T300 200 gsm twill 2 × 2 and BADGE epoxy monomer containing 1.5 Wt% of IOC-8 SbF$_6$ (PAG) and 1.5 Wt% of TPED (RTI). Four fabric layers, each weighing 0.15 g, were laid into a silicone mould with a sample dimension of 12 × 60 mm and a thickness of $3mm$. The front was initiated through UV irradiation via an optical fibre for a duration of 10 s.

Similar to the previous samples, a separate sample is thermally bulk cured at 80° C for 3 $hours$ for comparison. These two samples are then characterized with the DMTA and the tensile tests. The results of these tests are summarized in Table 2.3. As in the case of the GFRP composite, this study also noted that the T_g of the RICFP-cured composites is higher than that of thermally cured compos-

ites. This difference is explained as a consequence of the formation of different polymer networks. The mechanical analysis showed that composites obtained via the two methods have the same rigidity, but the tensile strength is compromised in the case of the RICFP composite.

Table 2.3: Mechanical properties of crosslinked epoxy–carbon fibre composites obtained via thermal curing and RICFP[11]

Sample	Tensile strength$(MPa)^2$	Tensile Modulus $E(GPa)^3$
Thermally cured composite	715±54	61±5
Frontally cured composite	447±81	61±4

Finally, Dung Tran et al.[39] utilized VARTM to manufacture CFRP composites containing 8 fabric layers of woven carbon fibres. The epoxy formulation used consisted of BADGE monomer with 4 mol% TPED as the RTI and 0.2 mol% I-Al (bis (4-tert-butylphenyl) iodonium tetrakis(perfluoro-tert-butyloxy) aluminate) as the PAG. Additionally, 40 mol% of the solution contained HDDGE (1,6-hexanediol diglycidylether) and EOM (3-ethyloxetan-3-yl) methanol) as reactive diluents.

For a successful FP, the monomers must possess the required energy density and reactivity. However, not all monomers meet these basic requirements. To overcome this issue, reactive diluents can be added to the FP formulation. In this formulation, HDDGE has a viscosity-reducing effect, and EOM provides increased reactivity. The fibre volume fraction (V_f) of the final layup with the formulation was 35%. For comparison, a sample containing a similar amount of carbon fibre V_f was produced via thermal bulk curing.

Both these samples were characterized through differential scanning calorimetry (DSC) and fourier transform infrared (FTIR) analyses. Conventionally, monomer conversions are usually measured via the FTIR method. However, conventionally cured samples can have an overlap of epoxy and anhydride signals. As a result, DSC analysis was also used for comparison. The data from the comparison study is summarized in Table 2.4.

Table 2.4: Conversion and fibre content of woven carbon fibre reinforced epoxy composites cured by RICFP and thermal bulk curing [39]

Sample	Conversion by		Fibre content
	DSC	FT-IR	
Thermal cured	93.1±2.5	97.1±1.1	34.2±1.2
RICFP Cured	97.7±0.6	98.3±1.6	35.2±1.0

2.4. Heat Transfer Considerations

A successful FP requires a fine balance between the reaction rates, the exothermic heat released and the heat transfer into the unpolymerized monomer medium [14], as well as the surroundings. As previously discussed, the reaction rates and the exothermicity of the FP formulation are indeed dependent on the choice of the monomer and concentration of RTI and the PAG. However, in addition to these, to manufacture FRPs cured via FP, it is also important to understand the governing physics of heat transfer.

To understand heat transport in a frontal system, a brief introduction to the various modes of heat transfer is warranted. There are primarily four modes of heat transfer: conduction, convection, advection, and radiation [14].

Conduction occurs due to the direct contact between two bodies. Vibrating atoms and molecules directly transfer kinetic energy to their immediate neighbours through collision. Conduction is the predominant mode of heat transfer in solids, but it also occurs in liquids and gases to a lesser extent [14].

Heat transfer through a bulk fluid flow is referred to as convection. Convection couples both mass and energy diffusion within a fluid. Convection is caused due to external forces such as gravity driving a density-driven fluid motion. As hotter objects are less dense than colder ones, mass diffusion of hot and cold bodies within a fluid system provides the opportunity for the associated molecules to transfer kinetic energy [14].

On the other hand, advection is similar to, but not the same as convection. Advection occurs due to the non-diffusive movement of the fluid. A flowing fluid moves molecules with high kinetic energy through space, leading to the transfer of energy between molecules [14].

The final form of heat transfer, radiation, is based on photon energy changes. In this process, high-energy molecules undergo photo-relaxation and as a result, release a wave-like photon. Radiation, unlike the other methods of heat transfer, can occur in a vacuum as well and hence does not need any contact between the source and the sink [14].

In the context of FP, heat transfer plays a role in two phases. The first phase involves the transport of the heat generated by polymerization via thermal diffusion (convection) through the monomer and polymer phases. The second phase of heat transfer involves heat loss to the surrounding primarily via convection and conduction, and to a lesser extent, advection and radiation [14]. Convection causes heat loss to the unreacted monomer, while heat is lost to the reinforcement (carbon fibres) through conduction.

with an understanding of the basics of heat transfer in FP, it is necessary to take a few factors into consideration in order to successfully implement FP in the manufacturing of FRPs:

- **Heat Generation vs Heat Loss:** The FP formulation should exhibit very low reaction rates at the room temperature (initial temperature), as well as a high reaction rate between the room temperature and the adiabatic reaction temperature (temperature the formulation would reach without heat loss). This is crucial for an FP formulation because the basic requirement for a successful formulation is that the reaction is exothermic in nature. Such a formulation allows for a situation in which the rate of heat production exceeds the rate of heat loss. This is essential for sustaining the thermal front, as there must be sufficient energy available to cleave the initiators [9][43].

- **Temperature and Front properties:** Front properties, such as front velocity, are often temperature dependent. For instance, front temperature and front velocity have a linear relationship between them. Fast-moving fronts have higher front temperatures than slow-moving ones [44]. In a frontal system, the temperature is studied as a function of space and time. In an FP experiment, thermocouples at fixed junctions or infrared thermographs are used to record temperatures. Both these methods show three distinct regimes [14], as illustrated in Figure 2.11: (1) monomer

preheating, which results from heat transfer from the ignition source or from the polymerization enthalpy and is represented as a smooth curve in both space and time; (2) reaction front, resulting from the concurrent heat released from the rapid conversion of monomer to polymer, represented as a sharp gradient in both space and time; and (3) polymer cooling after polymerization due to heat loss to the surroundings.
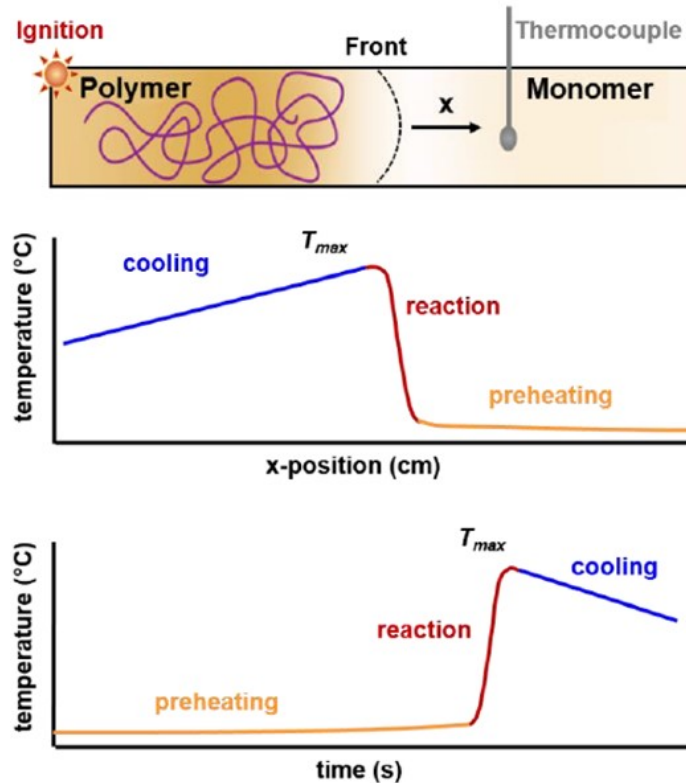
Figure 2.11: The three temperature regimes in frontal polymerization [14]

Moreover, Goli et al. [45] demonstrated that convective heat losses to the surroundings often result in a front temperature lower than the trigger temperature (the temperature that triggered a travelling front). Furthermore, Birkner et al.[46] reported that RICFP leads to a high degree of monomer conversion as compared to traditional curing and they argue that this is due to high polymerization front temperature which results in high conversion in a short period. It has also been shown that excessively high front temperatures can cause the initiator to completely decompose before all the monomer has reacted. This condition is termed initiator burnout and is said to decrease conversion and front velocity [43].

- **Effect of Fillers:** Fillers are often added to monomer formulation to incorporate or improve specific properties. When fillers are added to FP formulations, they can significantly affect the initiation and propagation of a front. For example, Bomze et al.[28] studied the effect of mica fillers and found that UV-initiated FP becomes difficult due to the scattering of light on the filler particles. Additionally, the heat uptake by filler material can have a significant effect on FP as it can reduce the energy available for the decomposition of the thermal initiator.

Dung Tran et al.[39] tested a variety of fillers, both insulating and conductive, and concluded that filler contents reduce the front velocity and frontal temperature. They explained this observation as a result of the decrease in monomer concentration and the heat uptake of the fillers. The study also showed that the use of conductive fillers could have an impact on FP, which is of particular importance in the manufacturing of composites as the thermal conductivity of the reinforcements

has an impact on the propagation of the front. The presence of a continuous conductive element like carbon fibre alters the thermal transport of the front.

Goli et al.[47] showed that conductive elements allow the heat from the polymerization reaction to travel ahead into the unreacted monomer, thereby increasing the reaction rate and frontal velocity. Different fibre materials facilitate FP dynamics in different ways with the spacing between the fibres limiting or facilitating the travel of the Front. They also observed that the presence of a conductive element changes the shape of the front, likely due to the monomer being subjected to higher preheating near the fibres with no preheating away from it.

Finally, Klikovits et al.[48] showed that the addition of insulating fillers like SiO_2 to the formulation has a positive effect on FP. The heat-retaining ability of these insulating fillers helps create a locally heated zone at the initiation point, helping create a self-sustaining front.

- **Effect of Boundary Layer Heat Loss:** Frontal polymerization works on the principle of thermal equilibrium between the heat generated by the exothermic reaction of the resin system and the heat diffused by the propagating front. However, this equilibrium may be affected by the heat loss from the system to the surrounding. Goli et al.[49] tested the effects of boundary layer heat losses on FP. They mainly investigated the effects of two types of boundary layer heat losses. The first one was the convective heat loss from the resin channel, which is the boundary of the reaction, and the second one was the contact heat loss due to the interaction between the resin channel and the tool plate. Both these boundary conditions led to a decrease in frontal velocity, with substantial heat loss leading to frontal quenching. They also observed that convective heat loss affected the maximum degree of cure in the channel, particularly in the region of the channel boundary. Additionally, they also demonstrate that convective heat losses, when combined with narrow channels, often lead to frontal quenching [50].

3

Research Scope

As described in chapter 2, a significant portion of the work carried out in the field of frontal polymerization has focused on studying the effectiveness of new FP formulations. These studies have examined the use of different monomer, PAG and RTI architectures for the successful propagation of the front. Additionally, the relationship between the type of monomer and the initiator concentrations and the properties of the front, such as front velocity and the front temperature have been explored. Successful demonstrations of the use of FP to cure GFRP and CFRP composites have been conducted, and the qualities of the resulting samples have been compared against similar FRP samples cured via traditional methods.

While the research so far has established the necessary foundation for the implementation of FP as a viable alternative to bulk curing methods, a significant knowledge gap still exists in our understanding of the behaviour of the front when in relation to FRPs. Moreover, the FRPs cured via FP until now have been flat rectangular samples with uniform V_f. Although these samples are a good starting point to demonstrate the feasibility of FP in composite manufacturing, they are hardly a representation of the composites that finds structural applications. Therefore, the goal of this research would be to demonstrate the feasibility of manufacturing FRP samples with varying V_fs within the sample and varying geometric shapes.

3.1. Research Questions

Based on the introduction of this chapter, different research questions have been developed and the main research question is as follows:

"Can we control the heat losses in frontal polymerization to maintain the heat generation-diffusion equilibrium under geometrically complex conditions? "

In order to answer this main question, the research question has been further divided into sub-questions:

1. What is the influence of the variation of the V_fs within the sample on the propagation of the front through the sample?

2. Does the geometrical complexity of a composite part have an influence on FP?

3. What characteristics are desired in a test setup to cure composite samples via FP?

Answering these research questions will aid the extensive characterization of FP in the manufacturing of FRPs. The developed mould test setup will be used to investigate the influence of varying V_fs within the sample on the propagation of the front and demonstrate the feasibility of manufacturing composite samples with different geometries cured via FP. The results from these sub-questions will

help determine whether the heat balance required for the sustenance of the front can be achieved, hence affirming FP's viability as an alternative to traditional bulk curing methods currently used in the manufacturing of composite parts.

3.2. Research Hypothesis

In this section, the hypotheses based on the questions presented in the previous section will be discussed. As described in chapter 2, the thermal front can only propagate when a heat balance is maintained between exothermic heat generated and the heat diffused through the unreacted monomers and fibres, as well as the loss of heat to the surrounding. Therefore, before studying the effects of the changing V_fs and geometry on the behaviour of the front, an effective and predictable system is required to manufacture composite laminates cured via FP. The question regarding the appropriate mould test setup is thus posed, with the hypothesis that a mould test setup comprising insulating elements will be able to maintain the required heat balance for the propagation of the front [51].

In parallel with the development of a mould test setup, an optimization of the manufacturing process required to achieve samples of repeatable quality would be necessary. This optimization process will involve testing for the most optimal method for initiating the front, as well as determining the optimal quantity of resin required to achieve saturation of the fabric layers. Optical analysis will be performed to assess if there is an improvement in the quality of samples. Additionally, samples with increasing V_fs will also be manufactured. It is assumed that a system beyond a certain value of V_f will not be able to sustain a front due to disruption of the heat balance, based on the conclusions of previous studies reported in the previous sections.

Once the highest achievable V_f is determined, experiments will be performed to study the influence of changing V_fs within the sample on the propagation of the front through it. Composite samples with changing V_fs will be manufactured, and the sample surface area will be divided into two regions with different V_f values. One of the regions will have a lower V_f as compared to the other, and the front on initiation will propagate through the lower V_f region before reaching the higher V_f region. The hypothesis here is that if the V_f in both regions is below the highest achievable V_f, the front should propagate smoothly from one region to another. However, if the V_f in the higher V_f region exceeds the highest achievable V_f of the test setup, the front will either quench at the interface or at a short distance from it. The propagation of the front from one region to another will be quantified through the collection of temperature data. This data will then be used to speculate the thermal behaviour of the front at different points during its propagation.

Finally, the possibility of curing composites with different geometries via FP will be examined. A flat, in-plane "L" shaped geometry will be selected, and the front will be started from one of the arms. The assumption here is that the front should traverse through any flat, in-plane geometry as long as the heat balance within the system is favourable to FP. The highest V_f achievable for these L-shaped samples is expected to be the same as those achieved in sub-question one. If the L-shaped samples with uniform V_f are successful, the complexity of the sample will be increased by introducing changing V_fs within the sample. The samples are expected to cure in the same way as the flat rectangular samples manufactured in the second sub-question, and this is based on the assumption that propagation of the front will not depend on the shape of the sample but rather on the ability to maintain the complimentary heat balance.

3.3. Research Objectives

The research objective for this master thesis is:

> " To study the influence of varying V_fs within the sample on the propagation of the front and to demonstrate the feasibility of manufacturing samples with varying geometry by designing an appropriate test setup that would allow effective control of the heat generation-diffusion equilibrium."

To achieve this objective, different sub-goals are set. First, a mould test-up that allows for the repeatable manufacturing of composite samples will be built through trial and error. Second, the highest achievable V_f that can be consistently achieved with the test setup will be determined. Once the mould test setup is in place, the influence of changing V_fs within the sample on the propagation of the front will be studied. Third, composite samples with varying V_fs will be manufactured, followed by the fourth sub-goal, which will involve incorporating thermocouples to study the propagation of the front from one V_f region to another. This will then be followed by the fifth sub-goal, which entails the manufacturing of composite samples with a different geometrical shape while keeping the V_f uniform. This will determine whether the same highest achievable V_f as in the second sub-goal is repeatable. Based on these results, the final sub-goal is to vary the V_f within the sample of this new shape to validate if the observations in sub-goals three and four also apply to the behaviour of the front when the shape of the sample is changed.

4

Manufacturing by FP

To answer the research question posed it is imperative that the right kind of experiments were designed to perform the required tests. This chapter provides the details of the evolution of manufacturing composite samples cured via FP.

4.1. FP Formulation & Characterization

The manufacturing of composite samples began with the preparation of the frontal polymerization solution mixture. This solution mixture contained components that enabled frontal curing based on the RICFP mechanism, as discussed in chapter 2. The RICFP curing mechanism involved three active components: (1) epoxy monomer, (2) RTI, and (3) PAG. Additionally, a photosensitizer was added to shift the initiation wavelength spectrum. The list of chemicals used for to prepare the solution mixture can be found in Table 4.1. Two different sources of epoxy monomer were used to manufacture the composite samples. The first set of samples used IGM Omnilane OC1005, procured from IGM Resins, while the latter set of experiments used UViCure S105, procured from Arkema.

Table 4.1: Componensts of frontal polymerization solution mixture

FP component	Chemical	CAS Number
Epoxy resin	3,4-Epoxycyclohexylmethyl-3',4'-epoxycyclohexane carboxylate	CAS 2386-87-0
Radical Thermal Initiator	Benzopinacol	CAS 464-72-2
Photo acid Generator	(4-(Octyloxy)phenyl)(phenyl) iodonium hexafluorostibate	CAS 121239-75-6
Photosensitizer	Isopropylthioxanthone (ITX)	CAS 5495-84-1

The preparation of the solution mixture began with the removal of volatiles from the resin. The required amount of resin was measured and placed in a beaker, which was then put in a vacuum oven. The resin was subjected to a vacuum at a temperature below its boiling point for a specific duration. The vacuum created an inert environment that prevented the resin from absorbing any moisture from the surrounding air. Care had to be taken to ensure that the resin did not boil in the oven and evaporate, as a liquid under vacuum (reduced pressure) has a lower boiling point. Therefore, the vacuum was only pulled enough to remove the volatiles before any boiling was observed. Once the resin had been heated, the oven was turned off, and the resin was cooled under a vacuum. After the resin had completely cooled down, it was removed from the oven.

The resin required for the FP formulation was measured by weight percentage and transferred to a separate mixing beaker. Then, the necessary amounts of benzopinacol and ITX Photosensitizer were measured based on weight percentages and added to the beaker. To prevent exposure to UV light, the entire beaker was covered with aluminium foil. The components were mixed at high shear rates using a magnetic stirrer. Once the benzopinacol and the ITX had completely dissolved, the required amount

of photoinitiator IOC-8 SbF$_6$ was weighed and dissolved at high shear rates. The resulting solution mixture was stored in a storage bottle with its mouth covered by Parafilm, and the entire bottle was wrapped in aluminium foil before being kept in the refrigerator until use.

The percentage of the various components depended on whether the solution mixture was being used to make polymer samples or fabricate composite samples. These values were obtained from the literature [51]. The weight percentages of the different components based on their use have been presented in Table 4.2. The concentration of initiators used to manufacture composite samples cured via FP was larger than a regular polymer sample. The FP formulation utilized in composite manufacturing comprised 2.13 wt% and 0.75 wt% of benzopinacol and IOC-8 SbF$_6$, respectively.

Table 4.2: The weight percentages of the various FP components

FP Components	Composite Samples (wt%)	Polymer Samples (wt%)
Benzo pinacol	2.13	1
IOC -8 SbF6	0.75	0.4
ITX	0.05	0.05

In chapter 2, Frontal polymerization was described as a process that depends solely on the exothermic enthalpy of polymerization to convert the monomers into a polymer. To determine if the solution mixture prepared had the required enthalpy to successfully carry out frontal polymerization, it was characterized using the calorimetric technique known as Differential scanning calorimetry (DSC). The DSC (dynamic DSC) involves measuring the difference in the heat flow rates between the sample and a reference while they are being subjected to a controlled temperature program. It is important to note that DSC measures the change in property, namely the difference in the heat flow rate, which is a consequence of the variation of sample temperature. This means that no heat flow measurements can be made when there is no alteration in the sample temperature. Hence, a distinct "temperature program" is necessary for a DSC measurement [52].

The DSC furnace temperatures were equilibrated at -20$°C$ for $1min$ to ensure a constant scan rate and reliable temperature readout. The crucibles were then heated to a temperature of 250$°C$ at a heat ramp of 55$°C/min$. The obtained DSC data was further processed to determine the enthalpy of polymerization and the polymerization onset temperature for each batch of FP formulation. The results from the DSC analysis have been presented in chapter 5.

Before manufacturing the composite samples, each batch of the FP formulation underwent characterization via the DSC technique. A solution with an enthalpy of polymerization ranging between 400 J/g to 600 J/g is required for successful front propagation through the composite layup [39]. The initial batches of FP formulation mixed were small, consisting of 20g each, and all used the IGM Omnilane OC1005 epoxy monomer. As the need for the resin in the experiments increased, larger quantities ranging from 40g to 80g were mixed using IGM Omnilane OC1005 as the epoxy resin. However, these batches of the formulation showed inconsistencies in the enthalpy values due to the variations in the mixing apparatus and shear rates employed. To address these inconsistencies and improve the consistency of the mixture, standardisation was carried out.

The latter part of the experimental trials involved batches of FP formulations that utilized UViCure S105 as the epoxy resin. To ensure consistency, a standardized mixing approach was adopted, and the mixing beaker and magnetic stirrer were kept constant throughout. All batches had a weight of 80g and were mixed at a shear rate of 440rpm. The mixing time for all components was also standardized. Firstly, the resin was mixed with benzopinacol and ITX photosensitizer for a duration of 17 hours (overnight), followed by the mixing of IOC-8 SbF$_6$ for 7 hours.

4.2. Casting Silicone Moulds

To manufacture composite samples cured via frontal polymerization, it was important to choose the right test setup [51]. As mentioned in the previous chapters, for the successful propagation of the front it is necessary to maintain a balance between heat generation and diffusion. Therefore a material that could help maintain the required thermal heat balance while preserving its structural integrity at the elevated front temperatures was needed. To achieve this, Room Temperature Vulcanizing (RTV) silicone rubber was chosen as the appropriate material. The casting process started with the preparation of the box cavity with the pattern to be cast and the silicone mix. As shown in Figure 4.1, to ensure that the pattern cast was dimensionally precise, the core/pattern had to be made of rigid solid material like wood, metal, PLA, etc.
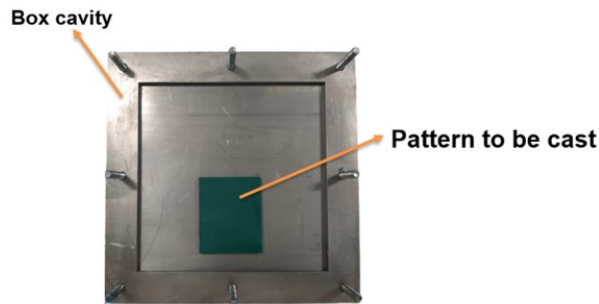
Figure 4.1: Preparation of mould setup for casting.

The next step was to mix the silicone base and catalyst using the recommended mixing ratio of 10:1 (base to curing agent). A clean container was used, and the required amount of base and catalyst were poured in proportion. The two components were mixed manually until the catalyst was completely dispersed in the base (see Figure 4.2 A). The mixture was then degassed for a minimum of 12 min in a vacuum chamber (see Figure 4.2 B). The mixture would take 16 hours to cure completely at room temperature. If the ambient temperature was any lower, it would take longer to cure. Conversely, heating accelerates the curing process, but could cause significant shrinkages due to the difference in cooling between the silicone mixture and the mould original. The silicone moulds made from SILASTIC^{TM} RTV-4136-M have high temperatures resistance, making them perfect for manufacturing samples cured via frontal polymerization. However, the silicone joint would loss its elastic properties upon repeated exposure to a temperature above 200° C [53]. Additional details on the preparation of the SILASTIC^{TM} RTV- 4136-M silicone mixture and the mould cavity have been presented in section B.1.
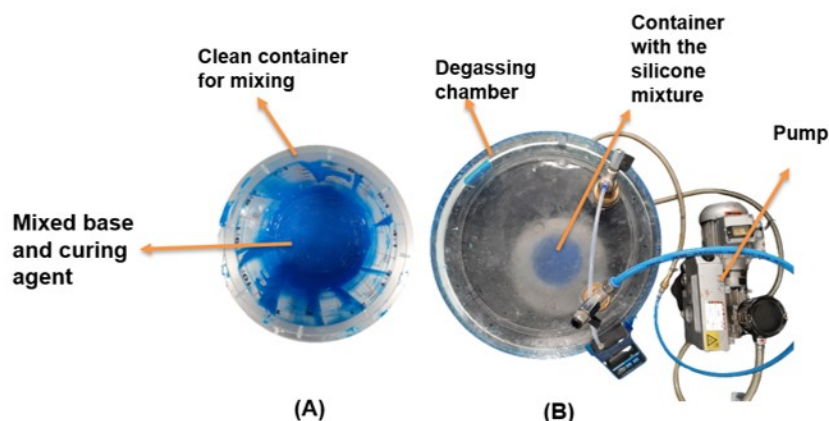
Figure 4.2: Silicone components mixing and degassing. **A:** Mixed SILASTIC^{TM} RTV- 4136-M base and curing agent. **B:** Vacuum chamber utilized to degas the liquid silicone mixture.

4.3. Manufacturing Composite Samples

A series of experiments were conducted to demonstrate the manufacturing of composites cured via frontal polymerization. These experiments were of increasing complexity, each subsequent trial built upon the failures and the know-how gained from the preceding set of experiments. These experiments helped determine the setup required for a sustaining front and the highest possible V_f achievable by combining the hand layup processing with FP-based curing. The experiments performed can be broadly classified into three separate categories based on the addition of elements to the mould setup, which allowed for better consistency and control over the sample manufacturing process.

The first set of experiments was performed in open silicone moulds cast to the required dimensions. In this experimental set, the samples were made in an open silicone mould with a cavity of dimensions $120\times60\times5\ mm$. The samples manufactured used only 1 or 2 fabric layers to determine the feasibility of a silicone-based mould for FP curing. A 2/2 twill weave carbon fabric was chosen as the reinforcement phase. As the corresponding technical data sheet was unavailable, the required parameters were either calculated or based on the standard values obtained from the literature.

To carry out the hand layup, a brush was used to spread a layer of resin on the cavity surface, followed by layup of the fabric layer pre-cut to a dimension of $11\times5.5\ cm$ via a guillotine shear (see Figure 4.3 A & B). The fabric layer was pressed into place with a wooden stick, followed by an additional layer of resin completely wetting the fabric layer (see Figure 4.3 C). After the layup was completed, a soldering iron was used to initiate the front. If the initiated front did not travel all the way to the end, curing the entire sample area, then a front was initiated again just in the vicinity of the uncured region (see Figure 4.3 E).
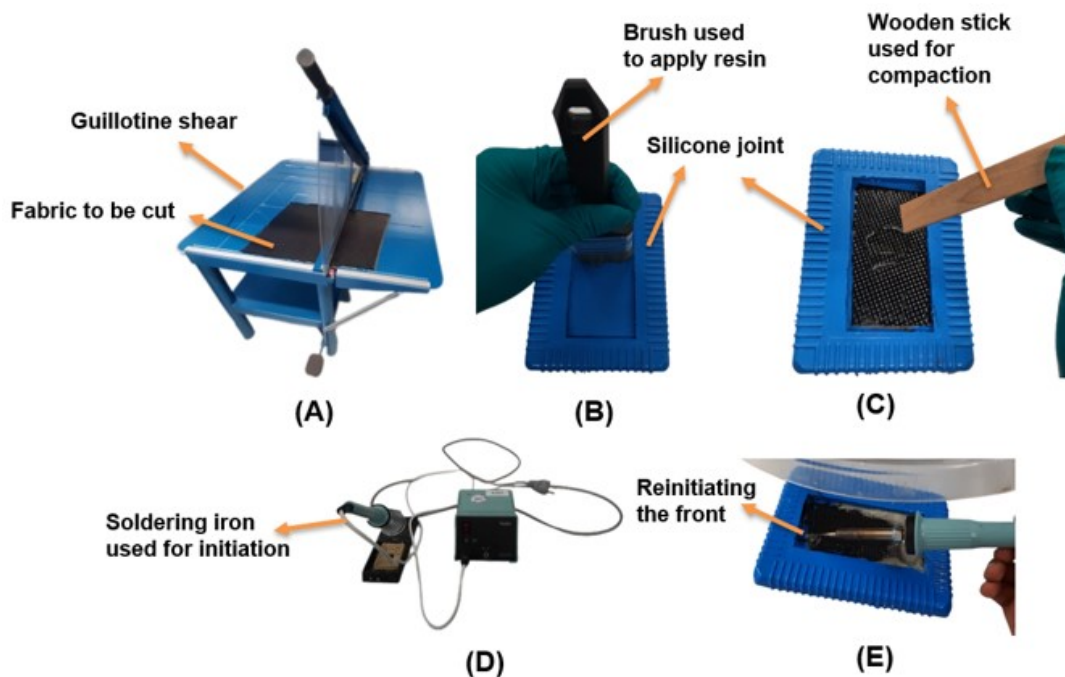
Figure 4.3: Manufacturing composite samples in an open silicone mould **A:** Guillotine shear. **B:** A brush was used to wet the mould cavity. **C** Compaction with a wooden stick. **D:** Soldering iron. **E:** Re-initiation of front.

The second set of experiments incorporated three new features based on observations from the previous stage. As shown in Figure 4.4, a $3mm$ Teflon plate was used to cover the cavity to prevent any loss of heat to the environment. A $7mm$ hole was drilled through the plate for FP initiation via the soldering iron (see Figure 4.4 D), and weights were kept on top of the Teflon plate to achieve uniform thickness (see Figure 4.4 D). Furthermore, samples were made of a size such that there was enough surface area for the provision of a resin pool (see Figure 4.4 C). This resin pool was now initiated directly, forcing the front to cure the pool first before moving on to cure the layup. This ensured that the

fabric did not stick to the hot iron when in contact. The silicone mould had a cavity with the dimensions of $60{\times}50{\times}5\ mm$.
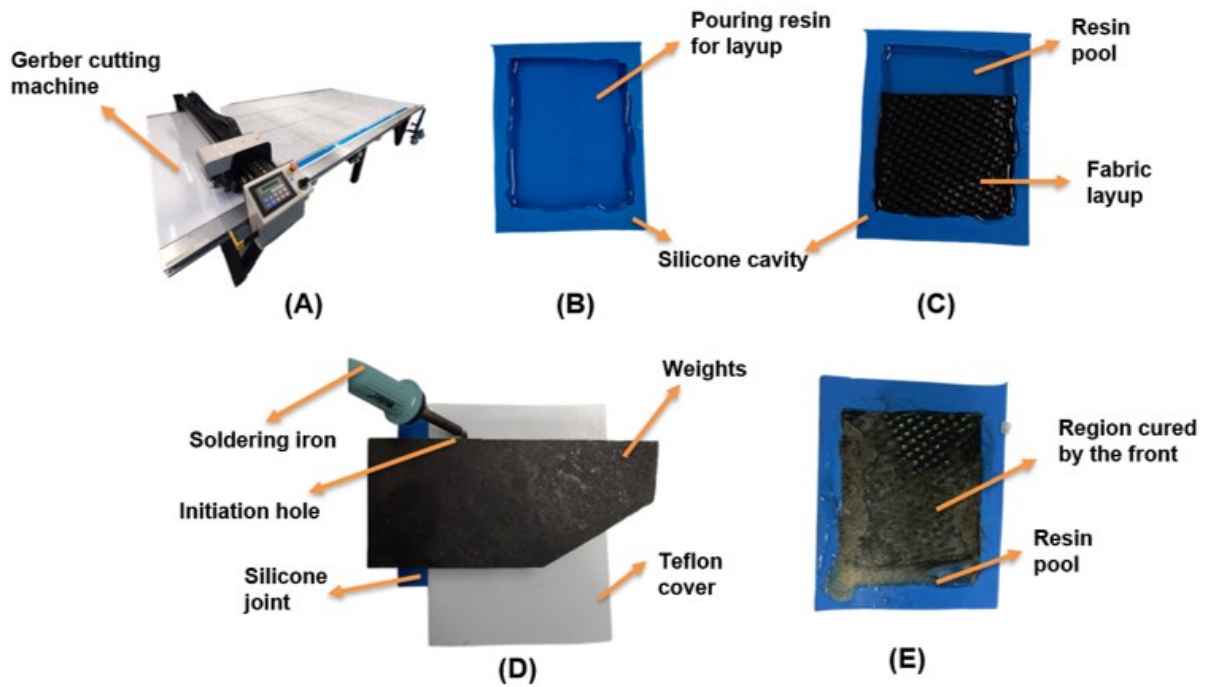
Figure 4.4: Manufacturing composites samples with a Teflon cover silicone mould. **A:** Gerber cutting machine. **B:** Pouring and spreading of resin **C:** Handlayup **D:** Placing a $3mm$ thick Teflon cover and the weights and initiating of the front using a soldering iron. **E:** Cured sample.

The hand layup process began by pouring and spreading some resin on top of the cavity surface (see Figure 4.4 B), followed by laying the first fabric layer cut to the appropriate dimensions via the Gerber cutting machine (see Figure 4.4 A). The fabric layer was then laid on the resin film, and a wooden stick was used to thoroughly wet the layer. This was repeated for the next resin and fabric layers until the required number of layers was in place. The number of layers and hence the corresponding theoretical fibre volume fraction was calculated via a formula derived based on the standard composite volume fraction formula-

$$V_f = \frac{n \times A_{textile}}{\rho_{fabric} \times d} \tag{4.1}$$

Where V_f is the fibre volume fraction, n is the number of fabric layers, $A_{textile}$ is the areal weight of 2/2 twill weave used as the reinforcement, ρ_{fabric} is the density of the fibre used in the 2/2 twill weave fabric and d is the intended/measured thickness of CFRP part.

The areal weight of the fabric was calculated by weighing a fabric with a surface area of $100cm^2$ ($10{\times}10cm$) and then calculating the areal weight of $1cm^2$. The calculated areal weight of the fabric was $276\ g/m^2$. The value of fibre density (ρ_{fabric}) was assumed to be $1.77g/cm^3$, based on the range of density values summarized in literature[54].

Once the predetermined number of layers were laid up, the resin pool was created in the remaining unused surface area ($1cm{\times}5cm$). Subsequently, the Teflon plate was placed above the cavity with the initiation hole right above the resin pool. The weights were then placed on the Teflon plate and the front was initiated via the soldering iron (see Figure 4.4 D). Multiple samples with different V_fs were manufactured until the highest V_f with this test setup was reached.

The last set of experiments was conducted using a specially designed closed mould setup, which was intended to achieve uniform thickness across the sample. The design of this mould was based on the observations of the behaviour of the front in the first two sets of experiments. The various components and the assembly of the closed mould setup are depicted in Figure 4.5. The mould setup was comprised of four separate elements: a frame, two Teflon plates, two steel plates and a silicone joint with a cutout pattern (see Figure 4.5 A). The frame and the silicone joint, each 5mm thick, were sandwiched between two Teflon plates, which were in turn sandwiched between two steel plates. The entire setup was held together by eight M6 nuts and bolts.
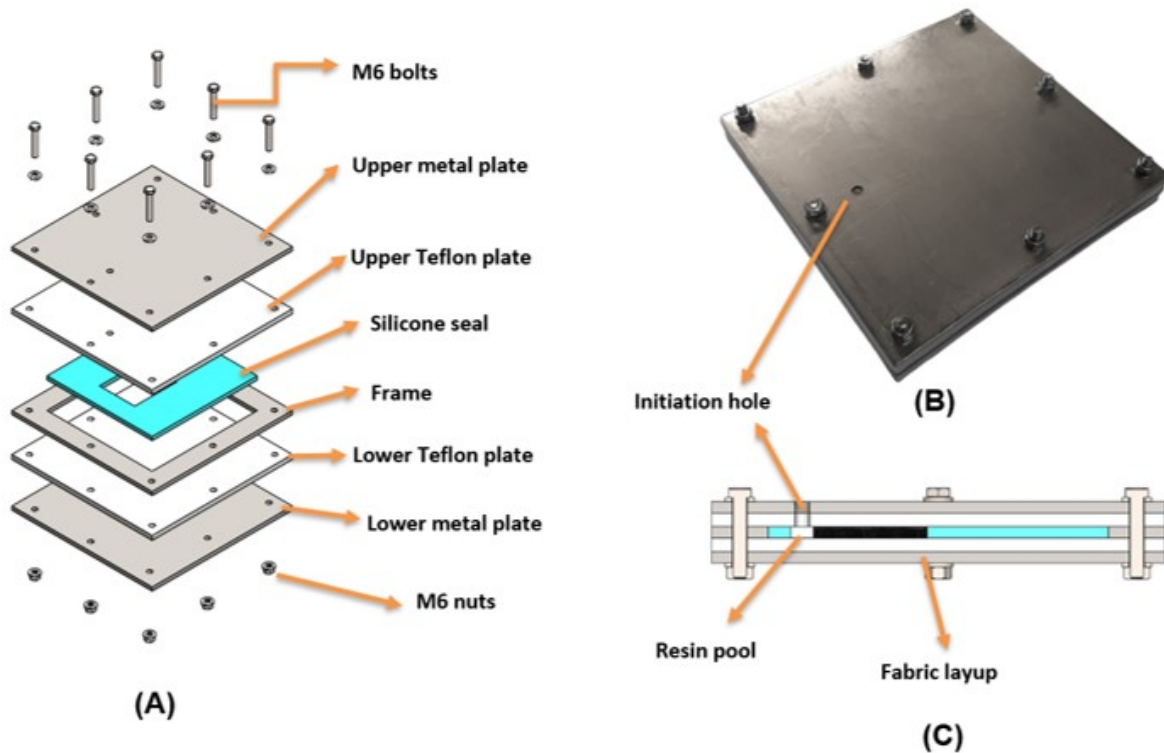
Figure 4.5: Assembly of the closed mould setup. **A:** Components of the closed mould test setup. **B:** Isometric view of the mould assembly. **C:** Cross-sectional view of the closed mould test setup

To manufacture the composite samples, the bottom Teflon and steel plates were aligned by inserting all eight bolts. The frame was then inserted to create a cavity for the silicone joint. To prevent leakage of resin through the interface between the Teflon plate and the silicone joint, a grease lubricant was applied along the cutout on the silicone surface in contact with the Teflon.

As illustrated in Figure 4.6, the silicone joint was put in place, and then the fabric layers were laid up in the cutout. Unlike the previous two sets of experiments where the resin was applied layer by layer, a large chunk of resin was now poured into the cavity, creating a pool where the fabric layers were subsequently placed into the cavity step by step (see Figure 4.6 A).

The layup process involved laying the fabric into the cavity and allowing the resin to wet the layer completely by capillary action before compressing the layer into the cavity with a wooden stick. This process was repeated until all the fabric layers were in place. During the layup, if the amount of resin appeared to be insufficient, additional resin was added to ensure that the cavity remained resin-rich.

Similar to the second set of experiments, the dimension of the cavity were $60{\times}50{\times}5\ mm$, and the fabric layers used were cut to the dimension of $5{\times}4.5\ cm$. The remaining area in the cavity was used to create a resin pool used to initiate FP. Once the last layer was in place, the entire lower half of the mould, along with the completed layup, was placed in the degassing chamber (see Figure 4.6 C). This
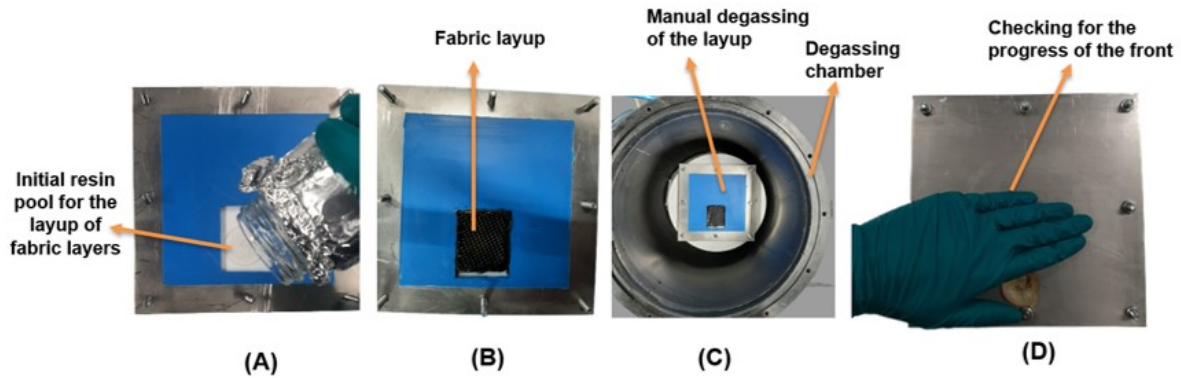
Figure 4.6: Manufacturing of a composite sample with the closed mould setup. **A:** Pouring the resin into the cavity. **B:** Layup of the fabric layers. **C:** Manual degassing in a vacuum chamber. **D:** Checking for heating of the steel plate over the sample to check the progression of the front.

was a simple manual degassing method used to remove the air entrapped in the FP formulation and between the fabric layers.

After degassing, the lower mould half was taken out of the vacuum chamber, and a final dose of resin was used to cover the fabric and fill the initiation pool. The mould was then closed with upper Teflon and steel plates. M6 nuts were tightened against the bolts, with the centre bolts being tightened first, followed by the corner bolts. To initiate FP, a hole large enough ($7mm$) for a soldering iron was provided through the upper steel and Teflon plate.

The front was initiated by touching the resin in the pool with a soldering iron. To check the progress of the front, the steel plates were checked for any release of heat. If the steel plates became hot directly over the cavity, then it was an indication of curing (see Figure 4.6 D). After 2 or 3 min, the mould was demoulded to remove the fully cured composite part.

Prior to manufacturing the stainless steel components, it was necessary to create a prototype first to test the feasibility of the setup. The prototype mould consisted of an aluminium plate for the outer covers and a 3D-printed frame made of polytetrafluoroethylene (PTFE). The Teflon covers and silicone seal, which were used to contain the heat within the system, were manufactured once and later reused with the stainless steel mould test setup. The success of the prototype mould led to the manufacturing of the actual stainless steel mould test setup.

The composite sample manufactured via the closed mould test setup exhibited observable variation in thickness, which led to variation in V_f across the length of the sample (further discussed in chapter 5). This variation was attributed to the thickness variation across the cavity in the silicone joint. To correct this issue, the source of the thickness variation across the silicone joint was investigated. For this purpose, a new silicone joint was manufactured using the exact same steps as mentioned in section 4.2. Furthermore, to check for possible thickness variation across the length of a composite laminate, a representative resin block was cured in the new cavity.

To perform this exercise the lower half of the mould, which included the lower Teflon plate, lower stainless steel cover, and stainless steel frame, was pre-cleaned and assembled. The newly cast silicone joint was then assembled to create a new cavity. For this exercise, EPIKOTE^{TM} resin and EPIKURE^{TM} curing agent (code number: 04908) from HEXION were used. This two-part mixture had a mixing ratio of 10:3 (resin to curing agent), and had a curing time of 4 to 6 hours at a temperature of 80°C. The mixture was degassed before use to remove any air bubbles formed during the mixing process. The mixture was then poured into the cavity before closing the mould. The mixture was allowed to cure overnight at room temperature, after which the cured resin block was demoulded, and its thickness variation was measured.

4.4. Void Fraction Study

The quality of the samples manufactured through the different mould test setups was assessed by observing them under a laser confocal microscope to check for void content. The preparation for the microscopy began with identifying the surface of the laminate to be observed under a microscope. Once the surface had been identified, a permanent marker was used to label the samples and indicate the surface to be cut (see Figure 4.7 B). The selection and labelling of the samples were followed by the cutting/sectioning process using an abrasive cutting saw lubricated with a coolant to prevent damage to the samples due to the heat generated during the cutting operation.
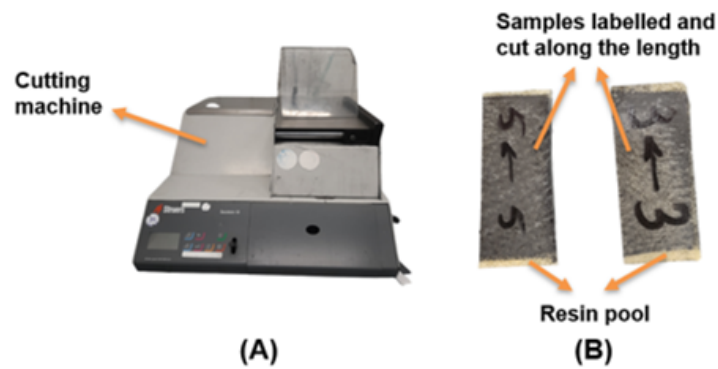
Figure 4.7: Labelling and cutting of samples.**A:** cutting machine.**B:** Labelling the samples.

As the objective of this study was to understand the reductions in void distribution among the different samples, it was more appropriate to study the void distribution along the entire length of front propagation. This need was also complemented by the small dimensions of the sample ($60{\times}50mm$). The samples were then cut through the exact centre along the entire length of the samples and further cut into two small sections of $30{\times}25mm$ to fits into the embedding mould. The cut samples were then cleaned in an ultrasonic bath to remove any particulate matter that might be left on the cut samples post-curing. The cleaned cut samples were then removed from the bath and dried using an air gun.

To observe any surface under a microscope, they were first embedded in a sample holding mould. To increase efficiency, many samples were embedded in one single holding mould, reducing the time spent in the remaining preparation steps namely, the grinding and polishing. To embed the samples, a plastic mould coated with a release agent was used (See Figure 4.8 A).
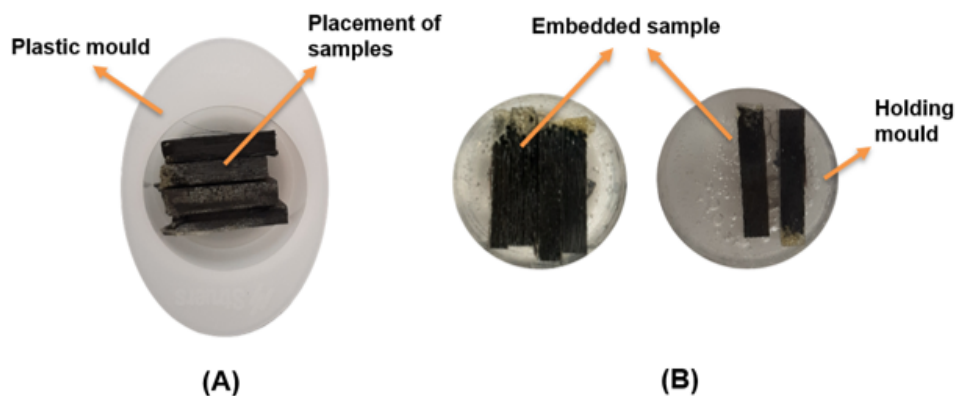
Figure 4.8: Embedded samples. **A:** Plastic mould used for embedding. **B:** Holding mould.

The pre-cleaned and dried samples were joined together with double-sided tape and lowered into the cavity. Epofix, a cold-setting resin based on two-fluid epoxy components, was used for embedding

the samples. With a mixing ratio of 25 parts resin to 3 parts hardener by weight, the required amount of resin was mixed. The mixture was then carefully poured into the plastic cavity to prevent air bubbles from getting caught. The mixture was then allowed to cure for about 8 hours before demolding to get the holding mould (See Figure 4.8 B).

Before the samples could be observed under a microscope, they had to be ground and polished to obtain a smooth and plain surface (see Figure 4.9). An automatic grinding and polishing machine was used for this purpose. The samples were first ground with silicone carbide paper. To increase the rate of material removal, increasing grades of the grinding papers were used, starting from grade 180, followed by 320,1000,2000 and grade 4000. After each grinding step, the sample (holding mould) was immediately cleaned via an ultrasonic bath and dried with an air gun to ensure that no particulate matter was carried onto the next grinding paper, which could have caused scratches on the sample surface.

To polish the samples, the grinding paper was replaced with a polishing cloth coated with a diamond abrasive paste. Different grades of diamond abrasive pastes were used, starting from $6\mu m$ to $3\mu m$ and $1\mu m$. Care was taken to ensure that the appropriate polishing cloth was used with the corresponding grade of polishing paste.

Figure 4.9: Ground and polished samples.

After the polishing step, the samples were ready to be observed under the microscope. Keyence laser scanning confocal microscope was utilized for the observations and the samples were observed at $10\times$ magnification.

The entire surface area of the sample was split into many sub-surfaces, each of which was observed and captured at $10\times$ magnification. The final image of the entire surface was obtained by stitching all the individual images of the sub-areas. All these steps were automatically performed by the inbuilt control software of the KEYENCE microscope. The stitched images of the entire surface area of the sample were then post-processed with an image processing software known as ImageJ.

4.5. Influence of Fiber Volume Fraction

To consider frontal polymerization an effective technique for curing thermoset-based composites, it was necessary to test its versatility in manufacturing composites that find everyday applications. Primary and secondary load-carrying structures made of composites are not flat, rectangular plates; they are complex structures with varying shapes and thicknesses. The thickness of composite samples can be varied by stacking a different number of fabric layers. However, no studies have yet demonstrated the feasibility of using frontal polymerization to manufacture composite samples with variations in the fibre volume fraction (V_f) within a single homogeneous structure.

Building on the know-how gained from various experimental trials using the closed mould test setup, a new set of experiments was designed to manufacture composite samples with varying V_fs within the sample.

In order to manufacture composite samples with varying V_fs, the surface area of the flat rectangular plate samples was divided into two separate regions of higher and lower V_f. Prior to manufacturing a composite sample, a silicone seal with dimensions of $90 \times 50\ mm$ was cast. With its large surface area, the cavity allowed for significant variations in the dimensions of the higher and lower V_f region. This flexibility in the dimensions of the different V_f regions enabled the manufacturing of a variety of samples.

Furthermore, the thickness of this cavity ($4.91 \pm 0.04\ mm$) was similar to the cavity utilized to manufacture flat rectangular laminates. As a result, the highest V_f achievable was consistent with that of the flat rectangular samples (up to 12 layers, theoretical V_f of 38%). The manufacturing process began with the same steps described in section 4.3. The initial steps involved the preparation and the assembly of the bottom mould half with the silicone seal to create the cavity for the layup of the fabric layers, and this step remains unchanged.

As illustrated in the schematic diagram in Figure 4.10, the surface area of the sample was divided into two separate regions of lower and higher V_f. The lower V_f region was adjacent to the resin pool and similarly, the higher V_f region was adjacent to the lower V_f region. The exact surface area of the lower and the higher V_f regions varied from sample to sample and the figure shows the case where the lower and higher V_f regions are equally split.
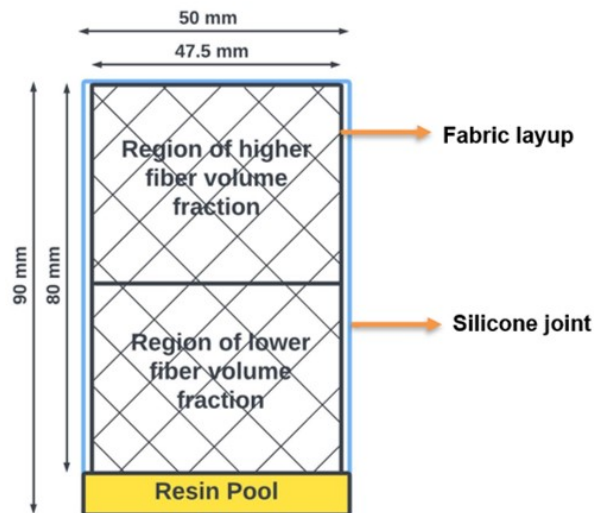
Figure 4.10: Schematic diagram showing the different regions of fibre volume fraction.

To achieve these two separate regions, a unique fabric layer stacking method, referred to as the "blended hand layup method" was used. To understand this stacking method, Let us take the example of a sample where the lower and the higher V_f regions were made of 11 and 13 fabric layers, respectively. To achieve the required layup, 11 continuous fabric layers with a dimension of $80 \times 49\ mm$ and 2 shorter fabric layers with a dimension of $40 \times 49\ mm$ were cut out.

To cut the fabric layers, the Gerber cutting machine was initially used. However, later on, manual cutting methods were utilized, where a large piece of fabric was sandwiched between two plastic films. The entire setup was then stuck to a cutting table using masking tape (as shown in Figure 4.11 A). The tape was pulled in tension and stuck to the table to ensure that no wrinkles were formed on the fabric. To cut out the fabric layer, a roll cutter was traced along the edges of a 3D printed template, printed to the dimensions of the fabric layer (as shown in Figure 4.11 B).
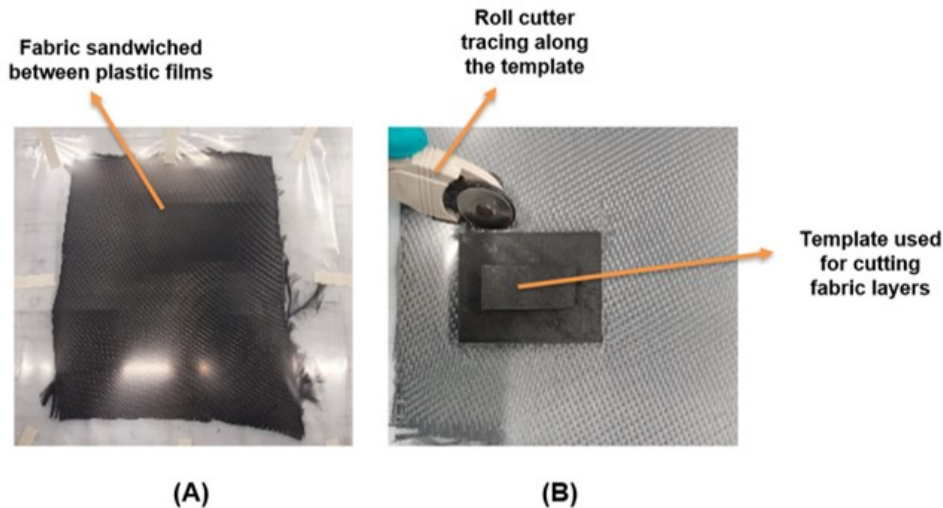
Figure 4.11: Cutting of fabric layers manually via a roller cutter and a template. **A:** fabric cutout sandwiched between two plastic films and stuck to a cutting table with masking tapes. **B:** Cutting fabric layers with a role cutter.

Similar to the steps described in section 4.3, the layup process began by pouring some resin into the cavity creating a pool. The first of the long fabric layers was laid into the cavity, this layer was then allowed to be wetted via the capillary action. Then the layer was compacted using a wooden stick (See Figure 4.12 A). The remaining fabric layers were laid up in an exactly similar way. To build up the regions of the higher V_f the two small fabric layers were stacked in between appropriate layers of the longer fabric layers. This way the region of higher V_f was made of 11 continuous fabric layers and 2 shorter fabric layers while the region of lower V_f had only 11 layers. The shorter fabric layers were stacked appropriately between 3rd & 4th layers and 6th & 7th (See Figure 4.12). This unique method of stacking allowed for the formation of a continuous homogeneous sample without any physical demarcations between the two regions. The layup was then placed into the degassing chamber to remove the air entrapped between the layers. Following this, the remaining steps of mould closure and front initiation remained the same as in section 4.3.
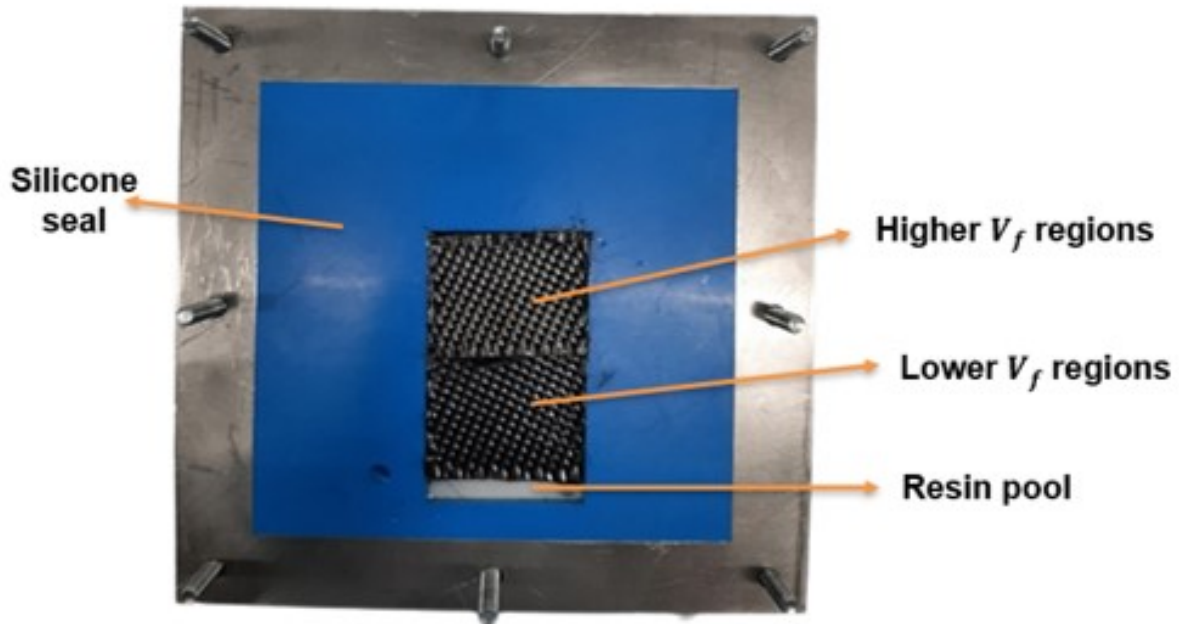
Figure 4.12: Manufacturing composite samples with the variation of V_fs within the sample.

4.5.1. Manufacturing Process Optimization

The initial composite samples, which were manufactured with two separate V_f regions, exhibited inconsistency and non-repeatability. These samples are presented in section 5.3. In order to identify the source of inconsistency, a study was conducted by manufacturing samples with equal regions of higher and lower V_f. The manufacturing steps used were documented and later examined to identify possible sources of inconsistency. The samples were manufactured following the exact steps outlined in section 4.5. The Gerber cutting machine was used to cut the fabrics to the required dimensions.

As a result of this exercise, four main sources of inconsistency were identified: (1) fraying of carbon fibre filaments from the fabric layers before and after layup, (2) an inadequate amount of resin during the layup process, (3) a small initiation pool size, and (4) movement of the layup and loss of resin during degassing. The following steps were taken to tackle these issues:

In all of the manufactured samples, two main sources of fraying have been identified: (1) fraying of filaments during cutting and subsequent storage and handling of the fabric layers, and (2) fraying of filaments during compaction with a wooden stick.

The fabric layers that were cut using the Gerber cutting machine exhibited filament fraying due to poor handling during transport from the cutting table and inadequate storage before use. To ensure fabric stability and reduce filament fraying during handling, an optimized cutting method was necessary. To achieve this objective, three separate approaches were devised and tested: (1) tow stabilization with an air tack spray, (2) pre-wetting and cutting technique, and (3) dry table cutting and placement.

The first method of tow stabilization, involving an air tack spray, consisted of applying a fine mist of adhesive that would create a temporary bond to hold the filaments at the edge of the fabric layer intact. As shown in Figure 4.13, a 3D-printed mask was placed on top of the fabric layer, and the air tack spray was gently applied to the exposed edges to stabilize it.
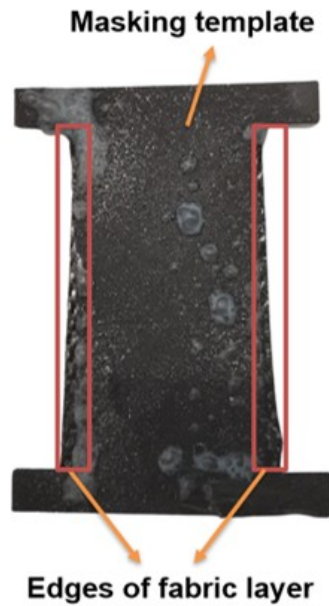
Figure 4.13: Using air tack spray to arrest the tows at the edges of the fabric layers.

The second method of tow stabilization involved prewetting and cutting fabric layers. In this method, the fabric layers were cut from a pre-wetted fabric sheet, which reduced or eliminated the separation of tows during the cutting process. To create a wetted fabric, a large piece of fabric was sandwiched between two plastic sheets, and resin was introduced between the plastic films and into the fabric layers to wet them (see Figure 4.14). The fabric layers were then cut from this sandwich using a roll cutter and a 3D-printed template.
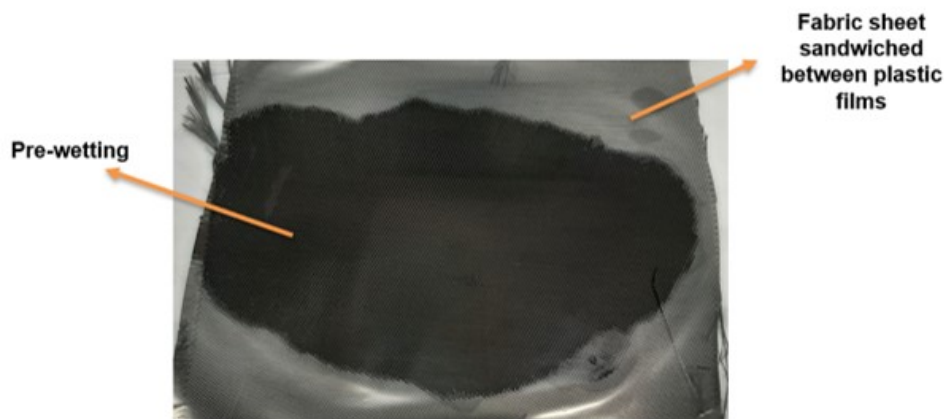
Figure 4.14: Pre-Wetting of the fabric layers sandwiched between two plastic films.

Both of these methods have some disadvantages, as discussed in subsection 5.3.1, which limit their usability. Following these two methods, the dry-cutting method was devised. After conducting various trials, the manual dry cutting method described in section 4.5 was selected as a replacement for the fabric cutting process that previously utilized the Gerber cutting machine.

The second source of fraying, which occurred during the compaction of the fabric layers, was more challenging to address. It was observed that even fabric layers of pristine quality experienced tow separations as a result of the outward flow of resin during the compaction process. To address this issue, minimum compaction was chosen with greater emphasis given to natural settling assisted by gravity and capillary action. However, if the tows did separate, they were not removed after degassing but

rather left untouched.

Two main causes of low levels of resin saturation were identified: (1) inadequate resin added during layup, and (2) resin escape during compaction. To overcome both of these problems, oversaturation of resin was considered to be the key solution. To achieve oversaturation of resin, the process of adding resin was standardized. This involved adding a predetermined quantity of resin during the layup process, with the number of layers at which the resin would be added also predetermined. The quantities of the resin used and the point of resin addition, determined through trial and error, have been presented in Table 4.3. To supplement the resin that escapes the cavity during degassing, $10g$ of resin was added. Prior to use, this resin was degassed to prevent any new sources of voids. Additionally, the resin was used to fill the pool up to the brim and create a thin layer of resin film over the layup. This ensured that despite the resin being squeezed out during compaction, sufficient resin was still available within the system to initiate the propagation of the front.

Table 4.3: The quantities and the point at which the resin is added during the handlayup porcess.

Layers at which the resin is added	Weight in g
The initial resin pool created for the layup (base)	16±0.5
Resin added after the layup of the 8th layer	6±0.5
Resin added after the layup of the 10th layer	5±0.5
Resin added after degassing and before mould closure	10±0.5

Another source of inconsistency that was identified was related to the size of the resin pool. The samples produced indicated that changing the initiation pool size had an impact, as shown in subsection 5.3.1. To address this issue, two separate steps were taken. First, the frayed tows were manually removed to ensure a pristine resin pool. Second, the physical size of the resin pool was increased from $10mm$ to $15mm$. These measures were taken based on the results of the trials.

Finally, disorientation of the stacked fabric layers during degassing was observed. The sudden rush of air into or out of the degassing chamber affected the orientation of the layup, causing it to rotate out of the cavity. This movement was also accompanied by an excessive loss of resin from the cavity, which affected the propagation of the front through the fabric layers. To tackle this challenge, a 3D-printed frame was used to stabilize the plies in the cavity. This frame surrounded the cavity, holding the layup and resin in the exact same orientation as before degassing.
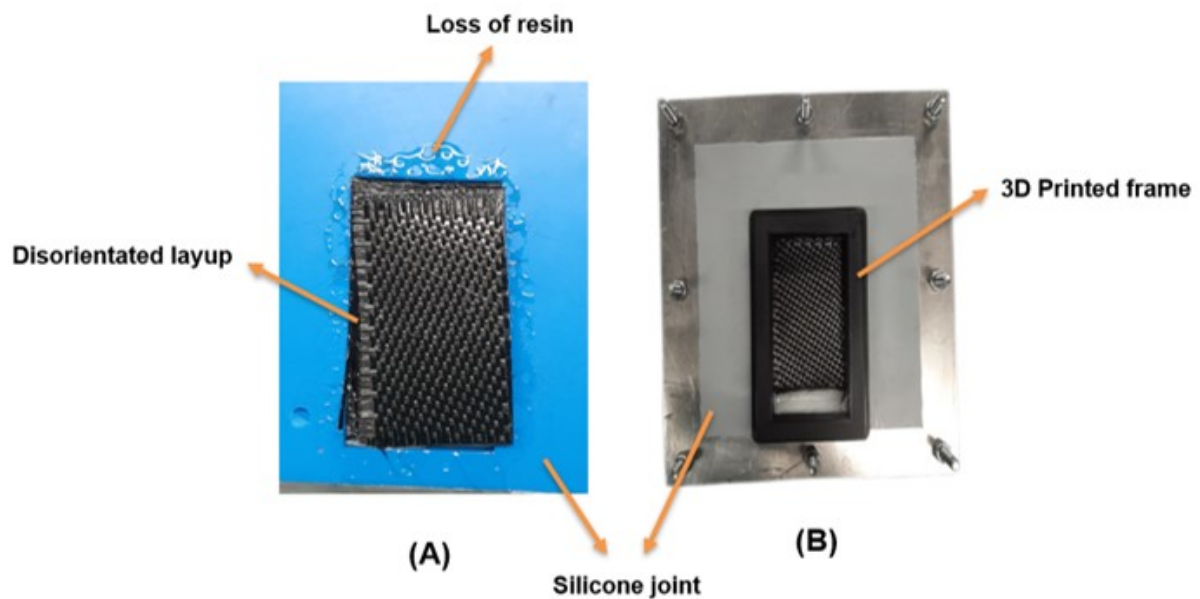
Figure 4.15: Movement of the stacked fabric layers while degassing. **A:** Disorientated fabric layers. **B:** 3D printed frame used to arrest the fabric layers in place during degassing.

4.5.2. Temperature Monitoring

To better understand the effects of varying V_fs on the propagation of the thermal front through a composite sample, a quantification system is required. This system should enable the measurement of the propagating front. One simple and effective quantification method for this purpose is the capture of temperature data at key locations on the sample surface.

The temperature data across the sample surface was captured by incorporating thermocouples into the layup. Type K thermocouples with a diameter of $0.5mm$ were used to capture temperature data. These thermocouples were manufactured in-house by stripping the thermocouple wire, which consists of two wires. The outer insulation and the shielding covering the metal wire were stripped, leaving the bare wires. These bare wires were then twisted together to maintain contact. The contact was made permanent by soldering the two wires together using an L60+ thermocouple & fine wire welder from LABFACILITY. The other end of the thermocouple was attached to a plug or connector, which was then connected to a device which measures temperature. For these experiments, a Keithley 2701 Ethernet-Based digital multi-meter was used for the acquisition of temperature data. The final data collection test setup utilized for temperature monitoring is illustrated in Figure 4.16.
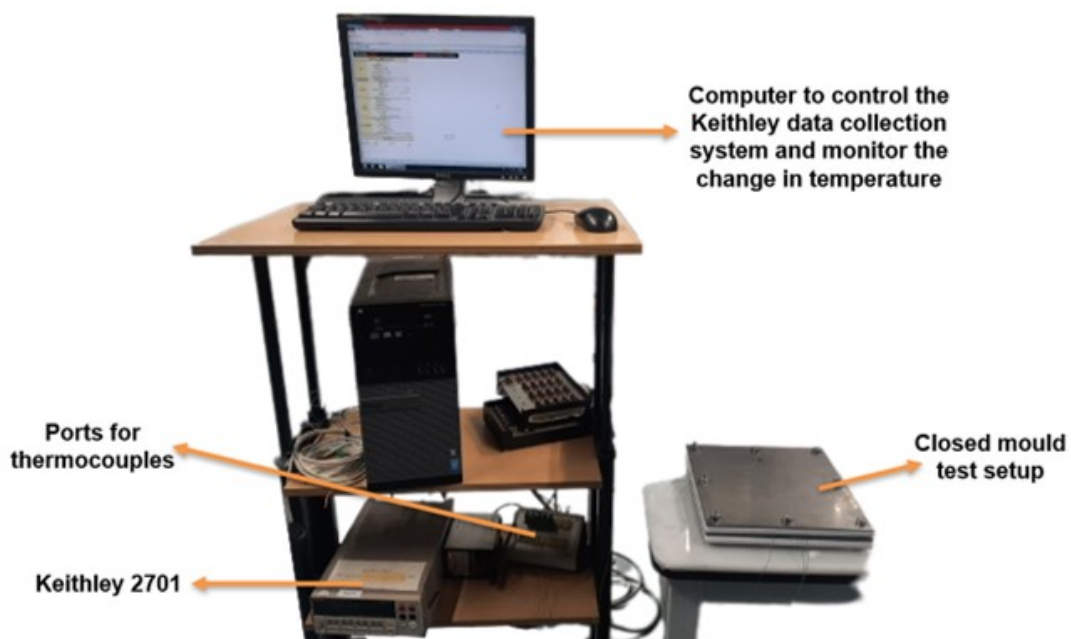
Figure 4.16: Data collection setup based on the Keithley 2701 digital multi-meter.

To 'better understand the placement of the thermocouples, let's Continue the example from section 4.5. The thermocouples were placed in key positions immediately after the last smaller fabric layer was laid to build the higher V_f region, between the 6th & 7th layers.

Figure 4.17 illustrates the placement of thermocouples during the hand layup process. Five thermocouples were used, with one placed on each of the lower and higher V_f regions (labelled as thermocouples 1 and 4). Two thermocouples were placed at the interface of the two V_f regions (labelled as thermocouples 2 and 3). Additionally, one thermocouple was placed at the edge of the sample on the higher V_f region (labelled as thermocouple 5). Thermocouples 1 and 4 were positioned approximately 10 mm away from the interface, while thermocouple 5 was positioned approximately 10 mm from the end of the sample (opposite end to the initiation point).
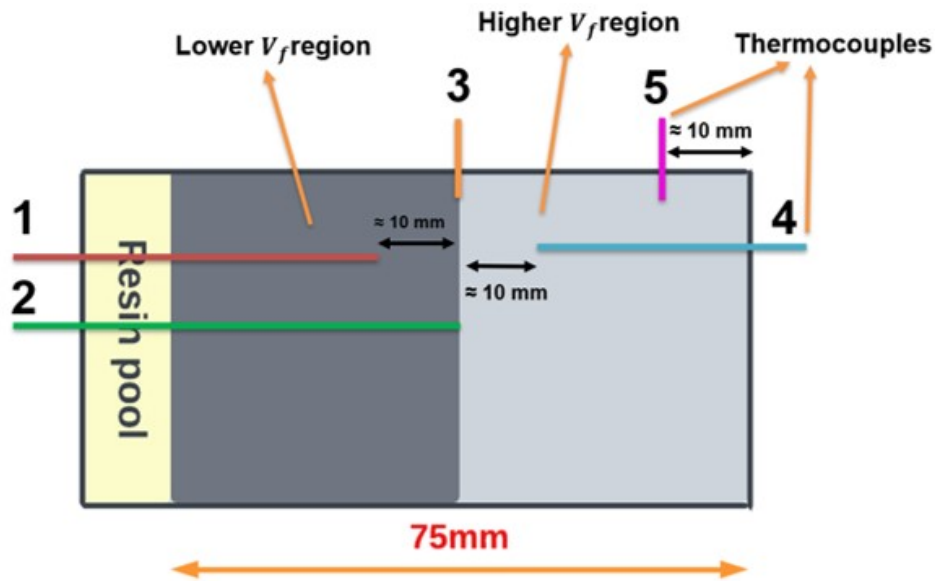
Figure 4.17: Schematic diagram showing Placement of thermocouples during layup of the laminae layer.

After the thermocouple was placed in the layup, their wires were attached to the silicone seal with masking tape. The remaining wires were then threaded through specially made grooves in the stainless steel mould (see Figure 4.18 A). The end plugs of all the thermocouples were connected to the data acquisition machine. The manufacturing process continued with the layup of the remaining layers, followed by degassing of the layup in the degassing chamber. Great Care was taken while moving the mould setup into the degassing chamber to avoid damaging the thermocouples, which could result in inaccurate temperature data readings(see Figure 4.18 B). Regular checks were carried out on the responsiveness of the thermocouples during the various steps of the manufacturing process to ensure they functioned correctly.
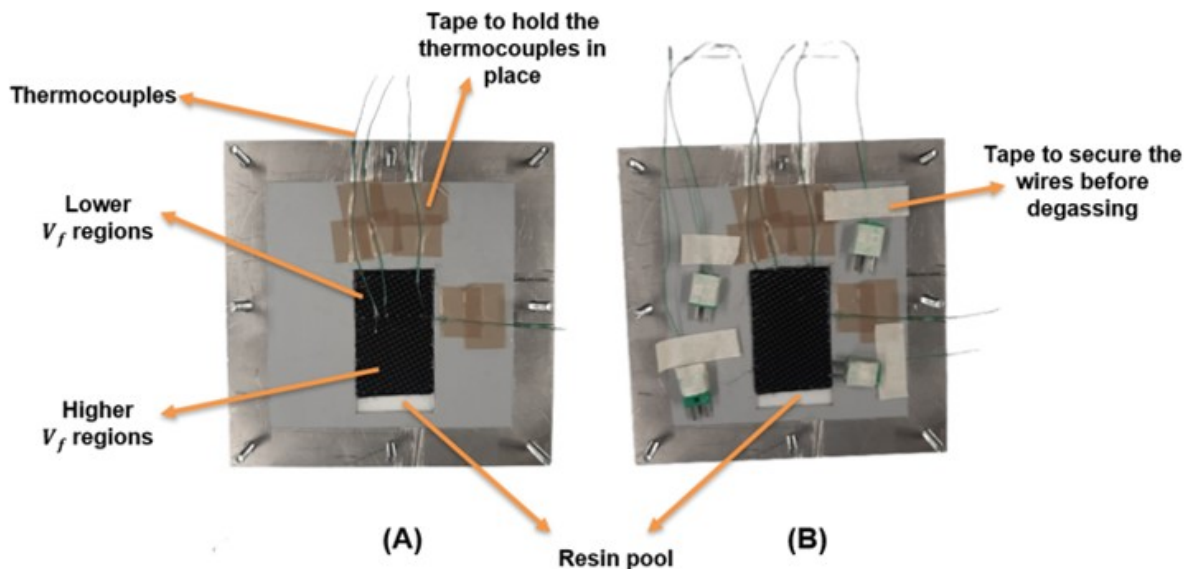
Figure 4.18: Incorporation of thermocouples into the layup. **A:** Addition of thermocouples. **B:** Sticking the end plugs to the mould before lowering the mould into the degassing chamber.

4.6. Geometrical Influences

In order to demonstrate the feasibility of manufacturing composite samples with irregular geometries cured via FP, a simple yet effective shape needed to be selected. The shape of the composite sample had to be the one that could be manufactured using the closed mould test setup used to manufacture simple flat rectangular samples, as demonstrated in section 4.3. This basic criterion narrowed down the pool of available geometries to simple in-plane shapes. Hence, the in-plane "L" shape was chosen for these experiments as it offered the possibility of FP-based curing (front initiation and propagation).

This "L" shape allowed for a natural progression from the straight rectangular samples and was a more reasonable choice in terms of the increase in manufacturing complexity compared to some of the other possible shapes, such as the in-plane "T" or "S" shaped geometries. Additionally, the L-shaped fabric layers with sharp $90°$ bends would be easier to cut via the Gerber cutting machine. Moreover, the hand-layup process would remain exactly the same as the one followed to manufacture flat rectangular samples.

The manufacturing of the "L" shaped composite samples began with casting a silicone seal to create the required cavity. A symmetric "L" shape with both arms of equal length was chosen, as shown in Figure 4.19. The length of the longer arm and the shorter arms was $80mm$ and $40mm$, respectively, with both arms having a width of $40mm$ each.

The manufacturing process started by cutting the L-shaped fabric layers to the required dimensions via a Gerber cutting machine. The longer end of the arms of "L" shaped fabrics had a length of 65 and 75 mm, respectively, while the shorter end of the arms had a length of 30 and 40 mm, respectively. The width of both arms was $35mm$ each. The arms towards the initiation point were shorter than the arm away from the initiation point, which provided a resin pool for initiation. These dimensions were chosen to ensure the best fit of the individual fabric layers in the silicone cavity while preventing the warping of the fabric layers on the closure of the mould.
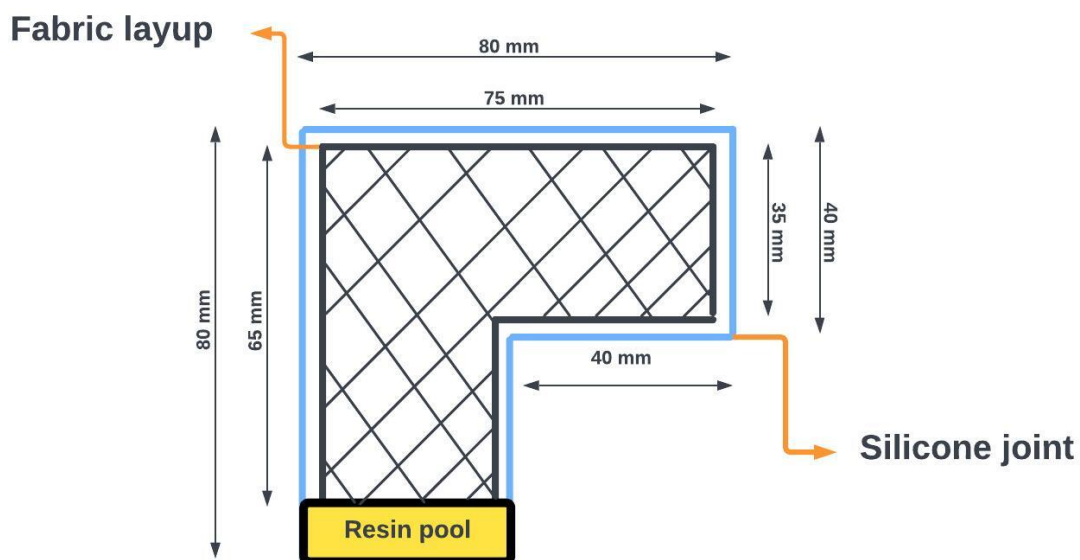
Figure 4.19: Schematic diagram showing the dimensions of the L-shaped cavity and the L-shaped fabric layers

The manufacturing process for the L-shaped composite samples with uniform V_f was exactly similar to that of the regular rectangular samples discussed in section 4.3. The final layup of the L-shaped fabric layers has been shown in Figure 4.20.
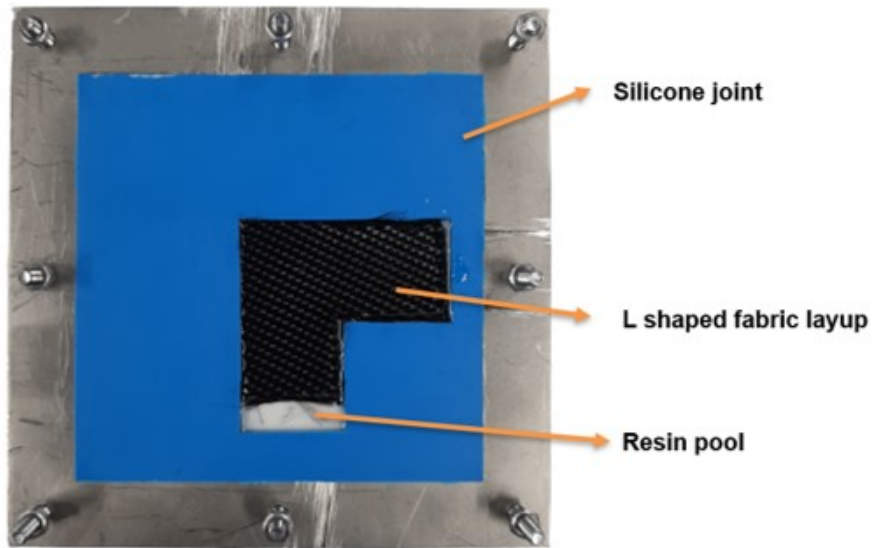
Figure 4.20: Hand layup of L-shaped fabric layup in an L-shaped cavity

4.6.1. Variation of V_f within the Sample

To demonstrate the effectiveness of using FP as a viable curing technique in the manufacturing of composite structures that find everyday applications, samples with varying geometries and varying V_fs within the sample were manufactured. The manufacturing methodology was based on the understanding gained from the previous set of experiments.

After successfully manufacturing an "L" shaped sample with uniform V_f, the decision was made to use this geometry for further trials. The "L" shaped cavity, shown schematically in Figure 4.19, provided a sufficiently large surface area that allowed for flexibility in adjusting the dimensions of the higher and lower V_f region. The manufacturing of the "L" shaped composite samples with varying V_fs followed the same steps as those used for the production of flat rectangular samples with varying V_fs. The blended hand layup method described in section 4.5 was utilized for the creation of the regions with higher and lower V_f.

As shown in Figure 4.21, to increase the V_f of a region and create a higher V_f region of, an additional fabric layer with the necessary dimensions was laid in between the continuous "L" shaped fabric layers. This method offers consistency and flexibility, which allowed for the manufacturing of samples with various dimensions of the lower V_f region. As a result of this flexibility many different samples were manufactured, the results of which have been summarised in chapter 5.
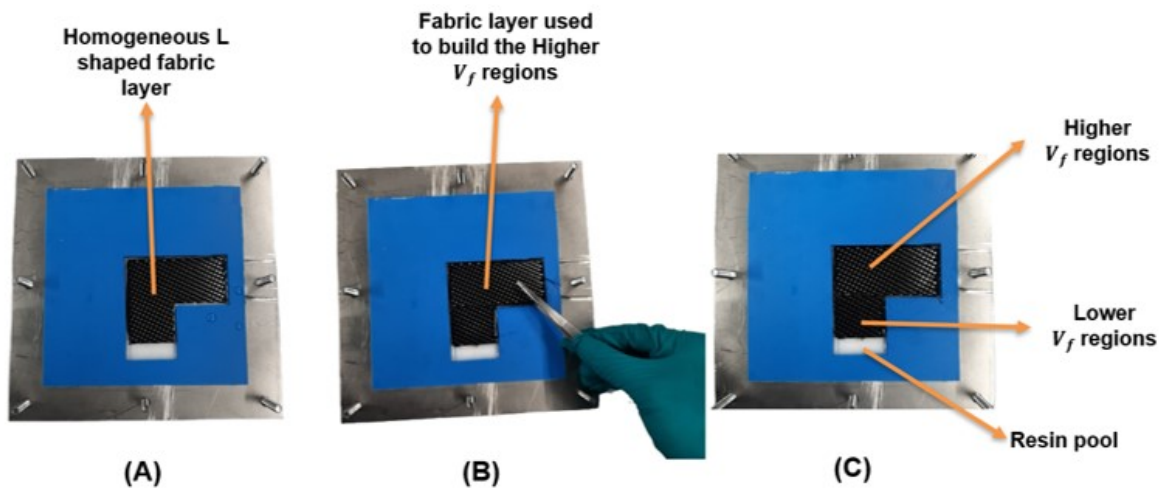
Figure 4.21: Blended hand layup of the fabric layers to create the different V_f regions in an "L" shaped sample. **A:** Layup of the first fabric. **B & C:** Layup of the rectangular fabric between the appropriate continuous "L" layers to create a region of higher V_f.

5

Results & Discussion

The results and observations from the various trials and experiments have been presented in this chapter. An attempt has also been made to explain the various observations by either providing an appropriate hypothesis for the physical observations or by analysis of the collected data.

5.1. FP Formulation Characterization

An example curve obtained from the DSC 250 machine on the characterization of a sample crucible containing 3.1 mg of the FP formulation from a total mixture of $20g$ has been depicted in Figure 5.1.
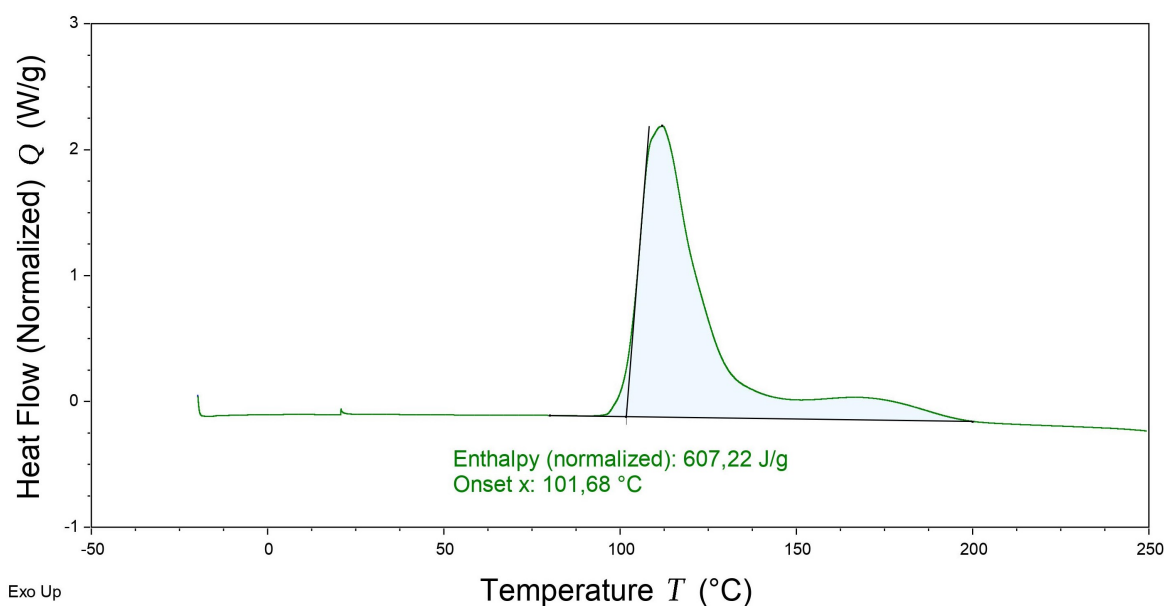
Figure 5.1: Example of a DSC curve obtained through the characterization of a batch of FP formulation

This DSC curve is an appropriate representation of a thermoset resin, with its large peaks indicating the exothermic energy released during the conversion of the monomer into a polymer. The area under the curve is a measure of the enthalpy of polymerization for the solution mixture. The area under the curve, measured between a temperature range of 80 to 200 $^\circ$ C, was taken as the enthalpy of the solution mixture. This span represents the temperature range where the cross-linking reaction occurs and is evident due to the release of exothermic heat, which can be used for FP. Additionally, another parameter of importance is the onset temperature, which is the temperature at which the cross-linking reaction starts. The onset temperature experimentally describes the minimum temperature required to cleave a sufficient amount of RTI and initiate the RICFP process [39]. This implies that the RICFP

38

process can be initiated by external heat when it is above the onset temperature of polymerization ($\gg100°$C). In practice, this corresponds to the temperature of the soldering iron used to provide the initial heat input to initiate the front.

The DSC curves of the earliest batch of FP formulations, which were mixed in small quantities of 20 g each, are depicted in Figure 5.2. These DSC measurements showed significant variations in the values of enthalpy of polymerization.
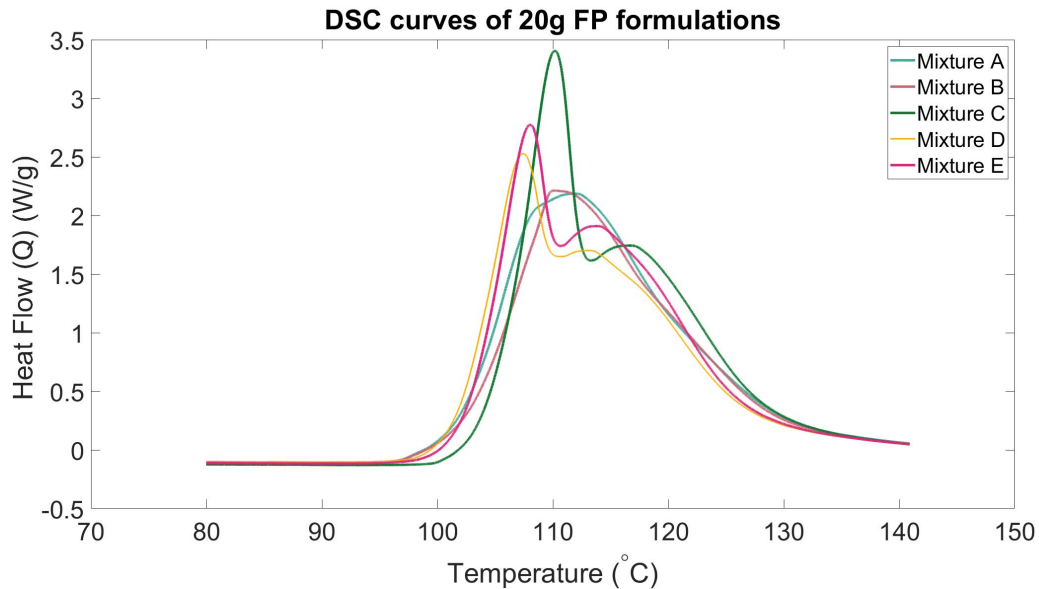
Figure 5.2: Magnified view of DSC curves of the various 20g FP formulation

Table 5.1 presents the corresponding values of the enthalpy of polymerization and onset temperatures for the five separate mixtures. The 20 g mixtures have a mean enthalpy of polymerization of 598.2 $\pm$ 20.5 J/g. At this stage of the experimental trials, the DSC measurements suggested that the mixing procedure was independent of the accessories associated with mixing the formulation, such as the beaker used and the individual time allotted to mix both the benzopinacol and ITX Photosensitizer combination and the photoinitiator IOC-8 SbF$_6$.

Table 5.1: The enthalpy of polymerization and the onset temperatures for the five 20g FP formulations.

Batch Name	Enthalpy(J/g)	Onset Temperature ($°$ C)
Mixture A	607.22	101.68
Mixture B	575.38	102,15
Mixture C	626.16	104.83
Mixture D	573.55	101.73
Mixture E	608.69	102.59

As the need for resin in the experiments increased, larger quantities of resin ranging from 40g to 80g were subsequently mixed. A scatter plot was created to compare the enthalpy values of all the separate batches of 20g, 40g, 60g, and 80g (see Figure 5.3). The weight of the formulations is assumed as the independent variable (x-axis) and the enthalpy of polymerization as the dependent variable (y-axis). The random scatter of the data suggests that there is no evident correlation between the two variables. The large scatter of data is attributed to errors in the mixing process, including inconsistencies caused by the choice of the beaker and the stirring magnet. Inappropriate combinations of the beaker and mixing magnet resulted in the incoherent mixing of the components with the resin.

These observations have also highlighted the influence of shear rates on the quality of the mixtures. Batches that were mixed at shear rates lower than 300 rpm, coupled with inconsistencies in the apparatus, yielded low enthalpy values. Conversely, batches that were mixed at shear rates higher than
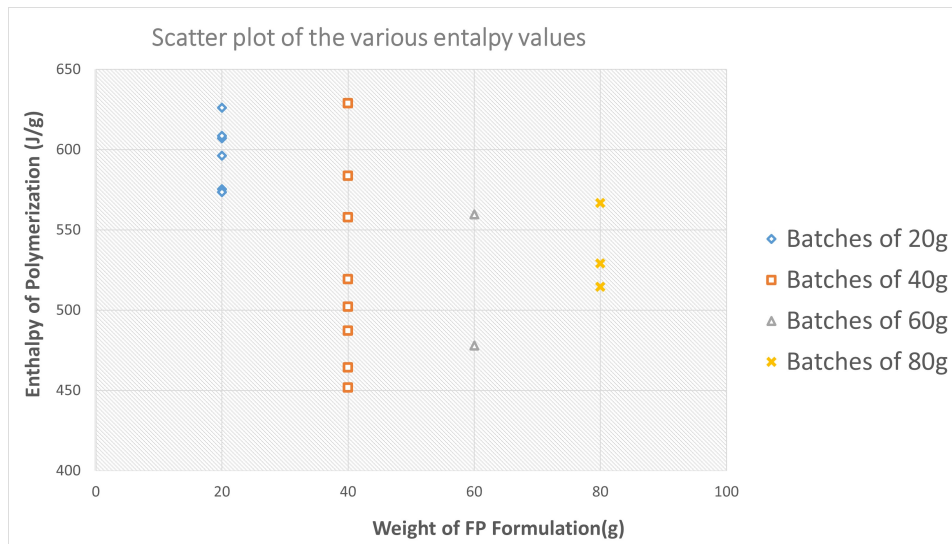
Figure 5.3: Variation of enthalpy of different batches of FP formulation

400 rpm, with some consistency in apparatus, showed high values of enthalpy. This observation was strongly supported by the $20g$ and a few $40g$ mixtures, with all these batches having an enthalpy value greater than 550 J/g. As a result of these observations, standardization of the mixing process as described in section 4.1 was carried out.

The DSC plots in Figure 5.4 show the results of the first five batches of $80g$ FP formulation mixed with the standardized approach. These steps have significantly improved the mix quality, resulting in a mean enthalpy value of 621.46 $\pm$ 13.72 J/g. The higher enthalpy values observed were attributed to the use of UViCure S105 as the epoxy resin. The lower deviation in enthalpy values indicates improved accuracy in the mixing process after standardization. However, the remaining deviation observed was attributed to differences in monomer conversion percentages among the different batches of mixtures.
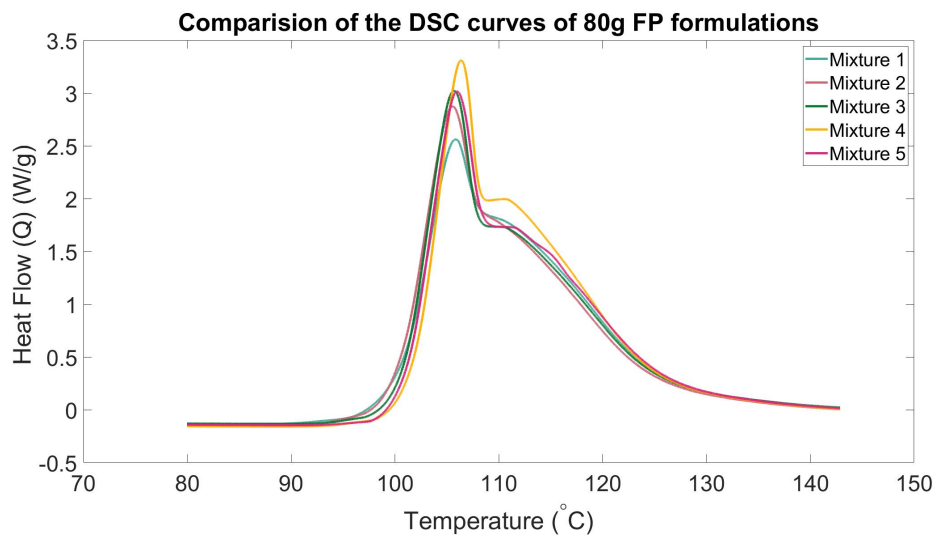
Figure 5.4: Comparison of the first five $80g$ batches made with standardized mixing process.

Table 5.2: The enthalpy of polymerization and the onset temperatures for the first five $80g$ FP formulations, mixed after standardization.

Batch Name	Enthalpy (J/g)	Onset Temperature ($^\circ$ C)
Mixture 1	609.04	100.22
Mixture 2	622.01	99.98
Mixture 3	610.48	100.44
Mixture 4	647.12	101.52
Mixture 5	618.65	100.74

5.2. Composite Samples

As described in section 4.3, the demonstration of the feasibility of manufacturing composite samples was performed under three separate categories of trials, with each category based on the type of mould setup utilized. The progressive results of each of these trial categories are as follows:

5.2.1. Open Mould Test Setup

The samples manufactured in an open mould test setup demonstrated the feasibility of manufacturing composites cured via FP. In the earliest stages of this set of experiments, samples were manufactured to gain an intuitive cognizance of the resin saturation levels, required to achieve samples of reasonable quality.

(a) Sample 1 shows the degradation and unevenness of the top surface.

(b) Sample 2 shows the unevenness of the top surface.
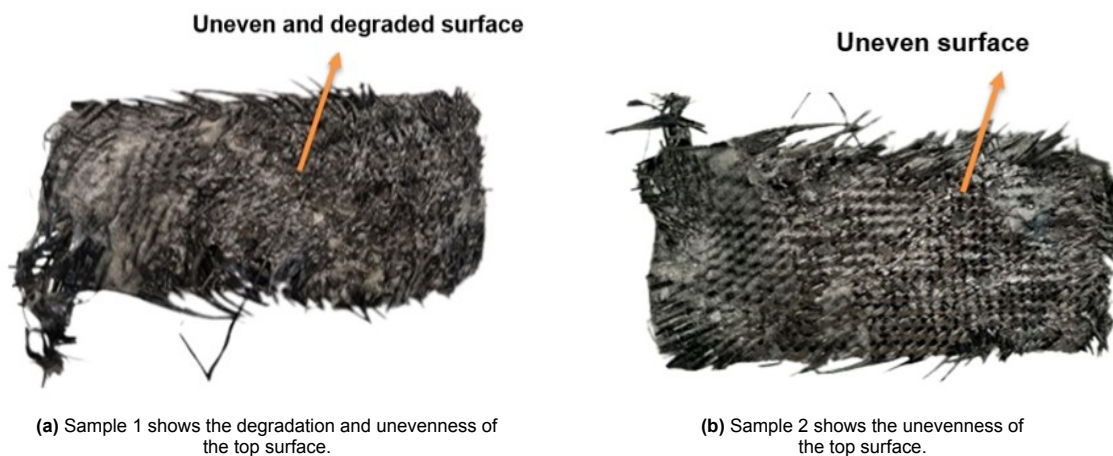
Figure 5.5: Samples manufactured in an open mould test setup

The samples presented in Figure 5.5 exhibited several observations. Firstly, it was noted that upon initiation, the front did not propagate throughout the entire surface area of the sample. Multiple initiations were required across the surface area of the sample to completely cure the composite. Additionally, the soldering iron had to be held constantly over the surface of the fabric to continuously supply heat energy to sustain the front. Two separate causes were identified for these observations: incomplete saturation of resin in the fabric layers and disruption of the thermal equilibrium due to heat loss to the surroundings. The two causes were observed to be complementary, implying that in an open mould test setup, incomplete resin saturation of the layup would lead to a system with insufficient resin. This insufficiency of the resin in the layup would then lead to a level of heat generation which could not sustain the front. As the disruption of the heat balance required to maintain the front would occur due to the loss of heat to the surroundings and the uptake of heat by the carbon fiber. The samples produced during this stage had poor quality, with the surface of all the samples being uneven and apparent degradation of the top surface due to the fabric layer sticking to the soldering iron as a result of the curing of the FP formulation in the vicinity. Therefore, an auxiliary initiation resin pool was introduced to one end of the

sample in the later set of experiments.

(a) Sample with initiation pool along the width (Top surface)   **(b)** Sample with initiation pool along the width (bottom surface)
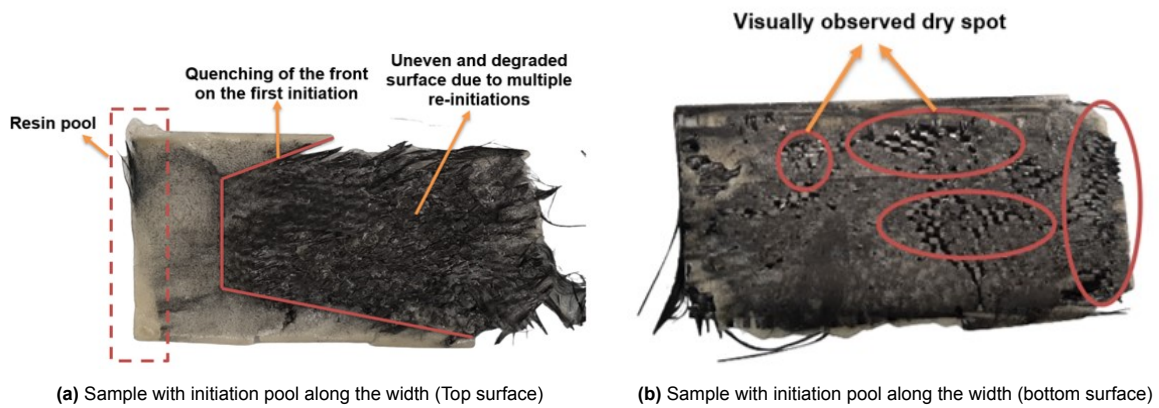
Figure 5.6: Samples manufactured in an open mould test setup

As shown in Figure 5.6a, the initiation resin pool was introduced along the width of the fabric by cutting it shorter than the cavity dimensions by a length of 0.5 cm. On initiation, the front would first travel along the pool before propagating over to the layup. It was observed that if the adjacent layup was adequately saturated, the front would propagate a certain distance before quenching. Conversely, if the saturation was inadequate, the front would only propagate along the pool without running over into the fabric layup. Similar to the earlier set of samples, the remaining sample area was cured via multiple re-initiations. Additionally, dry spots were visually observed on the bottom surface of the sample, indicating incomplete saturation. The outcome of manufacturing these samples was that a setup with the ability to maintain thermal heat equilibrium is necessary to manufacture samples cured via FP. If such a system can be complemented by (1) a layup with sufficient resin saturation and (2) a resin pool for the initiation of the front, it may be possible to manufacture samples of repeatable quality.

5.2.2. Teflon Covered Silicone Mould

The second set of experiments was designed and performed as a follow-up to the results of the previous experiments. This set of experiments had four notable changes: Firstly, a $3mm$ Teflon plate was used instead of the silicone mould to limit the loss of heat to the surroundings due to its low thermal conductivity of $0.3W/mk$ [55]. Secondly, weights were used to ensure uniform thickness of the laminate. Thirdly, an initiation resin pool was created to facilitate ease of manufacturing. Lastly, substantial resin was used to ensure high levels of saturation. Additionally, attempts were made to achieve the highest possible volume fraction (V_f) of the samples, with values ranging from 20% to 40% being tested.

The first phase of this experimental set saw the manufacturing of samples with V_fs greater than 30%. The number of layers and the corresponding V_fs were calculated using Equation 4.1. The summary of a few samples manufactured has been presented in Table 5.3.

Table 5.3: Samples with V_f greater than 30%.

Sample number	Sample dimensions (mm)(l×b)	Average height of the cavity (mm)	Number of layers(n)	Theoretical V_f (%)(V_{f_t})	Average thickness of the cured sample (mm)
1	50×47	4.85±0.39	12	38.59	5.99±0.81
2	40×45	4.85±0.39	10	32.16	6.08±0.40
3	50×45	4.66±0.24	10	33.50	5.37±0.64
4	50×45	4.66±0.24	9	30.15	5.35±0.42

In the earliest stages of these experiments, it was observed that when the theoretical volume fraction (V_{f_t}) of the layup was greater than 30%, the front would propagate through the resin pool but not into the layup. To continue the propagation of the front, the weights and Teflon sheet were removed, and the hot soldering iron was pressed into the fabric layup. The front was then noted to travel throughout the sample area. The inability of the front to propagate through the layup on the first initiation could be due to the disruption of the heat balance caused by excessive heat uptake at these high V_f values. Additionally, front propagation was accompanied by bubble formation. In this context, the high exothermic heat released during FP leads to the decomposition of either the monomer or the initiators, generating low vapour pressure byproducts. The evaporation or boiling of these small molecules physically manifests as bubbles in the reacted formulation. As the front progresses through the laminate area, it carries the formed bubbles along with it. Upon reaching the edge of the sample, the natural outlet for these bubbles in the absence of a compaction system (Teflon sheet pressed down by weights) is to escape beyond the perimeter of the samples/cavity. Upon observing Figure 5.7a, it is evident that the top surface of the samples was uneven. Similar to the first set of experiments, these surface irregularities were caused by the contact between the soldering iron and the fabric. The act of pressing the hot soldering iron on the layup caused localized upward movement of the front towards the soldering iron. This resulted in uneven distribution of resin which, upon curing, led to the formation of irregularities on the surface. Furthermore, during the examination of the same samples (as shown in Figure 5.7b), dry spots were visually observed. This was attributed to incomplete resin saturation of the fabric layup.

Throughout the subset of these experiments, both the test apparatus and the manufacturing process were also modified. Table 5.3 illustrates samples that were manufactured using silicone joints of varying average thicknesses. Sample 1 and 2 (from Table 5.3) were made using a silicone joint that had patterned surface undulations. These irregularities caused the Teflon sheet to not be in perfect contact with the layup, resulting in inconsistencies in the repeatability of the manufacturing steps and sample quality. In contrast, sample 3 and 4 (from Table 5.3) were manufactured in a new silicone mould that was cast in such a way that the Teflon sheet, along with the placement of weights, led to improved surface compaction. Furthermore, modifications were made to the sample dimensions. The sample width was varied to ensure that the fabric on the sides fit snugly into the cavity without curling upwards against the mould walls. As a result, the sample width was reduced from $47mm$, used for manufacturing sample 1, to $45mm$ for the remaining samples.

(a) Sample showing the unevenness of the surface caused due to multiple re-initiations (top side)

(b) Sample showing a visually observable dry spot (bottom side)
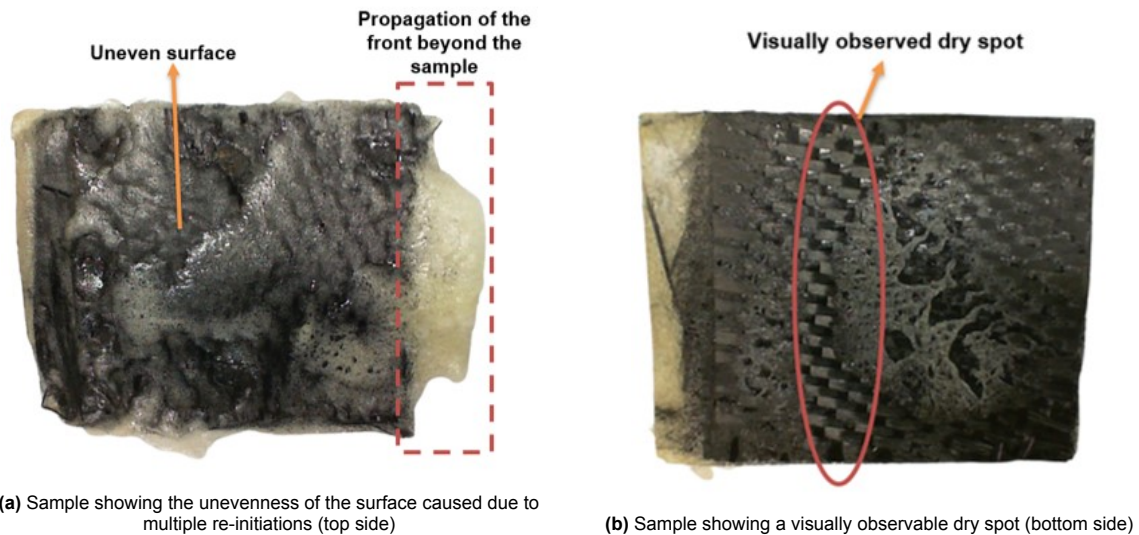
Figure 5.7: Samples manufactured in an open mould with a Teflon cover

The length of the initiation resin pool was also modified to determine the required dimensions for the successful initiation of the front. It was determined that an initiation pool with a length of $1cm$ was sufficient for successful propagation of the front.

Table 5.4: Samples with V_f less than 30%.

Sample number	Sample dimensions (mm)(l×b)	Average height of the cavity (mm)	Number of layers(n)	Theoretical V_f (%)(V_{f_t})	Average thickness of the cured sample (mm)
1	50 × 45	4.66±0.24	7	23.51±1.21	4.49±0.36
2	50 × 45	4.66±0.24	8	26.87±1.39	4.23±0.11
3	50 × 45	3.17±0.08	6	29.53±0.78	3.90±0.11

Table 5.4 presents a few manufactured samples with V_{f_t}s less than 30%. Unlike the previous samples, these samples cured completely with just the initiation of the resin pool. This meant that when the front was initiated at the resin pool, it would seamlessly propagate across the layup.

(a) Sample with a smooth surface

(b) Sample showing surface unevenness.
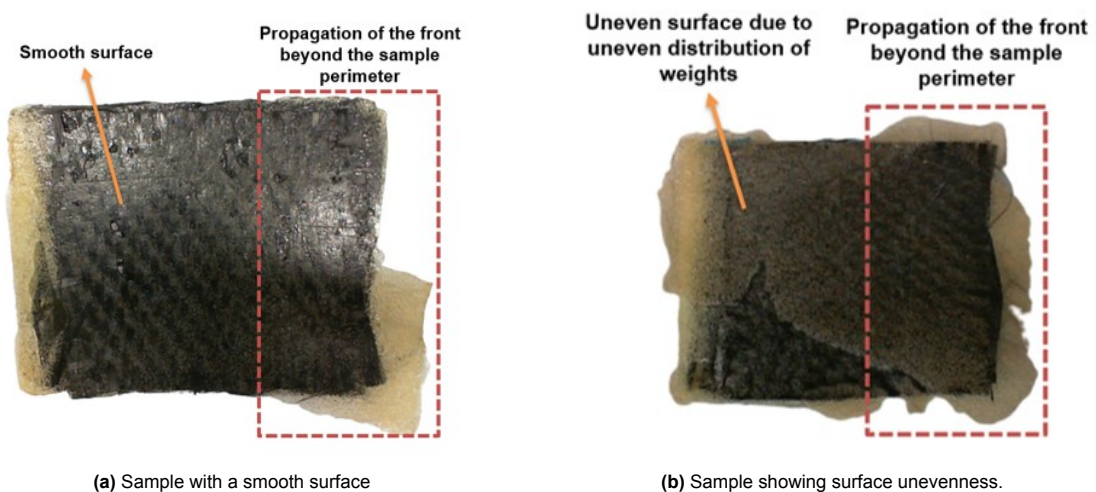
Figure 5.8: Samples manufactured in an open mould with a Teflon cover

The quality of the samples varied significantly, with some having smooth, uniform surfaces and oth-

ers riddled with undulated surfaces. Figure 5.8b serve as the best examples of the observed surface irregularities. These irregularities were attributed to the unequal distribution of weight across the surface area of the sample, which led to an uneven distribution of resin on the top surface. When the resin cured, it resulted in these surface irregularities. Despite being subjected to a Teflon plate pressed down by weights, some bubbles were able to escape beyond the perimeter of the sample, suggesting that the compaction provided by the Teflon plate setup was insufficient to physically collapse all the bubbles. Dry spots were visually observed in a few samples due to incomplete saturation, which was resolved by ensuring that adequate resin was used at every layer. In addition, a new silicone mould was utilized to manufacture samples at the later end of the experimental regime, like sample 3 in Table 5.4. This silicone mould was manufactured to remove the inconsistency in the manufacturing process arising from the undulations found on the walls of the cavity. The removal of undulations on both the top and interior cavity surfaces of the silicone mould allowed for a higher degree of repeatability in the sample manufacturing process.

The inability to cure composite samples with V_{f_t} larger than 30% was largely attributed to two factors: (1) the imbalance in the thermal equilibrium (heat generation - diffusion equilibrium) and (2) inconsistencies in the manufacturing test apparatus. At these high V_f values, not enough FP formulation was present in the system to ensure that the thermal equilibrium was in favour of FP. This was despite the large negation of the effects of heat loss to the surroundings due to the presence of the Teflon cover and high levels of resin saturation across the layup. Moreover, the poor quality of the test setup surely contributed to uncertainties in the manufacturing process, thereby reducing the highest achievable V_f.

5.2.3. Closed Mould Test Setup

The design of the closed mould test setup used to manufacture composites cured via FP was based on the outcomes of the previous set of experiments. The objective of the closed mould test setup was twofold: (1) to achieve high levels of repeatability in the manufacturing process by reducing the inconsistencies arising from the poor quality of the test setup, and (2) to improve the overall quality of the samples. To achieve these objectives, a closed mould test setup comprising components with good dimensional tolerances was conceptualized. The final manufactured closed mould was presented in section 4.3.

Table 5.5: Samples manufactured with the prototype mould setup

Sample number	Sample dimensions (l × b) (mm)	Average height of the silicone cavity (mm)	Number Of Layers (n)	Theoretical V_f (%)	Average thickness of the cured sample (mm)	Actual V_f (%)
1	50 × 45	5.86±0.17	8	21.30±0.63	6.27±0.39	19.99±1.28
2	50 × 45	5.86±0.17	10	26.62±0.79	6.24±0.30	25.08±1.25
3	50 × 45	5.86±0.17	12	31.95±0.95	6.01±0.24	31.22±1.31
4	50 × 45	5.86±0.17	14	37.25±1.13	6.18±0.20	35.43±1.24
5	50 × 45	5.86±0.17	15	39.94±1.19	6.04±0.31	38.84±2.03

The summary of a few cured samples, manufactured with the prototype mould, has been presented in Table 5.5. This prototype test setup allowed for a high degree of repeatability, with samples ranging from a V_{f_t} of 21 to 39 % successfully manufactured. However, the repeatability was much higher for samples with 12 fabric layers or less, while curing samples with 13 fabric layers or more was rare. Additionally, the average percentage error between the actual and theoretical V_fs from all the manufactured samples was estimated to be around 4.5%. This variation in V_f was directly correlated with the higher average thickness values of the cured samples, indicating insufficient compaction of the layup. This lack of compaction was attributed to two reasons: (1) the low stiffness provided by the aluminium cover plates and the 3D printed frame, and (2) the variation of thickness across the silicone cavity. At this stage of the experimental trials, the reasons for the variation in the thickness of the cavity in the silicone joint had yet to be identified.

(a) sample 1,n:8,V_{f_t}:21.28%,V_{f_a}:19.92%   (b) sample 4 ,n:14,V_{f_t}:37.25%,V_{f_a}:35.39%
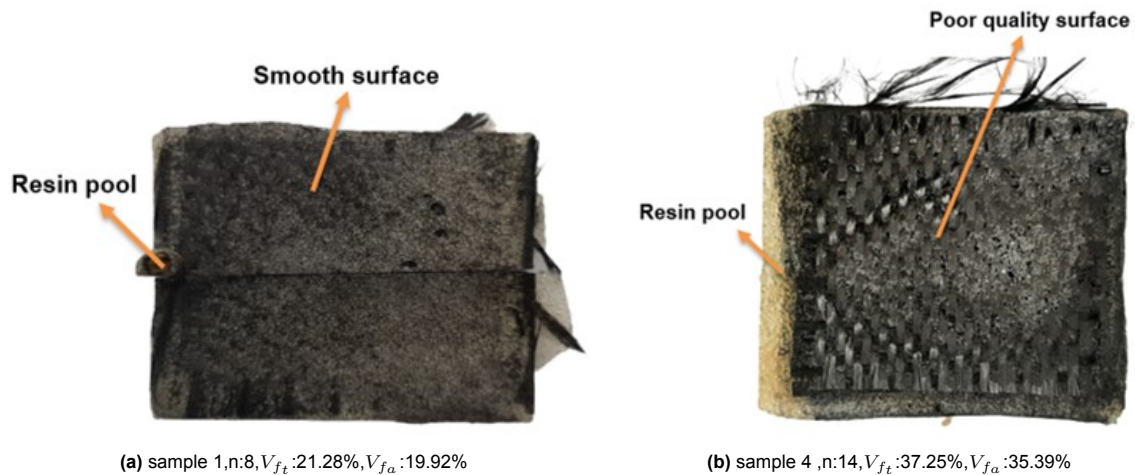
Figure 5.9: Samples manufactured in a prototype closed mould test setup

As shown in Figure 5.9a, samples with V_f values below 30% exhibited visibly improved surface quality after curing. This improvement in surface quality was attributed to changes in the hand layup method, which involved filling the cavity with a large amount of resin followed by laying up the fabric layers assisted by capillary wetting. The test setup provided sufficient compaction, preventing the propagation of bubbles through the front and allowing the cured resin to remain within the cavity boundaries. In contrast, samples with V_{f_t} greater than 35% showed low repeatability, with only a few samples curing successfully. Moreover, even the samples that did cure exhibited poor surface finish, despite consistent manufacturing steps (see Figure 5.9b). This poor surface quality was likely caused by the easy escape of resin during compaction, particularly from the top surface of the laminate, due to the non-wettability of the Teflon covers. This resin escape, along with the imbalance of thermal equilibrium resulting from the higher rate of heat loss, was speculated to be among the causes of low manufacturing repeatability.

At high V_fs, the heat generated during curing is often drawn away by the fibres, leaving insufficient heat for the reaction of the monomers and resulting in the quenching of the curing front. The heat drawn away from the front can be dissipated through two channels: (1) preheating of the monomers further away from the front or (2) transfer of heat to the mould components. If the rate of heat generation is much larger than the rate of heat diffusion, then the heat drawn away for preheating could aid the movement of the front. However, when the difference in these rates is minuscule or in equilibrium, the transfer of heat will lead to frontal quenching. Similarly, the rate of heat loss to the mould components must also be in favour of equilibrium to avoid frontal quenching.

Furthermore, these samples exhibited the formation of "race tracking fronts", which resulted from the narrower widths of the fabric layers chosen to ensure the best fit within the cavity (See Figure 5.10a). These narrower fabric layers led to the formation of small channels filled with resin along the edges of the laminate. Upon initiation, the front moved directly from the pool through these channels before continuing to propagate into the layup. Additionally, lateral movement of the front upon mould closure was observed (See Figure 5.10b). When the mould was closed, the fabric layup was pushed laterally into the initiation pool. This phenomenon is evident in the cured resin region visible on the other end of the sample, which was caused by the displacement of the resin into the empty space created.

(a) Race tracking front

(b) Cured resin region caused by the lateral movement of the fabric layup.
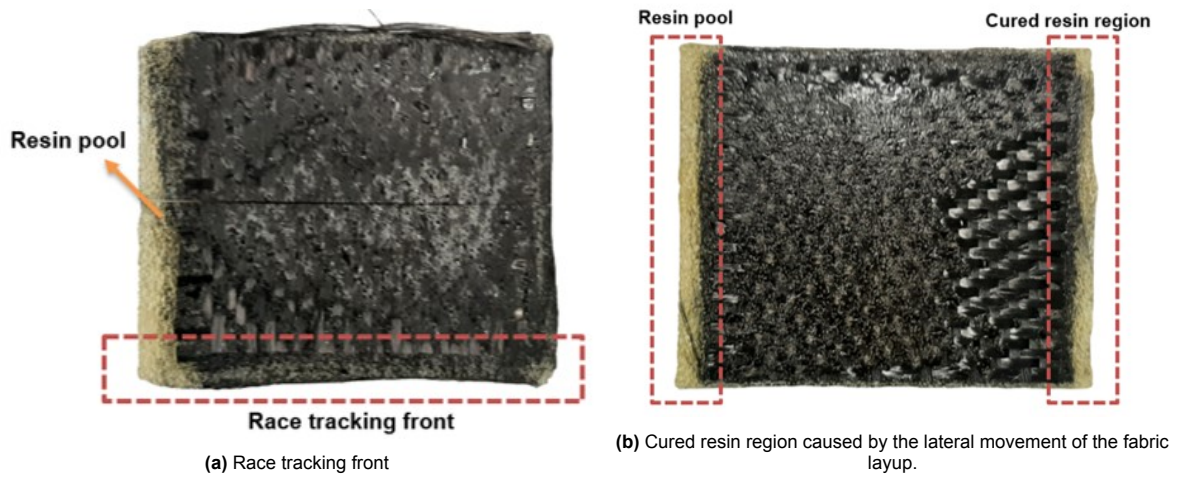
Figure 5.10: Race tracking fronts and lateral movement of fabric layup.

As a result of the findings from these trials, a new mould was fabricated with stainless steel cover plates and frame. The components were made of stainless steel grade 304, which has a maximum service temperature of $924°C$ and a tensile strength of $620 \ MPa$. Several samples successfully manufactured with the new mould have been presented in Table 5.6.

Table 5.6: Samples manufactured with the stainless steel mould setup

Sample number	Sample dimensions (l × b) (mm)	Average height of the silicone cavity (mm)	Number Of Layers (n)	Theoretical V_f (%)	Average thickness of the cured sample (mm)	Actual V_f (%)
6	50 × 45	5.86±0.17	10	26.62±0.79	5.70±0.23	27.09±0.98
7	50 × 45	5.86±0.17	12	31.95±0.95	5.79±0.19	32.37±1.11
8	50 × 45	5.86±0.17	12	31.95±0.95	5.71±0.22	32.82±1.31
9	50 × 45	5.86±0.17	12	31.95±0.95	5.76±0.18	32.54±1.02
10	50 × 45	5.86±0.17	12	31.95±0.95	5.82±0.19	32.09±1.11
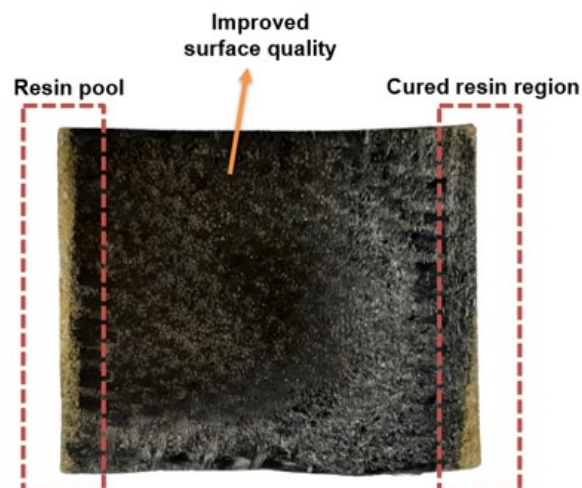
Figure 5.11: Samples manufactured in stainless steel closed mould test setup

As shown in Figure 5.11, the samples manufactured using the stainless steel test setup exhibited better surface quality. The high-stiffness stainless steel mould improved the compaction of the laminates,

resulting in improved manufacturing accuracy. This is evident from the comparison of the thickness of the cavity with that of the manufactured samples. The improved accuracy is also supported by the fact that the average percentage error between the actual and theoretical V_fs from all the manufactured samples was only 1.9%. However, curing was not possible for samples with 13 or more fabric layers due to the disruption of the thermal balance caused by the larger uptake of heat at these V_fs. In contrast, samples with 12 or fewer fabric layers cured successfully, indicating that the required heat balance was maintained to drive the front to complete the curing process. The formation of race-tracking fronts and lateral movement of the layup was also commonly observed.

5.2.4. Role of Silicone Joint

As previously mentioned, one of the factors that affected the uniform compaction of the laminates was the variation in thickness across the silicone joint. The schematic diagram of the silicone joint used in manufacturing the samples, as presented in Table 5.5 and Table 5.6, is shown in Figure 5.12. This silicone joint had an average thickness difference of 0.456 mm from one end to the other. In practical terms, this variation in thickness also resulted in variation in thickness across the sample surface. Table 5.7 presents the variation in thickness across the cured samples, which were manufactured in both the prototype mould and the stainless steel mould..

   From Equation 4.1, we know that V_f is inversely dependent on the thickness of the sample. Hence, a large variation in thickness across the laminate will also translate to a proportional variation of V_f across the length of the sample (see Table 5.7). Such variation in V_f is uncontrolled and not ideal for any practical application. Therefore, a subsequent exercise was conducted to achieve uniformity in thickness across the sample surface.
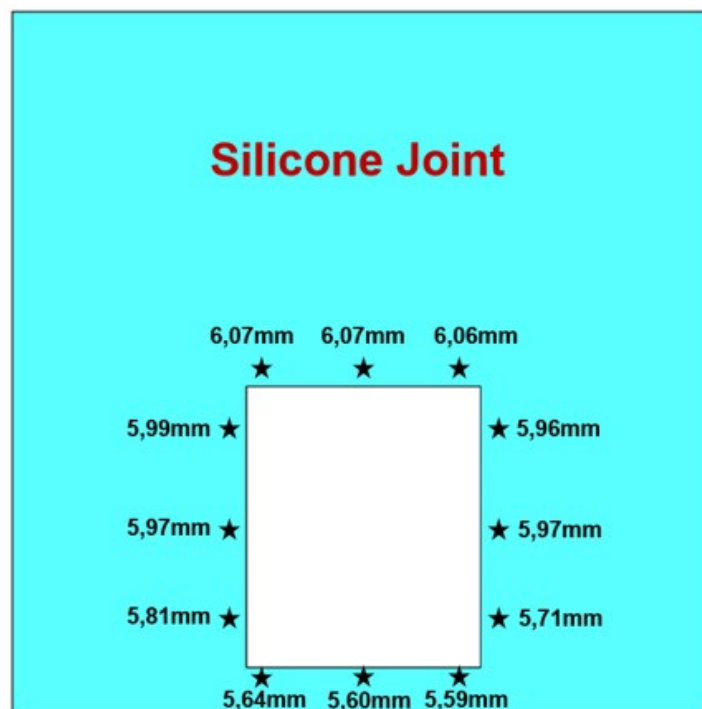
Figure 5.12: The variation of the thickness across the cavity in the silicone mould used to manufacture the samples presented in Table 5.5 and Table 5.6

Table 5.7: The variation of thickness and V_f between the two ends of the cured sample.

Sample number	Mould utilized for manufacturing	Number of layers(n)	Average difference in thickness between the two ends of the cured sample (mm)	Average difference in the V_fs across the two ends of the cured sample (%)
1	Prototype	8	0.99	3.2
2	Prototype	12	0.61	3.4
3	Prototype	14	0.51	2.9
4	Prototype	15	0.76	4.8
5	Stainless steel	10	0.66	3.2
6	Stainless steel	12	0.50	2.9

As thickness variations in the laminates are caused by the silicone joint, it was necessary to examine the manufacturing of these joints. As mentioned in section 4.3, a new silicone joint was manufactured. Despite careful considerations in the manufacturing process, an average thickness difference of 0.33 mm was still observed between the two ends, as seen in Figure 5.13a. Furthermore, the variation of thickness across the length of the representative resin block cast in this new cavity has been shown in Figure 5.13b. It was observed that the variation of thickness across the resin block was unlike the thickness distribution of the silicone joint itself, but the difference between the average thickness of the two ends remained almost the same ($0.32mm$). This difference in thickness could be due to the compaction of the silicone joint on mould closure, leading to variations in sample dimensions.

(a) Silicone joint manufactured without additional clamps

(b) The representative resin blocks cast with the silicone joint shown in Figure 5.13a.
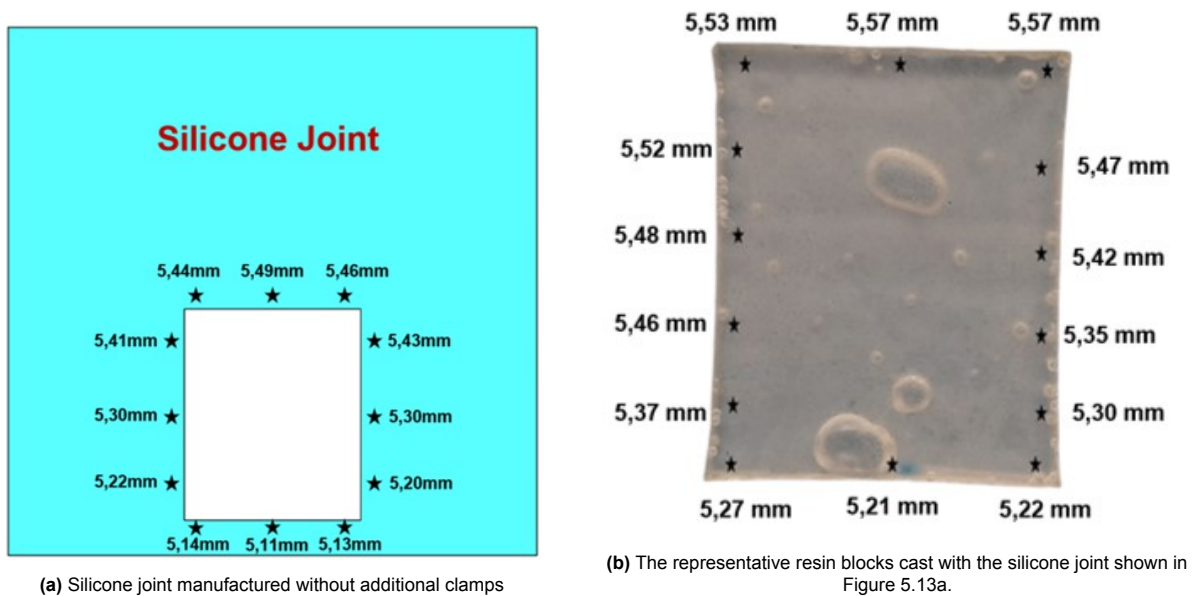
Figure 5.13: The variation of thickness across the silicone joints cast without additional clamps and the corresponding representative room temperature curing epoxy resin block.

On further deliberation, it was assumed that the most probable cause of the thickness variations across the silicone cavity was the buckling effect experienced by the mould plates during the closure of the mould via the tightening of the nuts and bolts. This buckling effect, combined with the fact that the cast cavity was not in the centre of the mould but rather at an offset, could have led to variations in thickness across the length of the cavity. The placement of the cavity was based on the position of the initiation hole, which was at the extreme edge of the mould and was a design choice made to accommodate a variety of experiments.

In order to verify this assumption, a new silicone joint was cast. However, in this instance, additional clamping was introduced to counteract the outward rise of the mould plates. The additional external clamping provided can be seen in Figure 5.14.
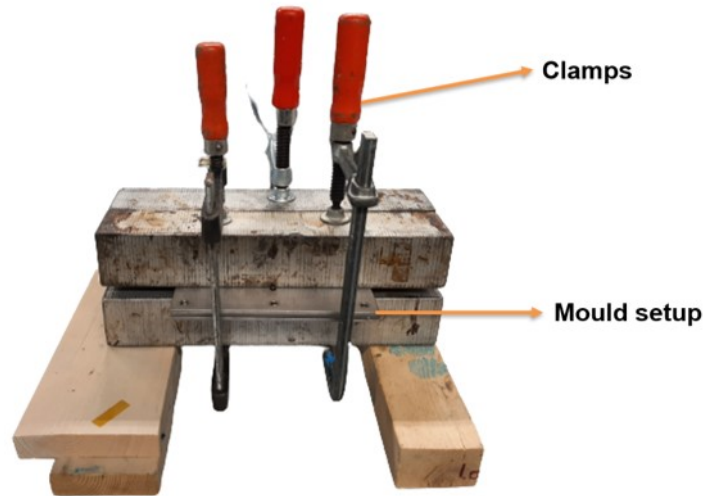
Figure 5.14: The use of external clamps in the manufacturing of silicone joints.

As illustrated in Figure Figure 5.15a, the thickness variation across the silicone mould cavity, which was cast with additional clamps, is displayed. The introduction of external clamps had a notable impact on the thickness distribution, leading to a decrease in the average difference between the two ends to $0.19mm$. This reduced variability in thickness was also observed in the resin block, which was cast using room-temperature epoxy resin. The average thickness difference between the two ends of the resin block was $0.12mm$. As a result of the diminished thickness difference, the new mould has the potential to facilitate the production of samples with increased dimensional accuracy.

(a) Silicone joint manufactured with additional clamps

(b) The representative resin blocks cast with the silicone joint shown in Figure 5.15a.
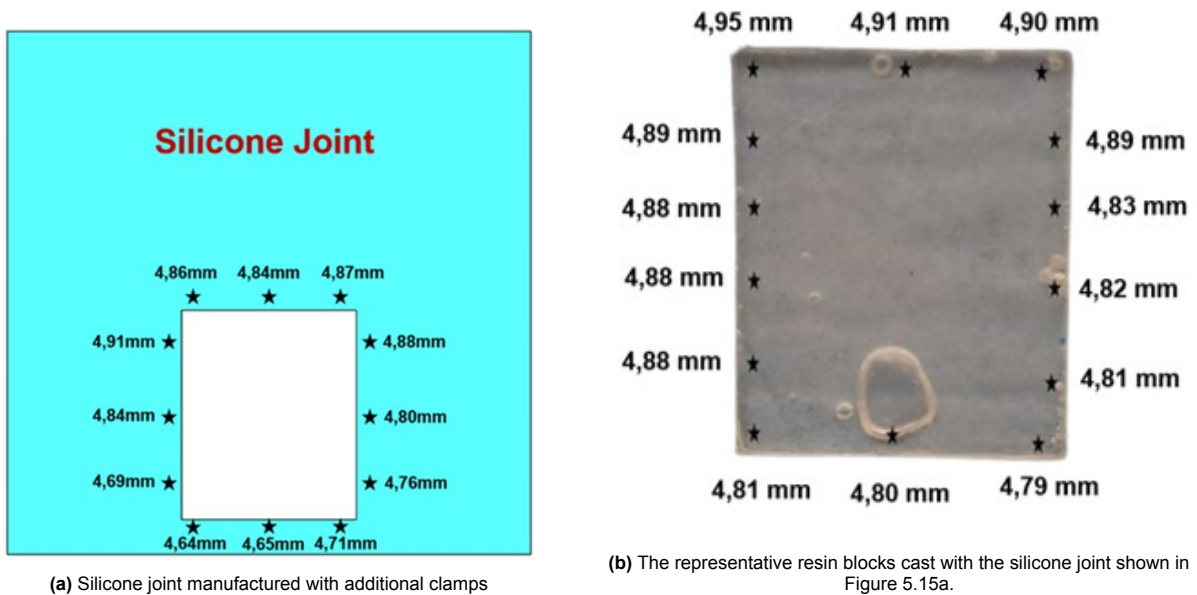
Figure 5.15: The variation of thickness across the silicone joints cast with additional clamps and the corresponding representative room temperature curing epoxy resin block.

Finally, based on these results, a new set of samples were manufactured with the optimized silicone joint. The summary of these samples has been presented in Table 5.8.

Table 5.8: Samples manufactured with the optimized silicone joint

Sample number	Sample dimensions (l × b) (mm)	Average thickness of the silicone cavity (mm)	Number Of Layers (n)	Theoretical V_f (%)	Average thickness of the cured sample (mm)	Actual V_f (%)
1	50 × 45	4.78±0.09	9	29.38 ±0.56	4.76±0.04	29.5±0.26
2	50 × 45	4.78±0.09	10	32.65±0.62	4.81±0.06	32.45±0.46
3	50 × 45	4.78±0.09	11	35.92±0.69	4.75±0.03	36.12±0.25

The difference in the average thickness values and in turn the corresponding V_fs between the two ends of the samples is presented in Table 5.9. The use of an optimized silicone joint in the manufacturing process has resulted in improved accuracy of the samples. This is evident from the reduced difference in average thickness values between the two ends, indicating that the manufacturing process has become more consistent and precise. Moreover, the average percentage error between actual and theoretical V_f values from all the manufactured samples had decreased to 0.5%, further indicating that the samples more closely matched the intended specifications.

Table 5.9: The variation of thickness and V_fs between the two ends of the samples manufactured using the optimized silicone joint.

Sample number	Number of layers(n)	Average difference in thickness between the two ends of the cured sample (mm)	Average difference in the V_f across the two ends of the cured sample (%)
1	9	0.10	0.8
2	10	0.15	1.3
3	11	0.04	0.3

5.2.5. Void Fraction

To evaluate the quality of the samples produced using different mould setups, cross-sections of a few representative samples were observed under a confocal microscope. One representative sample was chosen for each of the different mould test setups, excluding the samples manufactured via the open mould test setup, which were of extremely poor quality. The chosen representative samples had good surface finishes and were among the best samples manufactured from their respective mould test setups.

The cross-sectional images of the various representative samples, captured under the microscope, have been presented in Figure 5.16. Subsequently, these cross-sectional images of the representative samples were analyzed to determine their void contents and fibre volume fractions, using an image segmentation process known as the thresholding process.
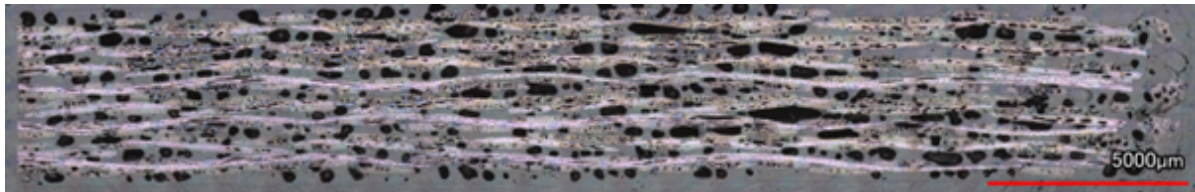
(a) Sample manufactured with a Teflon cover on top.
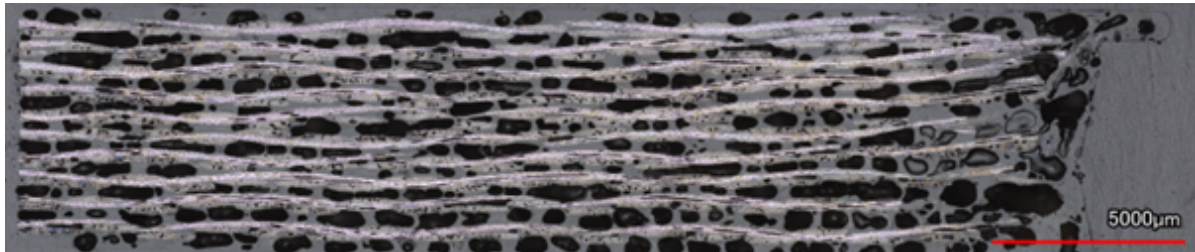
(b) Sample manufactured with the prototype mould
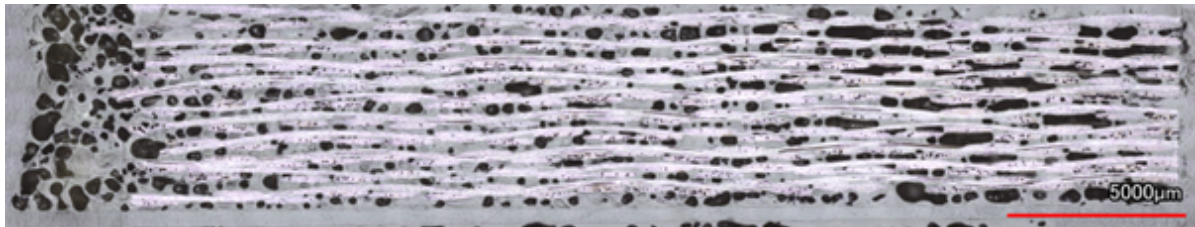
(c) Sample manufactured with a stainless steel mould

Figure 5.16: Representative samples observed under a laser confocal microscope at 10x magnification .

In thresholding, images are converted from grayscale or colour to binary images, which are simply black and white images. This method is used to select the features of interest while disregarding the rest. An example of the conversion of a grayscale image to a binary image has been shown in Figure 5.17. The highlighted features, in this case, the voids, can then be used to calculate their total area fraction with respect to the remaining space in the selected area.

(a) Grayscale image of the sample obtained from the microscope

(b) Selected area of intrest

(c) Thresholding
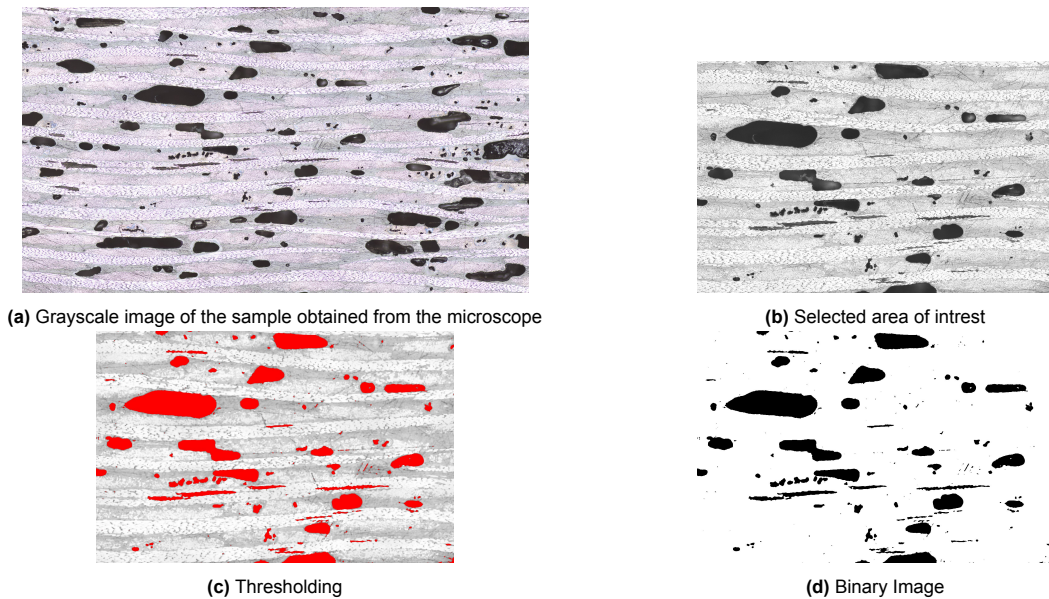
(d) Binary Image

Figure 5.17: Conversion of a grayscale image to a binary image via the thresholding process.

Three distinct samples were analyzed for their void volume fraction (V_v). The first sample was manufactured in an open mould that was covered with a Teflon cover, as shown in Figure 5.16a. The second sample was manufactured with a prototype mould setup that utilized aluminium cover plates and a 3D printed frame, as shown in Figure 5.16b. The third sample was manufactured with a closed mould test setup that was based on stainless steel, as shown in Figure 5.16c. When the void content of the samples with the same number of fabric layers was compared, a significant difference was observed in the void content between the prototype mould and the stainless steel mould. This difference was due to the increased compaction provided by the stainless steel setup, resulting in a reduction of 18.5% in void content for sample 3, as compared to sample 2, which was manufactured in the prototype mould with lower stiffness.

Additionally, the V_f values calculated via the thresholding process was compared to the measured theoretical V_f (V_{f_t}) and actual V_f (V_{f_a}) values. It was observed that the thresholding V_f values were fairly accurate in comparison. However, it is important to consider the thresholding measurements with caution, as they represent only a 2D cross-section of the sample rather than the entire 3D volume.

Table 5.10: The void fraction and the fiber volume fraction measured through the process of thresholding.

Sample number	Number Of Layers (n)	Theoretical V_f (%)	Actual V_f (%)	V_f obtained form thresholding (%)	Void fraction Obtained form thresholding (V_v) (%)
1	8	26.87$\pm$1.39	29.55$\pm$0.78	26.44	24.09
2	10	26.62$\pm$0.79	25.08$\pm$1.25	23.77	34.43
3	10	26.62$\pm$0.79	27.09$\pm$0.98	28.89	28.04

Based on these observations, a simple but effective method was devised to achieve samples with reduced void content. This method assumes that there are two separate sources of void formation in an FP sample: (1) the formation of voids due to the exothermic heat released during the reaction of the FP formulation, and (2) the formation of voids due to manually trapped air in the layup and resin mixture. To effectively control the exothermic heat release, the FP formulation itself would have to be optimized by varying the concentrations of initiators, making it reactive enough for front propagation yet with reduced frothing. However, as varying the initiator concentration to find the optimal values was a time-

consuming process, this method has been omitted from the scope of this thesis. On the other hand, a simple method of manual degassing was utilized to remove the air entrapped in the FP formulation and between the fabric layers. This method of manual degassing has already been described in section 4.3.

To investigate the impact of manual degassing on the reduction of voids, two separate samples were manufactured: one with manual degassing of the layup, and another without degassing. The cross-sections of the samples were observed under a microscope at 10x magnification. Upon analyzing the micrographs for void content using a thresholding process, a significant reduction in void content was observed in the sample manufactured with degassing compared to the one without. The results of the thresholding process are presented in Table 5.11. The void content was found to be reduced by 72.99% in the sample manufactured with degassing. The measured volume fractions (V_f) of both samples were in the vicinity of their respective V_{f_t} and V_{f_a} values. However, the accuracy of these values may be limited by the nature of the thresholding measurement process.

Table 5.11: Comparison of the void fraction in samples manufactured before and after degassing

Sample number	Number Of Layers (n)	Theoretical V_f (%)	Actual V_f (%)	V_f obtained form thresholding (%)	Void fraction Obtained form thresholding (V_v) (%)
1	12	31.95±0.95	32.09±1.11	34.86	14.33
2	12	31.95±0.95	32.54±1.02	31.41	3.87
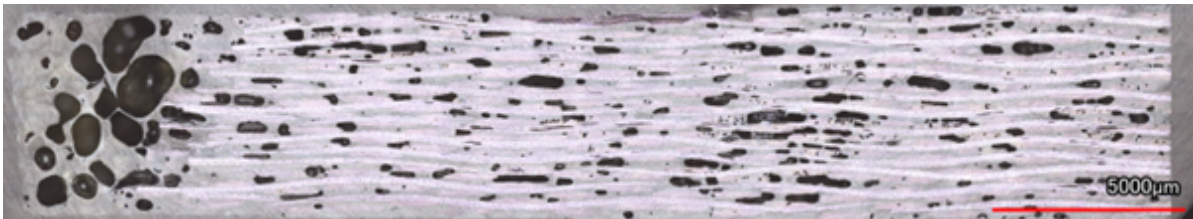
(a) Non degassed sample (sample 1 from Table 5.11)
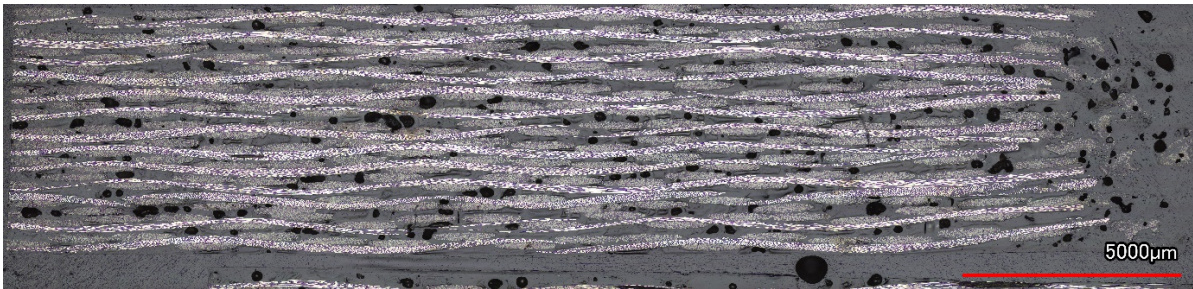
(b) Degassed sample(sample 2 from Table 5.11)

Figure 5.18: Microscope images of samples manufactured with and without degassing.

5.3. Samples with Varied Fiber Volume Fraction

To investigate the influence of varying V_f within the sample on the movement of the front through the sample, a systematic case study was conducted. As described in section 4.5, the entire surface area of the sample was divided into two separate regions with higher and lower V_f. The number of fabric layers in each region was chosen based on prior experience gained through the manufacturing of composite samples with constant V_f. The rationale for this choice was based on the assumption that the front would initiate from the resin pool and propagate to the lower V_f region. Once the front reached the higher V_f region, its temperature should still be sufficiently high to maintain the thermal heat balance necessary to sustain the front.

To test this conjecture, two sets of three samples each were manufactured. The first set of samples had equal lengths of the higher and lower V_f regions. The test results have been summarized in Table 5.12. To avoid the formation of race-tracking channels, which were discussed in subsection 5.2.3, the width of the fabric layers was chosen to be $49mm$.

Table 5.12: Samples manufactured as a part of a case study to understand the influence of varying V_fs on the propagation of the front.

Sample number	Dimensions of the 11 layer fabric (l×b)(mm)	Dimensions of the 13 layer fabric (l×b)(mm)	Average front propagation distance in the lower V_f region (mm)	Average front propagation distance in the higher V_f region (mm)
1	40×49	40×49	40	16
2	40×49	40×49	0	0
3	40×49	40×49	30	0
4	50×49	30×49	0	0
5	50×49	30×49	50	30
6	50×49	30×49	50	30

As shown in Figure 5.19, the samples manufactured with equal lengths of lower and higher V_f region showed rather inconsistent results. For instance, in the case of sample 1, the front reached the interface between the two regions and then propagated a certain distance into the higher V_f region before quenching. On the other hand, in sample 3 the front only moved a distance of 30 mm along the layup without reaching the interface between the two regions. The third sample (i.e., sample 2 from Table 5.12) in this set failed, with only the initiation pool completely curing.

(a) Sample 1 from Table 5.12   (b) Sample 3 from Table 5.12
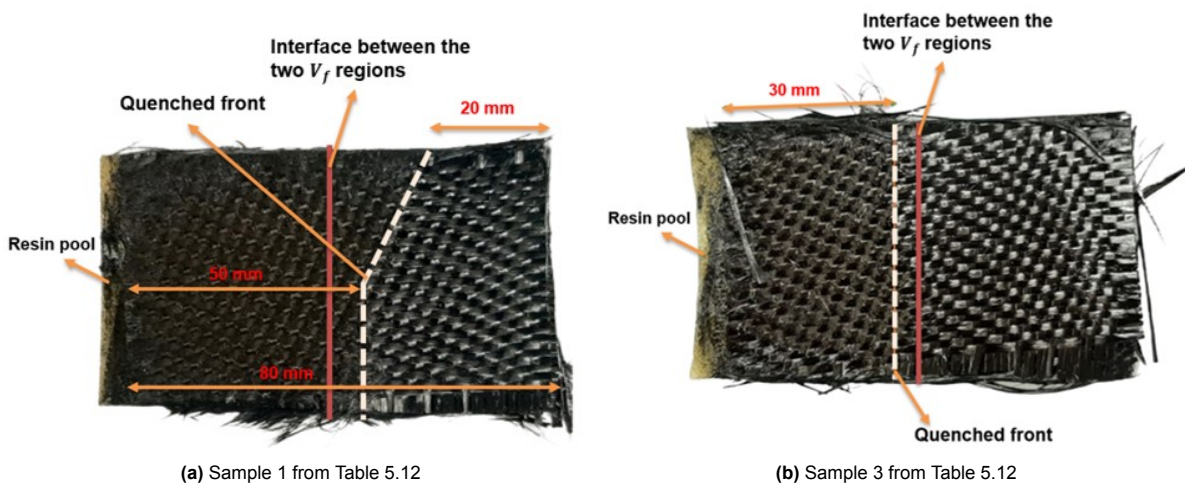
Figure 5.19: Samples with a lower V_f region of $40mm \times 49mm$

After observing that the front failed to propagate throughout the sample, the length of the lower V_f region was increased by 10 mm. As a result, it was observed that two out of the three samples were successfully cured, as depicted in Figure 5.20.

(a) Sample 5 from Table 5.12   **(b)** Sample 6 from Table 5.12
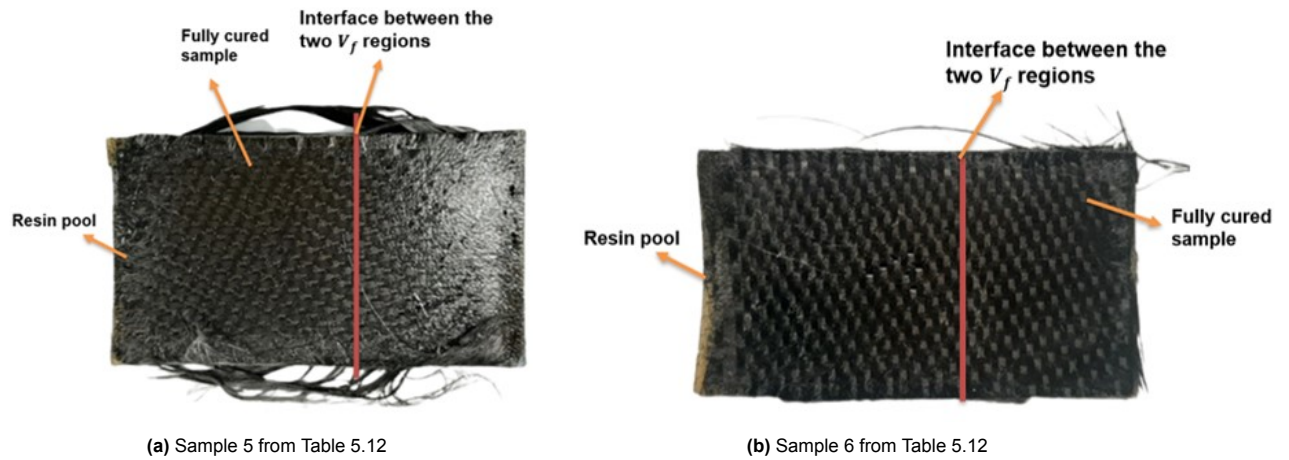
Figure 5.20: Samples with a lower V_f region of $50mm \times 49mm$

Curing the samples with a larger lower V_f region suggests that the length, and consequently the surface area, of the lower V_f region may determine the successful propagation of the front from one region to another. Based on this hypothesis, it can be inferred that for the given geometry, beyond a critical length of the lower V_f region, the front will always propagate into the higher V_f region, curing the entire sample. However, below this critical length, the front may simply quench at the interface of the two regions, or a few millimeters above or below it.

This assumption was based on the fact that the three regions: the initiation pool, the lower V_f region, and the higher V_f region would have different thermal equilibrium levels required to sustain the front. This difference in equilibrium levels is due to the variation in the rate of heat loss, caused by changes in fibre content, and the volume of FP formulation. Upon initiation, the front at the pool would have the highest temperature, which should be larger than the threshold temperature required to maintain the heat balance necessary to sustain the front. As a result, the front should smoothly propagate through the interface between the pool and the lower V_f region.

The front would then continue to propagate through the 11-layer region (lower V_f). The temperature of the front propagating through the lower V_f region should be sufficiently higher than the threshold temperature, despite the increased rate of heat loss due to the uptake by the fibres and the change in heat generation due to the change in the volume of available resin. As the front continues to propagate through the lower V_f region, its temperature would gradually reduce to the new equilibrium level. However, since this is not an immediate process, it means that the front temperature was initially high enough to sustain it through the region.

The aforementioned pattern is expected to continue as the front progresses through the 13-layer region, which has a higher V_f. However, when the front reaches the interface with the higher V_f region, the increased fiber content will abruptly divert more heat away from the front. This diversion will cause the heat to diffuse over a larger area, resulting in insufficient heating of the resin in the immediate vicinity of the front. This phenomenon, coupled with the reduction in resin volume (resulting in reduced heat generation) in the higher V_f region, will lead to a slowdown of the front and a much faster decrease in its temperature.

If the front temperature at the interface remains above the threshold temperature, it will propagate into the higher V_f region without interruption. However, if the temperature falls below the threshold, the front will quench at the interface. As the front progresses into the higher V_f region, the continued effect of heat loss will gradually reduce the front temperature, causing it to quench before traveling the

entire length of the region. If the length of the higher V_f region is short enough, the front will travel until the end. In the case of the manufactured samples, the short length of the higher V_f region translates to an increase in the length of the lower V_f region.

For samples 1 and 3, the shorter length of the lower V_f region may have caused the front to quench near the interface. The increased fiber content in the higher V_f region and reduced resin content led to a more significant effect of heat loss at the interface, resulting in frontal quenching.

In sample 2, the quenching of the front at the resin pool could be attributed to a reduction in heat generation caused by a decrease in the volume of resin in the pool. This reduction in volume was due to the separation of tows into the resin pool. The reduced heat generation likely caused the front temperature to fall below the threshold, resulting in the observed frontal quenching.

For samples 5 and 6, which had a longer lower V_f length, a lower rate of heat loss may have occurred at the interface of the higher V_f region. This lower heat loss to the fibers could have helped sustain the front as it propagated through the higher V_f region.

However, it's challenging to draw a strong conclusion about the behavior of the front based on the current set of samples manufactured. The inconsistent results and low repeatability of the experiments make it difficult to determine the physical phenomena of the front propagation or the influence of the change in the length of the lower V_f region. To address this issue, efforts were made to optimize the manufacturing process and achieve good-quality repeatable samples. The methods utilized to tackle the source of these inconsistencies have already been presented in Section 4.5.1.

5.3.1. Process Optimized Samples

The initial set of composite samples manufactured as part of the study conducted to identify the source of inconsistencies in the manufacturing process (described in subsection 4.5.1) utilized fabric layers cut with the Gerber cutting machine. However, during the cutting process, filament fraying was observed at the edges of the fabric layers. This was likely due to the small filaments at the cut edges sticking to the vacuum pores on the cutting table, leading to fraying as the fabric was removed. Furthermore, poor handling of the fabric layers during layup further aggravated the loss of filaments.

To address the issue of filament fraying, tow stabilization was tested using an adhesive air tack spray. Although the air tack spray was effective in stabilizing fabric layers, it had several drawbacks that made its use impractical. Firstly, the air tack sprays could only stabilize the fabric layers after they were cut and were unable to prevent the separation of the tows during the initial cutting process. Secondly, the time required for the adhesive spray to dry increased the preparation time necessary before the layup could commence. Thirdly, it was difficult to accurately control the amount of adhesive sprayed, as excess adhesive could cause the masking template and fabric layer to stick together. Any attempt to forcibly separate the two would result in the destruction of the layer's integrity. Lastly, the use of air tack spray on the fabric layer could potentially contaminate the layup and resin, thus affecting the propagation of the front through the layup.

To address some of these challenges, a wet layup approach was considered. Prewetting the fabric layers before cutting showed an observable reduction in filament fraying. However, this advantage was accompanied by some consequential disadvantages: (1) it increased the preparation time before layup without providing any leeway for possible buffer layers, which may be needed to replace imperfect layers due to mismatched cutting or handling, and (2) the resin levels in the layup could not be accurately controlled using this process, as the resin used for pre-wetting the fabric was insufficient to compensate for the amount of resin squeezed out during compaction.

Hence, to overcome these challenges, the dry-cutting method discussed in section 4.5 was implemented. This method had several advantages over the other two methods: (1) Reduced fraying with improved transport and handling of the layers, (2) No introduction of contaminants, (3) reduced preparation time. Finally, with the fabric layer stabilized the resin quantity was standardized to compensate for the loss of resin from the cavity on compaction. This standardization method has already been described in subsection 4.5.1.

In the study, repeated failure of the front to propagate beyond the pool into the region of lower V_f was observed mainly in samples with small resin pools (see Figure 5.21) . This phenomenon was attributed to the lower levels of heat generation due to the smaller volume of FP formulation, resulting in a front temperature that was closer to the threshold temperature required to maintain the heat balance. As the front came in contact with the fibres in the lower V_f region, the front temperature could have rapidly fallen below the threshold temperature required to maintain the front in the lower V_f region.
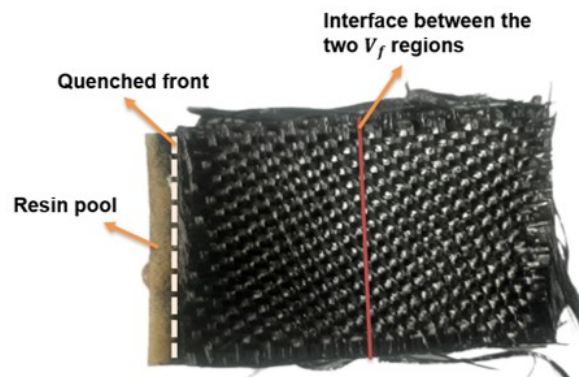
Figure 5.21: Sample manufactured with a small pool size.

Additionally, it was observed that the size of the resin pool decreased in size during the layup due to the tows fraying. The separated tows would accumulate in the pool, reducing the amount of resin while introducing fibre content into the pool. The presence of fibres in the pool could then result in a much lower front temperature, which would lead to immediate quenching upon reaching the lower V_f region, as the temperature falls below its threshold.

Based on the above discussion and the methods presented in subsection 4.5.1, a new batch of samples was produced. These samples were manufactured with the implementation of the proposed solutions simultaneously. This was necessary because during the optimization process, most inconsistencies were tackled in isolation, and hence the solutions developed were targeted to specific issues. These trials aimed to demonstrate the improvements gained in terms of sample repeatability and consistency.

As part of the trials, three samples were manufactured using the optimized manufacturing process. The summary of these samples is presented in Table 5.13. The fabric layers were dry-cut on the cutting table just before laying them into the cavity. The longer fabric layers used had dimensions of 75×49 mm, while the shorter ones used to build up to 13 layers had dimensions of 37.5×49 mm. The reduced dimensions of the samples automatically resulted in an increased length of the initiation pool, which was now 15mm.

Table 5.13: Samples manufactured measured with the optimized manufacturing steps.

Sample number	Dimensions of the 11 layer plies (l×b)(mm)	Dimensions of the 13 layer plies (l×b)(mm)	Average front propagation distance in the lower V_f region (mm)	Average front propagation distance in the higher V_f region (mm)
1	37.5×49	37.5×49	36	0
2	37.5×49	37.5×49	37	0
3	37.5×49	37.5×49	37.5	5.5

As shown in Figure 5.22, the front has successfully traversed the lower V_f region upon initiation. The samples showed a noticeable improvement in repeatability, with all three demonstrating consistent results. Additionally, the fraying of tows was almost negligible, with the observed fraying in the uncured region mainly occurring during the demolding process. Furthermore, distinct cured resin channels were also observed on the periphery of all samples, as depicted in Figures 5.22a and 5.22b.

(a) Sample 1 from Table 5.13   (b) Sample 3 from Table 5.13
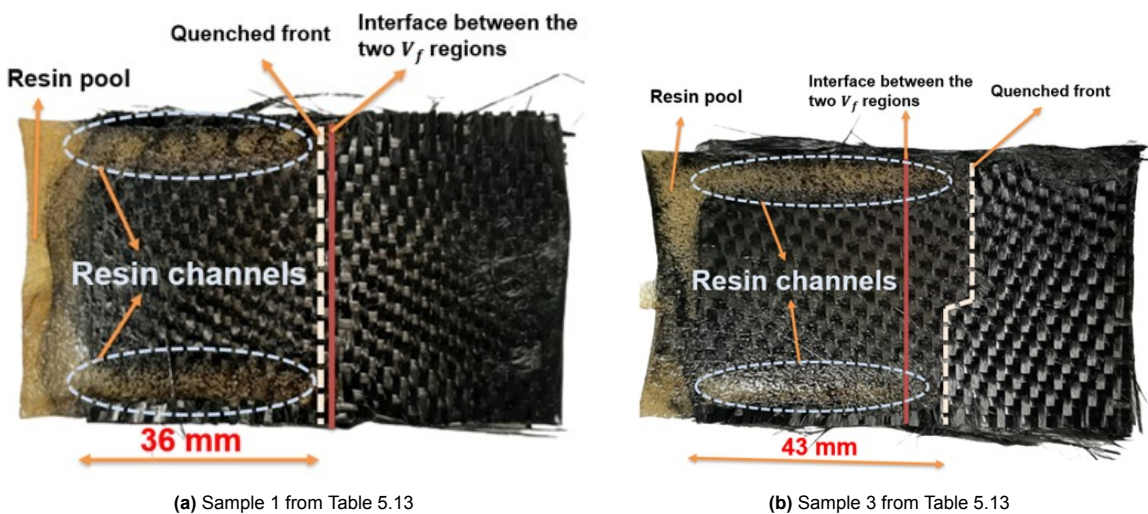
Figure 5.22: Samples manufactured with the optimized manufacturing process.

To conduct a more thorough investigation into the cause of the visible cured tracks, additional trials were carried out. The conclusion reached was that the cured resin tracks were a consequence of undulation created due to the imperfect fitting of the fabric layers into the cavity (as shown in Figure 5.23). These surface undulations of the fabrics were attributed to two identified causes: (1) the excessive width of the fabric layers and (2) the loss of elastic properties in the silicone joint, resulting in greater compression deformation.
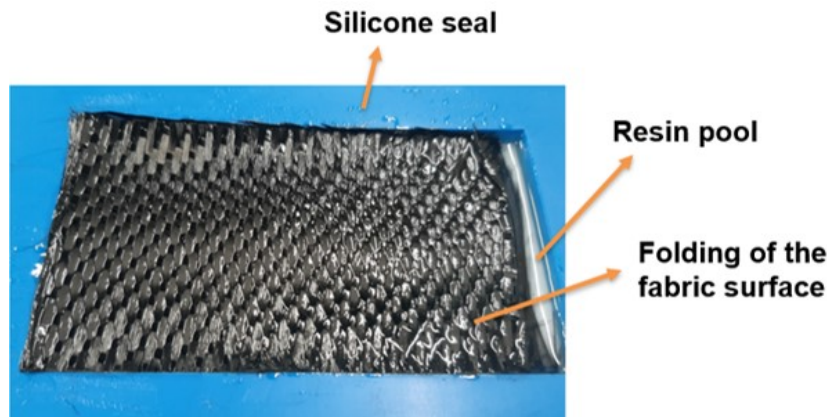
Figure 5.23: Warping of the fabric creating peaks and troughs in the fabric layup.

The excessive width of the layers caused the fabric layers to rise up against the walls of the silicone cavity during the layup process. As a result of this imperfect fitting, the fabric layer folded, resulting in regions of peaks and troughs. When the mould was closed, these shallow regions were filled with resin, creating a separate channel for the propagation of the front (as shown in Figure 5.24a). This phenomenon could potentially result in non-uniform movement of the front, as it may travel faster in the shallow regions compared to the peak regions. Furthermore, the larger width was exacerbated by the loss of elastic properties of the silicone joint due to prolonged usage. This loss of property led to greater deformation of the joint upon mould closure (as depicted in Figure 5.24b).
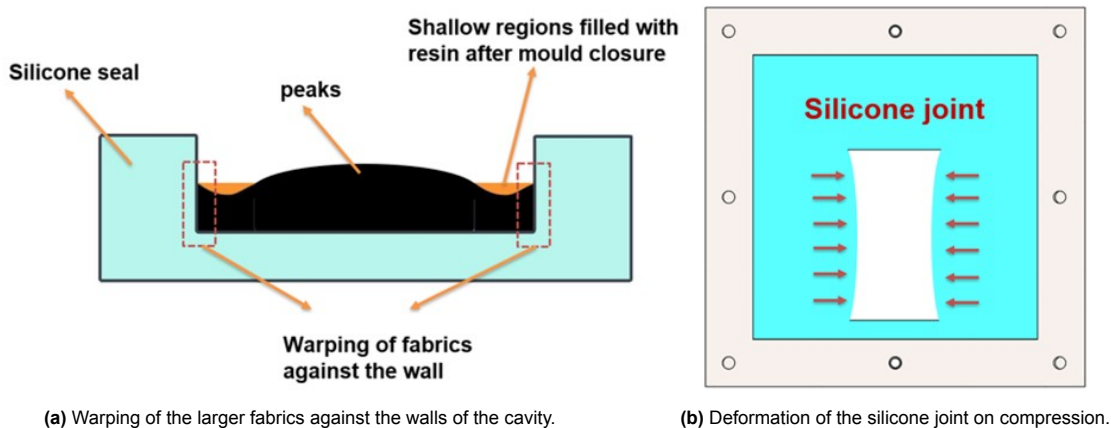
(a) Warping of the larger fabrics against the walls of the cavity.   (b) Deformation of the silicone joint on compression.

Figure 5.24: The causes leading to the formation of the resin channels.

To address this issue, two separate solutions were implemented. The first solution was to reduce the width of the fabric layers to ensure a better fit, and the second was to cast a new silicone joint. Table 5.14 presents the samples that were manufactured with the implemented changes. The reduction of the fabric width, coupled with a newly cast silicone joint, visibly improved the quality of the samples. As shown in Figure 5.25, these samples were devoid of resin channels, indicating the effectiveness of these simple solutions.

Table 5.14: Samples manufactured with a new silicone joint.

Sample number	Dimensions of the 11 layer fabric layers (l×b)(mm)	Dimensions of the 13 layer fabric layers (l×b)(mm)	Average front propagation distance in the lower V_f region (mm)	Average front propagation distance in the higher V_f region (mm)
1	42.5×47.5	32.5×47.5	41	0
2	47.5×47.5	27.5×47.5	47.5	27.5

(a) Sample 1 from Table 5.14

(b) Sample 2 from Table 5.14
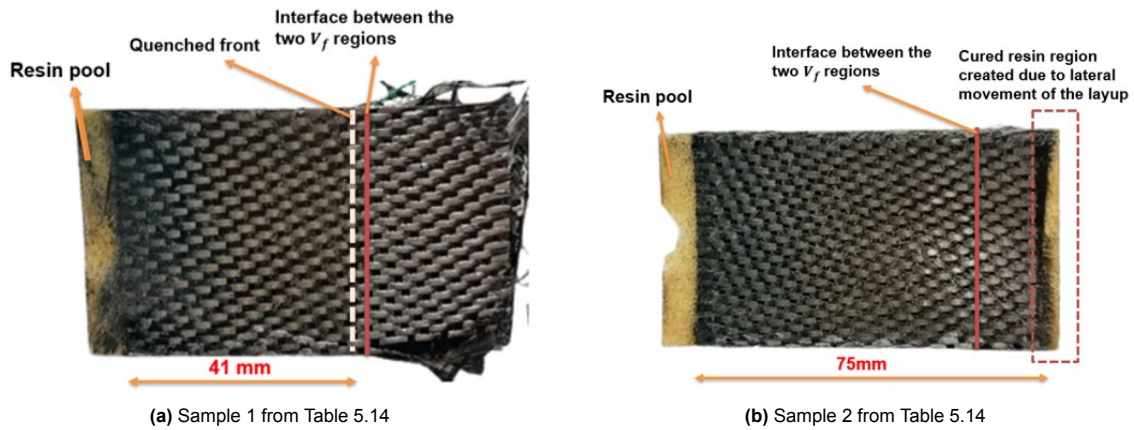
Figure 5.25: Samples manufactured with reduced width and a new silicone joint.

To investigate the impact of width optimization and the use of a new silicone, two separate representative samples with similar dimensions were observed under a microscope at 10x magnification. The first sample was manufactured before optimization and showed the formation of resin channels, whereas the second sample, manufactured after optimization, was devoid of any visible resin channels.

The cross-sectional microscopic images along the length of the samples were used to estimate the void fraction. The estimated void fractions in different V_f regions of the samples have been summarized in Table 5.15. Sample 1, which was manufactured before optimization, has a higher void content than the sample manufactured after optimization (sample 2). The void fraction decreased by 13.4% in the lower V_f regions and by 57.5% in the higher V_f regions.

Table 5.15: Comparison of the void fraction in samples manufactured before and after width optimization

Sample number	Dimensions of the lower V_f region (l×b)(mm)	Void fraction of the lower V_f region estimated via thresholding(%)	Dimensions of the higher V_f region (l×b)(mm)	Void fraction of the higher V_f region estimated via thresholding(%)
1	47.5×49	7.79	27.5×49	6.65
2	47.5×47.5	6.74	27.5×47.5	2.82

To visually confirm the elimination of resin channels, horizontal cross-sections of the same samples were observed at 10x magnification. Figure 5.26a shows fabric warping and the consequent formation of the resin channel. On the other hand, Figure 5.26b shows the absence of resin channels in a width-optimized sample.
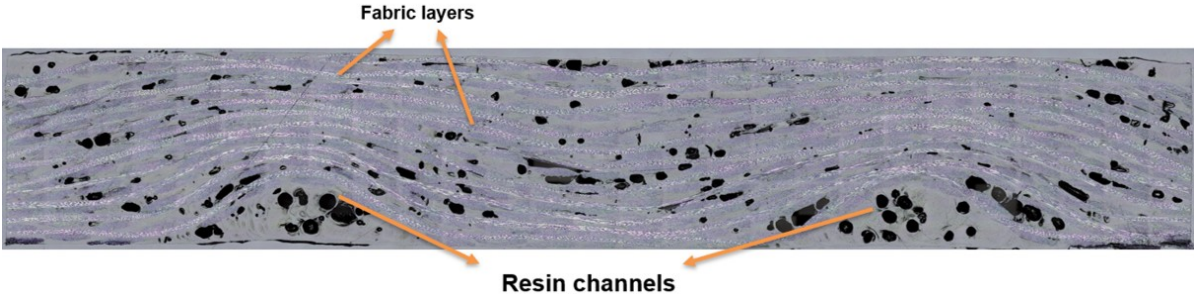
(a) Sample with a resin channel (sample 1 from Table 5.15)
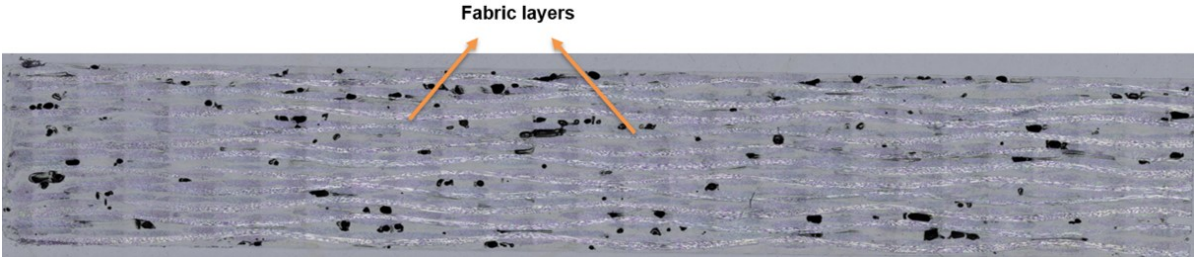
(b) Width optimized sample without resin channel (sample 2 from Table 5.15)

Figure 5.26: Microscope images depicting samples with and without resin channels.

5.4. Temperature Monitoring

As shown in section 5.3, it appears that changing the fiber volume fraction has a clear influence on the propagation of the front. Moreover, these experiments also revealed that the influence of varying V_fs is dependent on the relative surface areas of the two regions. To modify the surface areas of the two regions, the length of the lower V_f region was varied. It was observed that decreasing the length of the lower V_f region below a certain critical value acted as an inflection point in the front's behaviour. This phenomenon was explained by comparing the front temperature with the hypothetical threshold temperature of a particular region.

Furthermore, the samples shown in subsection 5.3.1 exhibited the formation of resin channels due to the warping of the fabrics against the cavity walls. The formation of these channels indicated the possibility of non-homogeneous movement of the front. To eliminate the formation of these resin channels, samples were manufactured with fabric layers of smaller width and a newly cast silicone joint. These corrections eliminated the formation of resin channels and suggested the formation of homogeneous fronts. However, further quantification was deemed necessary to validate these observations. As described in subsection 4.5.2, this quantification involved collecting temperature data across the sample's surface area.

To quantify the propagation of the front through the two regions with different V_fs and to determine the critical length of the lower V_f region, a study was conducted. In this study, a series of samples were manufactured by increasing the length of the lower V_f region, which was determined through trial and error. The different lengths of the lower V_f region used in the study are presented in Figure 5.27. Given the practical difficulties of introducing thermocouples into the layup, only two thermocouples were used initially as a precautionary measure, with one placed in each of the two V_f regions. Once some familiarity was gained with introducing the thermocouples between the fabric layers, an additional thermocouple was introduced at the interface in the samples manufactured towards the end of the study. It is worth noting that this study was conducted before the width correction was carried out, and therefore, resin channels are visible in all the samples.
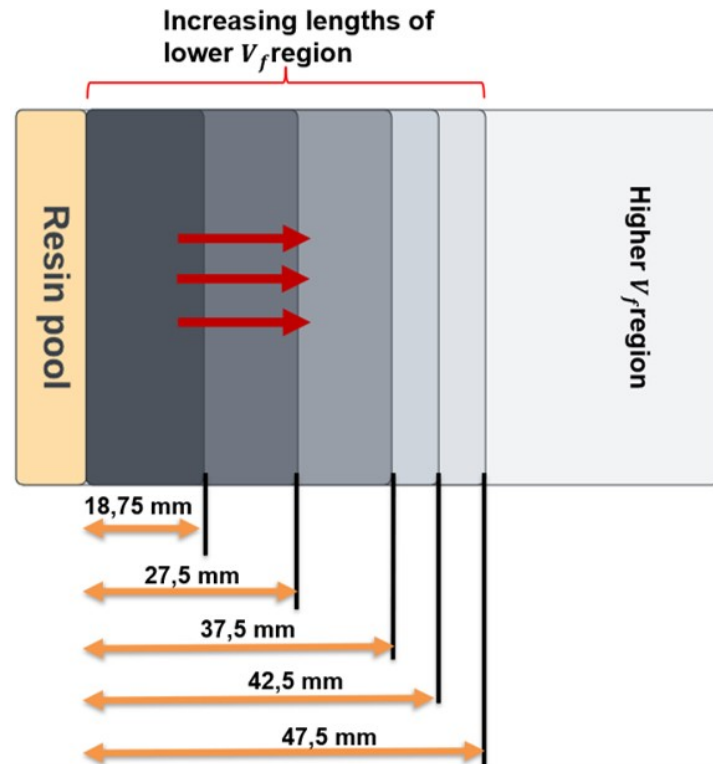
Figure 5.27: The different lengths of the lower V_f region used to manufacture samples.

The study began by manufacturing samples with a lower V_f region that had a length of 18.75 mm, which was exactly one-fourth of the total length of the layup (75 mm). As shown in Figure 5.28b, the front propagation stopped at the interface between the two regions. The temperature progression through the two regions was captured in Figure 5.28a.

Following these observations, two samples with a lower V_f region length of 27.5 mm and 37.5 mm were manufactured. These samples exhibited similar behaviour, with a sharp rise in temperatures observed in the thermocouple placed in the lower V_f region, while the thermocouple placed in the higher V_f region showed an almost flat curve, indicating that the front had not propagated through the higher V_f region.

On the other hand, samples with lower V_f regions with a length of 42.5 mm and 47.5 mm saw the complete progression of the front. The temperature progression for these lengths through the two regions is presented in Figure 5.28c and Figure 5.28e, respectively. A clear sharp rise in temperature across (T1 & T4) the two regions was observed, indicating the seamless propagation of the front from one region to another. The onset rise in temperature was in order with the movement of the front through the sample, with a clear distinction observed between the onset times of temperature rise in the two regions.
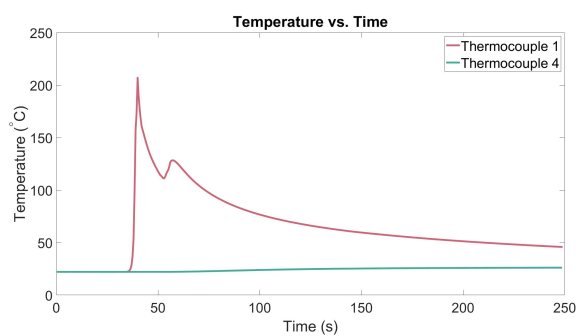
(a) Temperature readings (18.75mm)
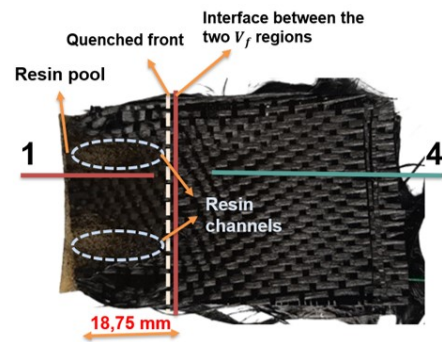
(b) Sample when the length of the lower V_f region is 18.75mm
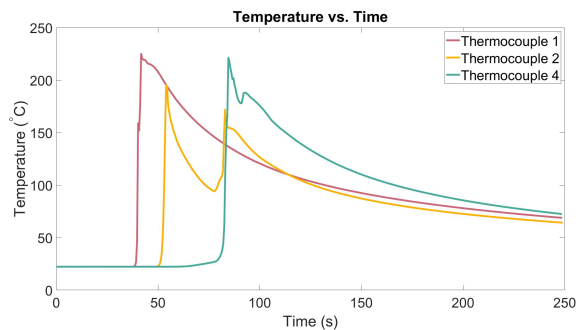
(c) Temperature readings (42.5mm)
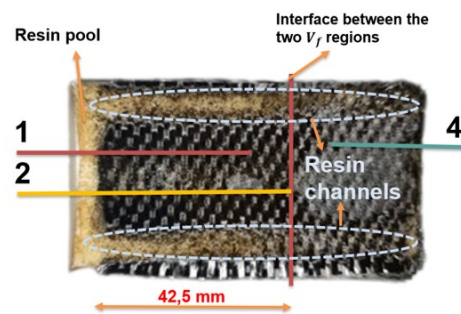
(d) Sample when the length of the lower V_f region is 42.5mm
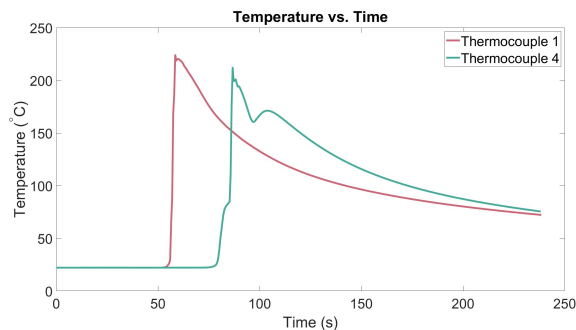
(e) Temperature readings (47.5mm)
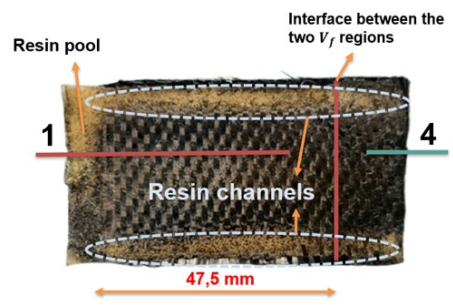
(f) Sample when the length of the lower V_f region is 47.5mm

Figure 5.28: Temperature vs. time plot representing the progression of the front in samples with different lengths of lower V_f region.

The scatter plot shown in Figure 5.29 provides clear evidence supporting the proposed hypothesis of a critical length (indicated by a vertical blue line). Specifically, the plot demonstrates that samples with lower V_f region lengths below 42.5 mm repeatedly experience frontal quenching at the interface.
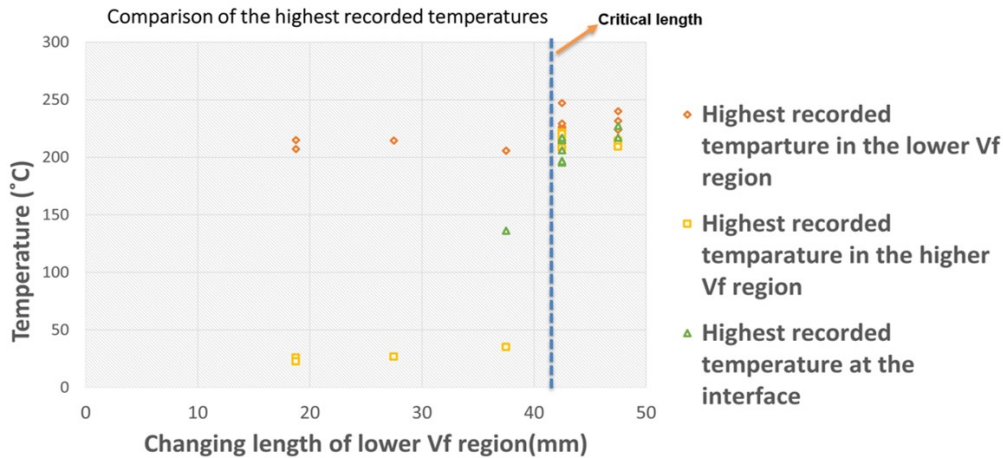
Figure 5.29: Comparison of the peak temperatures in the different regions.

The scatter plot also provides evidence supporting the necessary requirement to sustain the fronts through the different regions. Specifically, the peak temperatures of the front in the cured region were found to be above 200°C, indicating that the front had to be above this threshold to be sustained. In samples where the front quenched at the interface, the recorded peak temperature did not reach this threshold value. Furthermore, in all the samples that were manufactured, the peak temperature recorded in the lower V_f region was greater than those recorded at the interface and in the higher V_f region. This observation suggests that the front temperature gradually decreases as it propagates through the different regions. In samples with a length above the critical value, the front temperatures were sustained above the threshold, whereas in samples with a length below the critical value, the opposite was true.

Following these observations, a study was conducted to quantify the formation of a non-homogeneous front caused by the warping of the fabric layers. Subsequently, the formation of homogeneous fronts in samples manufactured after width optimization was also investigated. The warping of the fabric resulted in the creation of regions of peaks and troughs. This caused more resin to accumulate in the shallow regions, resulting in faster fronts in these areas as compared to the centre of the sample. Capturing temperature data at these specific locations would help quantify this assumption.

To address this requirement, two additional thermocouples were introduced: one placed at the interface (thermocouple 3), and the other placed at the edge of the sample (thermocouple 5). To confirm the non-homogeneous movement of the front, the onset point of temperature rise between thermocouples 2 and 3, and thermocouples 4 and 5 were compared. If the front moved non-homogeneously, then thermocouples at the interface (thermocouples 2 and 3) would not trigger simultaneously. The thermocouple in the shallow regions (thermocouple 3) would trigger first compared to the thermocouple in the centre (thermocouple 2). Similarly, if the front is non-homogeneous, then thermocouples 4 and 5 would also record this phenomenon.

To investigate the observed phenomena, samples were manufactured with a lower V_f region length of 42.5 mm. A summary of the peak temperatures recorded by the five thermocouples is presented in Table 5.16.

Table 5.16: Sample manufactured to study non-homogeneous fronts

Sample number	Dimensions lower V_f region (l×b) (mm)	T1 ($^{\circ}C$)	T4 ($^{\circ}C$)	T2 ($^{\circ}C$)	T3 ($^{\circ}C$)	T5 ($^{\circ}C$)	Distance moved by the front in the lower V_f region (mm)	Distance moved by the front in the higher V_f region (mm)
1	42.5×47.5	203.97	202.04	23.93	208.29	61.83	42.5	32.5
2	42.5×47.5	225.46	220.37	214.81	155.21	200.40	42.5	32.5

Similar to the previous study, it was observed that the peak temperature in the lower V_f region (T1) was higher than the peak temperature in the higher V_f region (T4) and at the interface temperatures (T2 and T3). However, in sample 1, slight variations were noticed in this trend where the peak temperature at the interface (T3) as recorded by thermocouple 3 was actually higher than the peak temperature in the lower V_f region (T1). This variation could be attributed to the non-homogeneous propagation of the front. The warping of the fabric in this sample resulted in the formation of resin channels (as shown in Figure 5.30b). Thermocouple 3, which was placed from the side, might have measured the front temperature of the resin channels formed in the shallow region, whereas Thermocouple 1, placed from the centre, could have measured the front temperature through the fabric. On the other hand, sample 2 did not have any visible resin channels, but the effects of warping were still evident in the form of uncured regions at the edges of the samples on both ends (see Figure 5.30d).

(a) Temperature readings of sample 1 from Table 5.16

(b) Sample 1 from Table 5.16

(c) Temperature readings of sample 2 from Table 5.16

(d) Sample 2 from Table 5.16
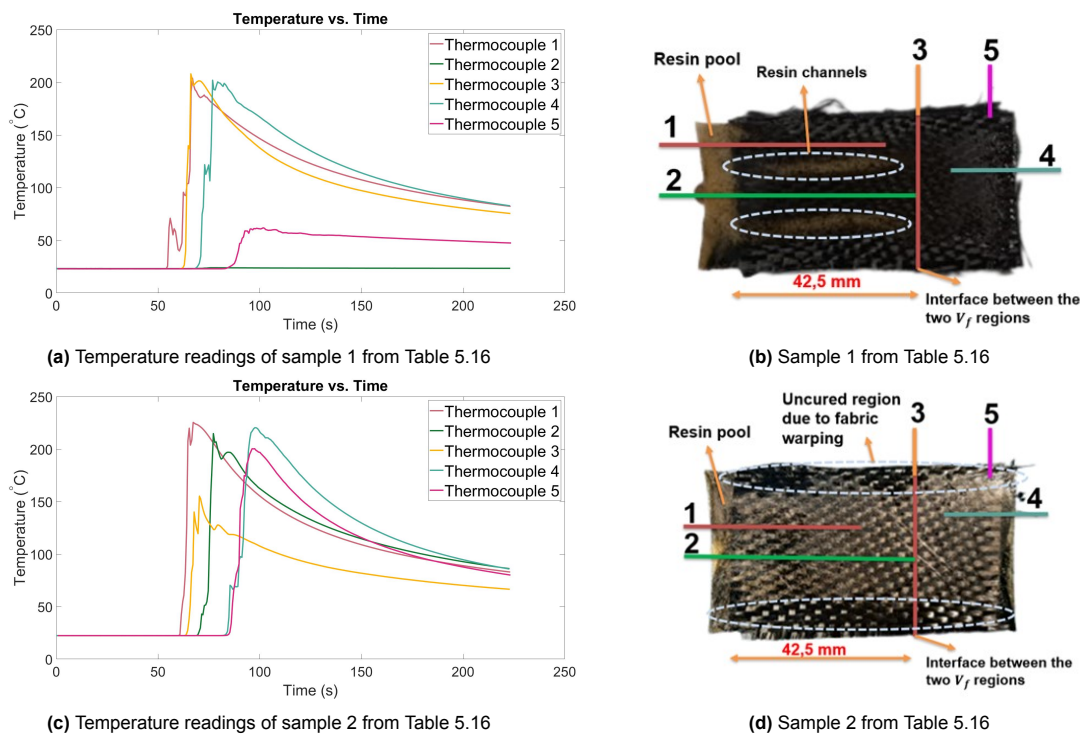
Figure 5.30: Temperature vs. time plot capturing non-homogeneous fronts.

Additional evidence of the formation of non-homogeneous fronts in these samples can be obtained by comparing the temperature curves. As shown in Figure 5.30c, there is a clear difference in trigger times between thermocouples 2 and 3, with thermocouple 3 triggering 6.3 seconds before thermocouple 2. Furthermore, thermocouples 4 and 5 triggered simultaneously, indicating that the front had reached both thermocouples at almost the exact same time. This would not be the case if the front had traveled in a homogeneous manner. If the front had been homogeneous, a concurrent triggering of thermocouples 2 and 3 would have been observed, with a delay in the onset of thermocouples 4 and

5, with the former capturing the front before the latter.

The behavior of the front for the samples manufactured after optimizing the fabric layer width and using a new silicone joint to eliminate warping of the fabric was investigated, and the peak temperatures captured by all the thermocouples are presented in Table 5.17. These samples had a lower length of V_f region of $46.5mm$, and the width of the fabric layers was reduced to $47.5mm$.

Table 5.17: Peak temperatures in samples manufactured with fabric width optimization and a new silicone joint.

Sample number	Dimensions lower V_f region (l×b) (mm)	T1 (°C)	T4 (°C)	T2 (°C)	T3 (°C)	T5 (°C)	Distance moved by the front in the lower V_f region (mm)	Distance moved by the front in the higher V_f region (mm)
1	46.5×47.5	223.83	189.38	199.64	209.01	-	46.5	28.5
2	46.5×47.5	231.58	214.20	227.24	212.86	214.20	46.5	28.5
3	46.5×47.5	239.83	209.44	216.91	224.32	222.36	46.5	28.5
4	-	279.16	55.20	217.82	-	-	0	0

For the samples with a lower V_f region length of $46.5mm$, the front propagation was observed until the end, indicating that this length is above the critical value. Across all samples, the peak temperature in the lower V_f region (T1) was found to be higher than the peak temperatures in the higher V_f region (T4) and the interface (T2 & T3).

(a) Temperature readings of sample 2 from Table 5.17
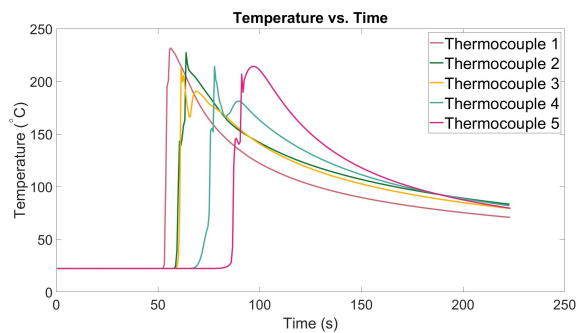
(b) Sample 2 from Table 5.17
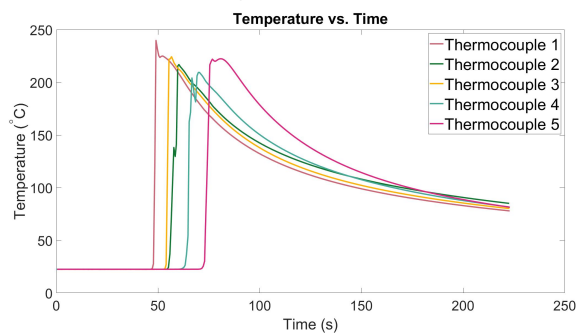
(c) Temperature readings of sample 3 from Table 5.17
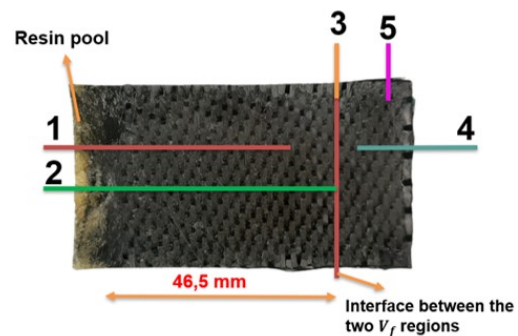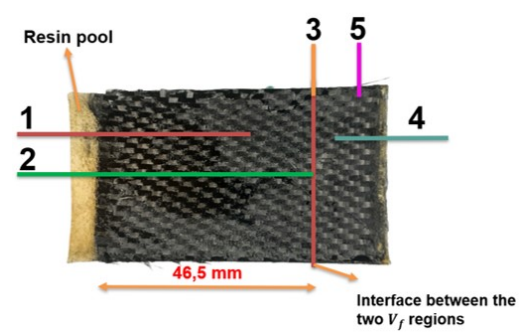
(d) Sample 3 from Table 5.17

Figure 5.31: Temperature vs. time plot capturing the progression of the front in samples manufactured with optimized width and silicone joints.

The analysis of the curves indicated that the propagation of the front through the sample's surface area appeared to be quite homogeneous. This is evident from Figure 5.31a and Figure 5.31c, where the onset rise in temperatures recorded by the thermocouples at the interface (thermocouples 2 & 3) occurred almost simultaneously. Additionally, the onset rise in temperature observed in thermocouples

4 was earlier than in thermocouple 5. These observations suggested that the propagation of the front was likely to be homogeneous.

Figure 5.32 depicts the three common features found in these curves: non-monotonic temperature increase, single peaks, and multiple peaks. These characteristics arise due to the micro-structure of the fabrics. The non-monotonic increase observed in many of the curves may indicate non-homogeneous fronts at the microscopic level. Each tow could have fronts moving at different speeds, causing the thermocouple to capture fronts moving in its vicinity before capturing the front propagating over it.

Furthermore, all the presented plots have shown two types of peak behaviours, namely (1) a single peak or (2) multiple peaks. The formation of these peaks may be related to the positioning of the thermocouples in relation to the micro-structure of the fabrics. If the tip of the thermocouple is placed in the resin pools between the tows, the temperature reading would show a single sharp peak. Conversely, if the tip of the thermocouple is placed on the tows, the reading would exhibit multiple peaks. The resin-filled region between the tows has a lower V_f, which means it polymerizes faster than the tows with a higher V_f. A thermocouple placed in this region would only detect the front moving through the pool, while the thermocouple placed on the tow would first register the front moving adjacent to it (the resin pool between tows). Subsequently, it would register the front that moves through the tow.
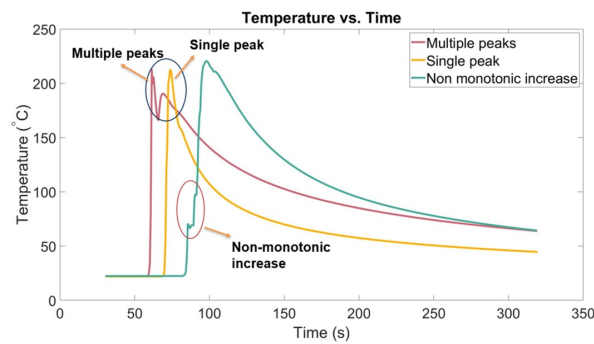
Figure 5.32: Curves showing Single peaks, multiple peaks and non-monotonic increases.

Finally, to provide a sense of closure to the experimental study conducted thus far, the length of the lower V_f region was reduced to 0 mm, while the length of the higher V_f region was increased to 75 mm (as shown in sample 4 in Table 5.17). As depicted in Figure 5.33b, the front has quenched precisely at the interface between the pool and the layup, which is a result consistent with those observed for samples with uniform V_f. In Figure 5.33a, the progression of temperature from the resin pool to the fabric layup is shown. As expected, the highest recorded temperature was observed in the resin pool (thermocouple 1). Moreover, the transfer of heat from the pool to the fabric is evident from the temperature rise recorded by the resin (thermocouple 3).
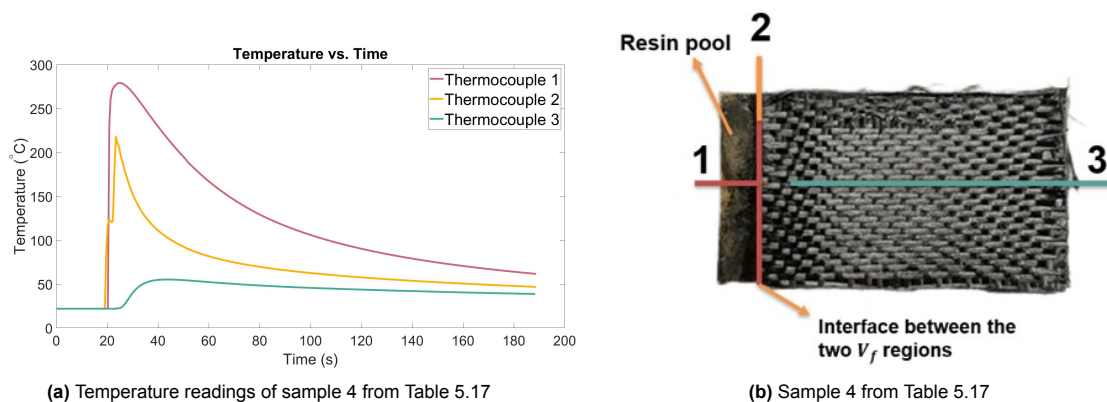
(a) Temperature readings of sample 4 from Table 5.17

(b) Sample 4 from Table 5.17

Figure 5.33: Temperature vs. time plot representing the progression of the front in samples with 13 layers

5.5. Non Rectangular Samples

The samples manufactured and the studies carried out in section 5.3 and section 5.4, respectively, made the first attempts at utilizing FP in curing laminates that mimic real-life applications. This exercise is the first step in making FP viable for different geometries. Continuing in this spirit, the next logical step was to test the feasibility of manufacturing composites with different geometrical shapes. As already discussed in section 4.6, composite laminates with in-plane "L" shaped samples were manufactured. Before varying the V_f within the L-shaped sample, the basic capability of the front to traverse the entirety of the sample was tested. To do this, a series of "L" shaped samples with uniform V_f were chosen based on the already exhibited results of rectangular flat plate samples. A summary of these samples has been provided in Table 5.18.

Table 5.18: L-shaped samples with uniform V_f across the surface area of the sample.

Sample number	Number Of Layers (n)	Average height of the silicone cavity (mm)	Theoretical V_f (%)	Average thickness of the cured sample (mm)	Actual V_f (%)
1	10	5.10±0.03	30.56±0.20	5.06±0.07	30.81±0.46
2	11	5.10±0.03	33.64±0.22	4.99±0.06	34.39±0.44
3	12	5.10±0.03	36.67±0.24	5.08±0.04	36.85±0.35

As illustrated in Figure 5.34, the L-shaped samples exhibited comparable surface quality to the rectangular samples with a uniform V_f, which were produced using the same stainless steel test setup. This surface quality indicated good resin saturation. The samples also showed reasonable accuracy, with an average percentage error between the actual and theoretical V_fs of 1.17%. The low error margin was an indication of the uniformity in the height of L shaped cavity of the silicone joint and the high compaction provided by the stainless steel setup.
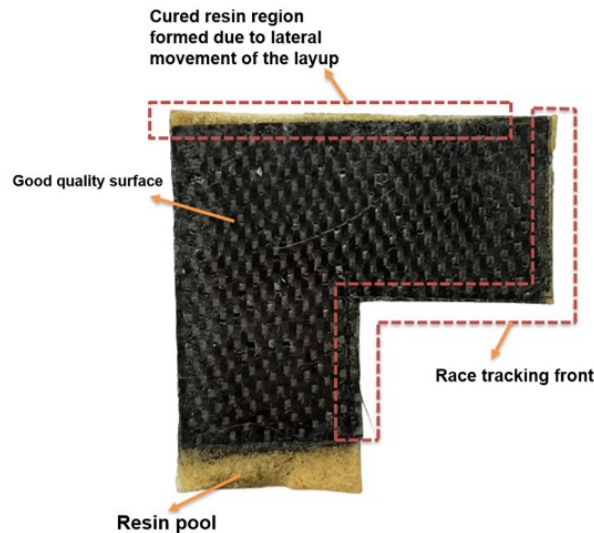
Figure 5.34: L-shaped sample with uniform V_f across the surface area of the sample.

The L-shaped samples with uniform V_f were manufactured immediately after the rectangular uniform V_f samples presented in subsection 5.2.3. At this stage, width optimization was not yet carried out and hence the L-shaped fabric layers were cut to dimensions that allowed for an easy fit into the cavity. These reduced dimensions resulted in two commonly observed features: the lateral movement of the layup on compaction evident from the cured resin regions at the edge opposite the resin pool and race-tracking fronts along the edges of the sample.

The sample with 13 fabric layers (with a corresponding V_{f_t} of 39.73±0.26) or more failed to cure. In these samples, the front was seen to quench at the interface between the resin pool and the fabric layup. The quenching of the front was attributed to the high fibre content and a small resin pool (10 mm). The small size of the pool may have resulted in lower heat generation, and subsequently, a lower front temperature. As the front reached the higher V_f region, the high fibre content may have directed a large amount of heat away, resulting in the slowing down of the front with a reduction in the front temperature. As a consequence, the front temperature may have fallen below the threshold temperature required to sustain the front through the fabric layup, leading to the observed curing failure in the samples with 13 or more layers.

The trials conducted in section 5.3 aimed to investigate the influence of varying V_f within the sample on the propagation of the front through the rectangular sample. These trials revealed that, in a rectangular sample of the tested dimensions (90 × 50 mm), the successful propagation of the front from a region of lower V_f to a region of higher V_f is dependent on the relative lengths of the two regions within the given sample dimensions. Specifically, the propagation of the front from one region to another occurred only when the length of the lower V_f region was greater than a critical value. Following the results of these trials, a study was conducted to investigate whether this critical length could also be observed in an L-shaped geometry.

In this study, a series of L-shaped samples with varied V_fs were manufactured. Similar to the rectangular samples with varied V_fs, the lower V_f region comprised of 11 layers while the higher V_f region comprised of 13 layers. The length of the lower V_f region was increased relative to the length of the higher V_f region. These lengths were determined through a trial and error process. Figure 5.35 illustrates the different lengths of the lower V_f region that were utilized in the study.
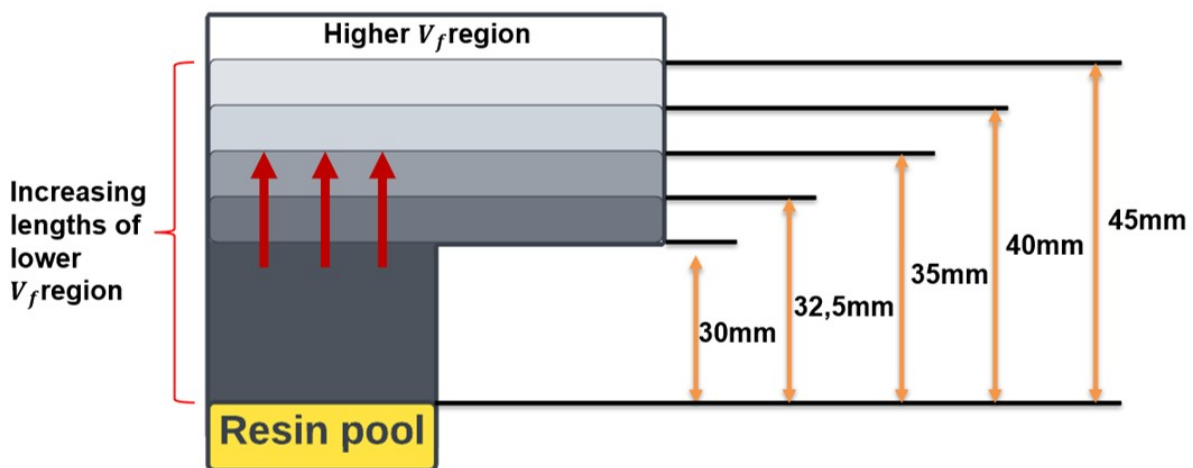
Figure 5.35: The different lengths of the lower V_f region used to study the existence of a critical length in an "L" shaped sample.

The results of these trials are summarized in Table 5.19. Notably, a critical point in the front's behaviour was observed at a lower V_f region length of 32.5mm. As shown in Figure 5.36, samples 1 and 2, which had V_f region lengths of 30mm and 32.5mm, respectively, showed quenching of the front at the interface. In contrast, samples with a longer length of the lower V_f region (greater than 32.5mm) exhibited complete front propagation during the curing process. Figure 5.36c illustrates the curing of a sample with a lower V_f region length of 35mm.

Sample number	Length of the lower V_f region (l)(mm)	Dimensions of the higher V_f region (l×b)(mm)	Average front propagation distance in the lower V_f region (mm)	Average front propagation distance in the higher V_f region (mm)
1	30	35×75	30	0
2	32.5	32.5×75	32.5	0
3	35	30×75	35	30
4	40	25×75	40	25
5	45	20×75	45	20

Table 5.19: L shaped samples with varied v_f manufactured to study the presence of a critical length.

(a) L shaped sample with a lower V_f region length of of 30mm

(b) L shaped sample with a lower V_f region length of of 32.5mm

(c) L-shaped samples with the lower V_f region length of 35mm.
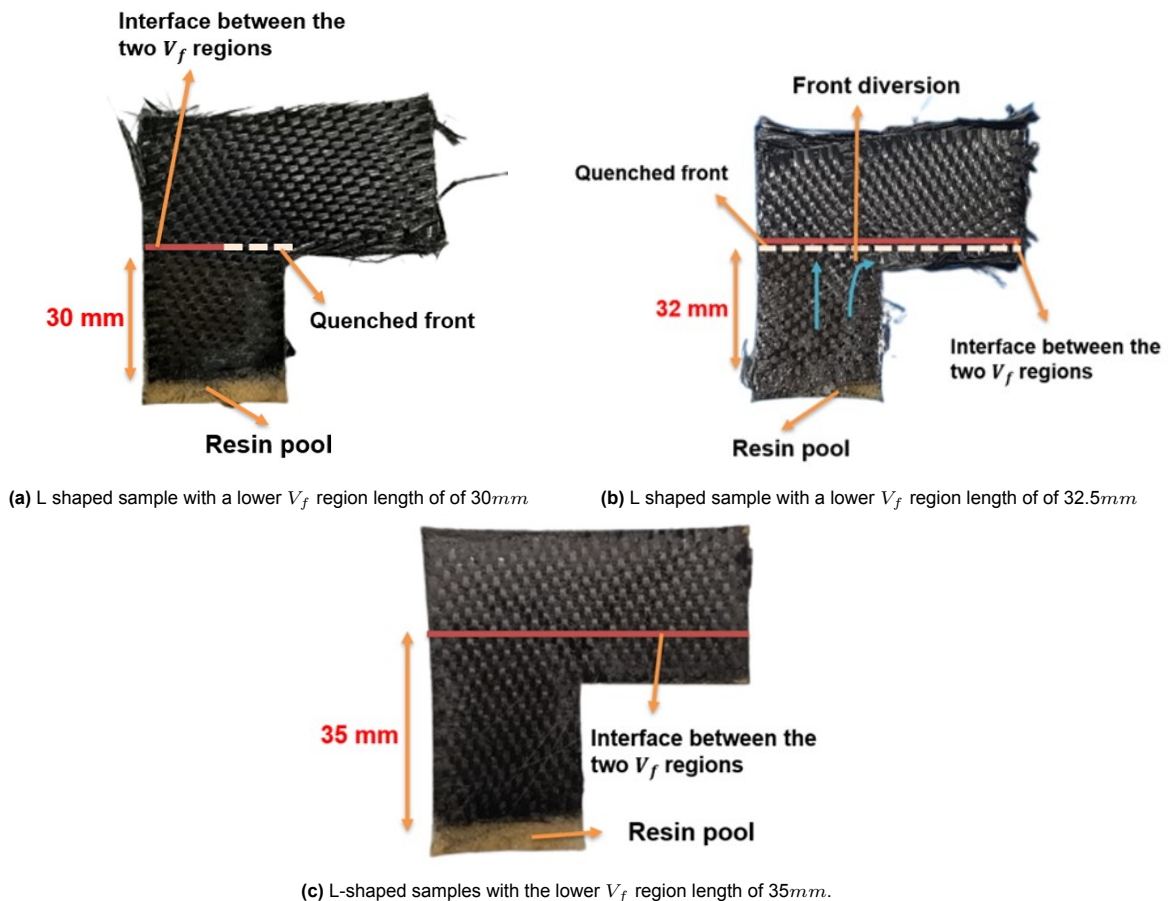
Figure 5.36: L-shaped samples with different lengths of lower V_f region.

These results were a clear indication that, as discussed for rectangular samples in section 5.3, the successful propagation of the front in an L-shaped sample is also dependent on the length of the lower V_f region. The successful propagation of the front in the sample with a lower V_f region length larger than $32.5mm$ provides clear evidence for the existence of a critical length.

The mechanism of front propagation in an L-shaped sample is similar to that of rectangular samples, with the only difference being the direction of propagation due to the variation in geometry. Initially, the front in the L-shaped sample would start propagating through one of its arms. Upon reaching the end of this arm, the front would then diverge into the next arm. The evidence supporting the diversion of the front can be found in the sample with a lower V_f region length of $32.5mm$ (Figure 5.36b). In this sample, the front has quenched at the interface, but the lower V_f region in both arms has fully cured.

The quenching of the front observed at the interface for samples with a lower V_f region below the critical length follows a similar mechanism to that of rectangular samples. Upon reaching the interface with the higher V_f region, the increased fibre content abruptly diverts more heat away from the front, which then diffused over a larger area, resulting in insufficient heating of the resin in the immediate neighbourhood of the front. This heat loss, coupled with the reduced volume of resin and thus reduced heat generation, eventually leads to a decrease in the temperature of the front and its slowing down.

Conversely, increasing the length of the lower V_f region would lead to a reduction in heat loss due to reduced fibre content in the higher V_f region. In these samples, if the front temperature remains above the threshold, it will continue to propagate some distance before it quenches due to the gradual effects of heat loss. The reduction of the front temperature below the threshold temperature would be a gradual process. If the length of the higher V_f region is small enough, the front should have adequate time to fully cure the region. However, if the length of the higher V_f region were longer, the front might not reach the end of the sample but instead, quench after travelling a certain distance.

As previously discussed, upon increasing the geometrical complexity from a flat rectangular sample to an L-shaped sample, the critical length phenomenon still held true. Additionally, the study of the critical length also highlighted the change in the direction of the propagating front due to the geometry of the L-shaped sample. To explore the effects of this directional change on the front's movement between different regions, two samples were manufactured with variations in the arrangement of the higher and lower V_f regions.

Figure 5.37 illustrates the schematic of the two samples manufactured. In the first sample (see Figure 5.37a), the length of the lower V_f region was smaller than the critical length. However, the smaller width of the higher V_f region allowed for the diverted front's progression into the lower V_f region in the other arm of the L-shaped sample. In the second sample (see Figure 5.37c), the length of the lower V_f region was increased to $65mm$ in one arm, while the other arm consisted of the higher V_f region. This arrangement of the V_f regions allowed for the investigation into the effects of the changing direction of the front on its ability to cure the samples.

In Sample 1 (see Figure 5.37b), the front propagated into the higher V_f region, curing the entire region. Since the length of the lower V_f region was smaller than the critical length, the propagating front should have quenched at the interface. However, due to the chosen width, the front may have diverted towards the lower V_f region in the other arm, potentially leading to the front approaching the higher V_f region from two directions. Additionally, the front approaching directly from the lower V_f region at the bottom (adjacent to the resin pool) could have preheated the fibres in the higher V_f region. This would mean that when the diverted front eventually reaches the higher V_f region, the fibres there would already be sufficiently heated, enabling the front to propagate seamlessly into the higher V_f region.

Furthermore, due to the smaller size of the higher V_f region (30×35), the heat loss due to the high fibre content should be much lower compared to the previous study conducted to study the critical length. Despite the larger size of the higher V_f region in this study (75×30), the front still propagated unimpeded. This low heat loss, combined with a two-sided front could mean that the front temperature in at least one of the arms should still be higher than the threshold temperature required to sustain

(a) Sample 1

(b) Manufactured sample 1

(c) Sample 2

(d) Manufactured sample 2
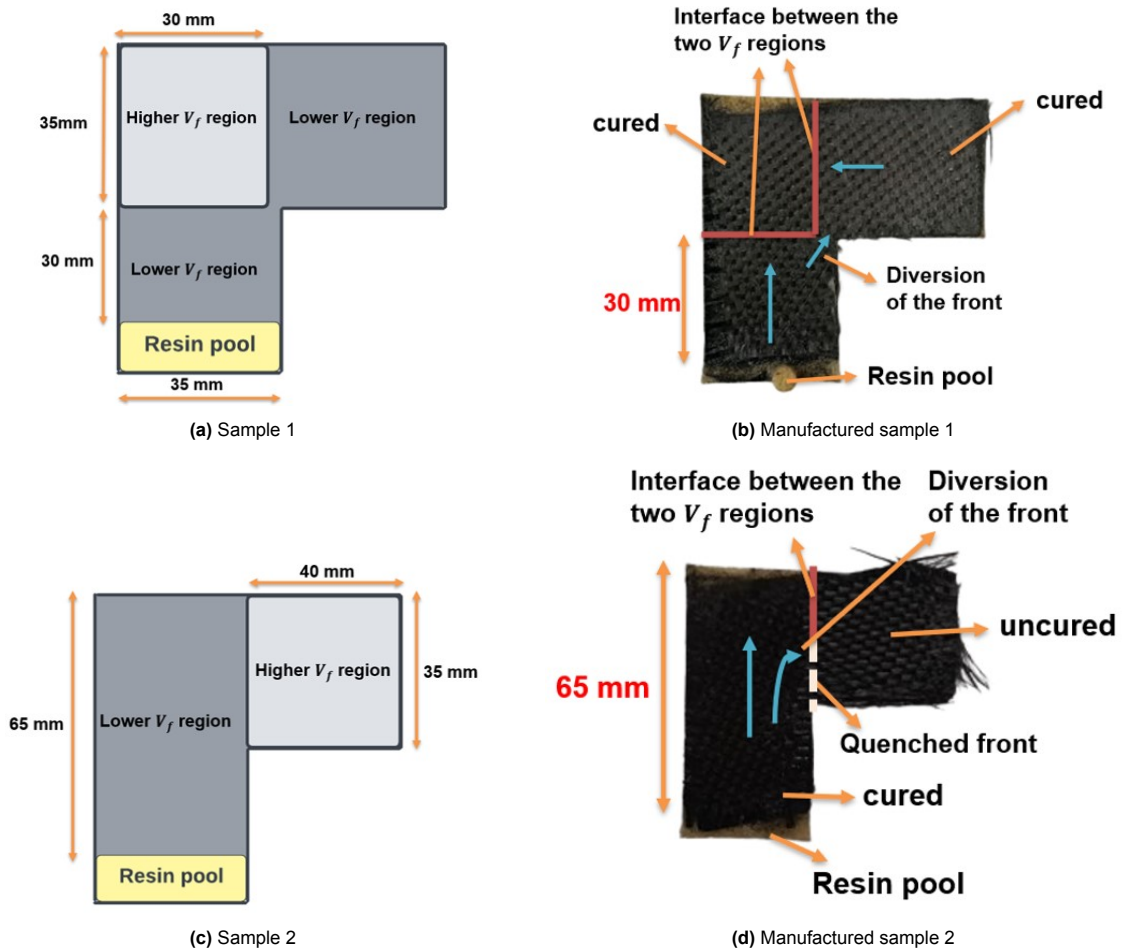
Figure 5.37: The samples manufactured to observe the effects of change in the direction of the propagation of the front in an L-shaped sample with varied geometry.

the front in the higher V_f region. Additionally, the dimension of the higher V_f region should be small enough to allow the front to propagate through it entirely before the front temperature falls below the threshold due to continued heat loss.

In sample 2 (see Figure 5.37d), the front propagated entirely through the lower V_f region in one arm of the sample while it quenched at the interface. The diverted front, upon reaching the interface, should experience a rapid slowing down and reduction in the front temperature due to the increased fibre content and reduced resin volume. Furthermore, the dimensions of the higher V_f region, and hence the fibre content, were large enough for the front temperature to rapidly fall below the threshold temperature, hence quenching at the interface.

These observations suggest that, for the L-shaped geometry with the selected dimensions, the behaviour of the front may not be influenced by the diversion resulting from the change in geometry. Instead, the propagation of the front seems to be impacted by the high fibre content and reduced resin volume, leading to a decrease in heat generation and consequently in front temperature. The experiments indicate that the propagation of the front relies on maintaining the necessary heat balance to sustain the front. If the diversion of the front were to have an effect on the heat balance, no definite conclusion about its influence can currently be drawn. Further experimentation and quantification are necessary to establish a relationship between the behaviour of the front and the change in its direction.

6

Conclusion

6.1. Conclusions

The objective of the current research was to examine frontal polymerization (FP) as a curing strategy for fibre-reinforced polymers (FRPs). The primary focus of this study was to investigate the behaviour of the propagating front in composite samples with varying fibre volume fractions (V_fs) within the sample and varying geometries. To achieve this, two primary sub-questions were initially posed, as outlined in chapter 3. These sub-questions have been adequately addressed, and the conclusions drawn based on the observations and interpretations made throughout the courses of this thesis are now presented.

To investigate the behaviour of the front in composites with varying V_fs and geometries, it was necessary to develop a mould test setup that would allow for the manufacturing of composite samples cured via FP. Therefore, several experimental trials were conducted to manufacture composite samples cured via FP, while also determining the optimal processing steps that would allow for easy and efficient initiation of the front, as well as its sustenance. To achieve this, several solutions were implemented, including the introduction of the initiation pool and optimization of the width of the fabric layers used in the layup. These trials helped to determine the most effective processing parameters and allowed for the development of a closed mould test setup, which was tested for viability using a prototype. The closed mould test setup utilized components made of materials with low thermal conductivity, such as silicone and PTFE, which provided the necessary insulation to maintain the thermal balance required to sustain a front in a composite sample.

Although composite samples were successfully manufactured using the prototype, the poor compaction provided by the mould resulted in an average percentage error of 4.5% between the actual and the theoretical V_f values in the manufactured samples. To improve accuracy, stainless steel-based components were incorporated. The improved compaction reduced the average percentage error between the V_fs to 1.9%. Further enhancement was achieved by optimizing the silicone joint, which improved dimensional precision and reduced the average percentage error to 0.5%. However, it was found that composite samples with V_f values greater than 36% could not sustain the front, likely due to the disruption of the heat balance resulting from the higher rates of heat loss and the reduction in the content of FP formulation in the fabric layup.

Based on these results, experiments were designed to investigate the influence of varying V_fs and geometries on the propagation of the front through the sample. As a result of these trials, the answer to the sub-questions is as follows:

1. What is the influence of the variation of the V_fs within the sample on the propagation of the front through the sample?

    Composite samples were manufactured with distinct regions of higher and lower V_fs. It was observed that, for the rectangular geometry considered, the length of the lower V_f region (interface position) relative to the higher V_f region had an impact on the propagation of the front. When

74

the length of the lower V_f region was below a critical value, the front would not propagate into the higher V_f region but would instead quench either at the interface or a few millimetres before or after it. Conversely, in samples with lower V_f region lengths above the critical value, the front would propagate unhindered to the higher V_f region, curing the entire sample. To quantify these observations, temperature data was captured by placing thermocouples at strategic locations throughout the sample.

The temperature data indicates that the peak temperature recorded in the lower V_f region was higher than that at the interface and the higher V_f region. This finding suggests that for the front to successfully propagate through a V_f region, the front temperature must be above the threshold temperature required to sustain the front. However, reducing the length of the lower V_f region below a critical value relative to the higher V_f, would increase the total number of fibres in the higher V_f region, which would divert more heat away from the front. This, combined with the reduction of resin quantity in the higher V_f region, could lead to insufficient heating of the resin near the front and result in a rapid decrease in the front temperature. If the front temperature falls below the threshold, it would quench the front at the interface.

If the front temperature remains above the threshold, the front may continue to propagate through the higher V_f region. However, the temperature of the front as it propagates through the higher V_f region would continue to decrease. If the distance the front has to travel through this region is short and if it happens before the temperature falls below the threshold, the front could cure the entire sample.

The study captured the non-homogeneous movement of the front, which was caused by the warping of the fabric against the walls of the silicone joint. This warping resulted in the formation of peaks and troughs, with the shallow regions containing more resin compared to the peaks. Upon initiation, the front would propagate through the shallow regions first before catching up with the front in the fabric region. Evidence for this behaviour was obtained by comparing the thermocouples placed at the interface. The difference in the trigger times of rise in temperatures measured by these thermocouples suggested that the front moved in this fashion. To achieve a more homogeneous front, the width of the fabric layer and silicone joint were optimized. This optimization yielded a seemingly homogeneous front, as evidenced by the comparison of the thermocouples at the interface. Additionally, the temperature curves obtained from the experiments showed the effects of the microstructure of the carbon fabric, which appeared in the form of single or multiple peaks and a non-monotonic increase in temperature.

2. Does the geometrical complexity of a composite part have an influence on FP?

The study successfully demonstrated the feasibility of manufacturing geometrically complex shapes by producing an in-plane L-shaped sample with uniform V_f. Tests were conducted to investigate the influence of variation of V_fs in the L-shaped samples. These tests involved manufacturing L-shaped samples with distinct regions of lower and higher V_f. In these tests, the length of the lower V_f region was varied with respect to the higher V_f region. The results clearly demonstrated that, similar to the rectangular samples, the behaviour of the front depended on the length of the lower V_f region, with a critical length acting as the inflexion point. Additionally, tests were conducted to study whether the change in the front's direction as it propagates from one arm to another affects its behaviour. Results from these tests suggest that changing the front direction did not affect its behaviour, as the front temperature still needs to be maintained above the threshold temperature to sustain it. However, further studies are needed to verify these claims.

Finally, answering the main research question,

” Can we control the heat losses in frontal polymerization to maintain the heat generation-diffusion equilibrium under geometrically complex conditions? ”

The results of all the experiments conducted in the study lead us to conclude that the propagation of the front is highly dependent on the test setup's ability to maintain the heat balance required to sustain it. This study has confirmed that a well-insulated test setup is one of the primary factors in the successful implementation of FP-based curing of FRPs. Additionally, higher fibre content coupled with a reduction in resin volume naturally affects the heat balance, leading to a rapid reduction in the front temperature below the threshold required for a sustained front. This governing principle seems to hold true despite changes in the geometry and, in turn, the direction of propagation. In summary, fronts can be sustained under geometrically complex conditions as long as the front temperature can be sustained above the threshold temperature.

6.2. Significance of the current work

This thesis effectively contributes to the knowledge base on the topic of frontal polymerization. Through the investigations of the behaviour of the front in composite parts with varying V_fs within the sample and varying geometries, this study provides insights into the use of frontal polymerization as an effective curing strategy in the manufacturing of fibre-reinforced polymers.

The current work presents a glimpse into the potential of FP, which lies in its ability to offer reduced curing times, potentially leading to increased production volumes with lower energy consumption. However, at present, its potential is limited by the lack of research that fully explores its capabilities. The understanding gained from this study will serve as a solid foundation for the design of manufacturing processes and setups tailored for the use of frontal polymerization.

7

Recommendation

This section introduces several recommendations for future research based on the study conducted in this thesis. In the stainless steel-based closed mould test setup, the manufacturing of composite samples was restricted to a maximum V_f of 36%. Samples with V_f greater than 36% were unable to sustain the propagating front, which was attributed to the disruption of the heat balance due to the excess heat loss to the surroundings. Therefore, future research should explore different methods to maintain the necessary heat balance to sustain the front at these higher V_fs. To achieve this, the first recommendation is to replace the Teflon plates with better-insulating materials, such as Fiberglass (foam glass) or polyurethane foam. Another method could be to optimize the concentration of the initiators (PAG and RTI) to achieve higher front velocity and temperature. Additionally, optimization to further reduce the void content can be explored. This can be achieved through an infusion process based on the resin transfer moulding process, such as VARTM, to create the fabric resin layup. A more controlled FRP processing technique like the VARTM can help reduce the formation of macrovoids and mesovoids. Another interesting area of research is the manufacturing of samples with two simultaneous fronts moving from the opposite side. This method could potentially allow for even faster manufacturing speeds. Furthermore, mechanical testing of the composite samples manufactured with the processes used in this thesis could be undertaken. These samples could be compared to complementary samples manufactured using traditional curing methods. The results from these tests could create a stronger case supporting the adoption of FP as a viable curing alternative.

The study of the influence of changing V_fs within the sample demonstrated the conditions necessary for the propagation of the front from one region to another. To enhance the understanding of the behaviour of the front, future research can look at increasing the size of the composite samples. This could involve doubling the dimensions of the samples used in this study to determine whether the observations made in smaller samples would still hold true at increased dimensions. In these studies, thermocouples can be placed strategically to study the relationship between the critical lengths, front temperature and the steady state of a certain V_f region. Furthermore, the propagation of the front through an L-shaped sample can be quantified through the use of thermocouples. Such data can perhaps provide insights into the behaviour of the front in regions with sharp bends or curves. Understanding the influence of these geometrical features on the propagation of the front can better help design structures that will be cured via FP. It is important to determine whether changes in the direction of the front have an influence on its properties (temperature, velocity,etc.) and behaviour. Studying the influence of variation of V_f within the L-shaped sample on the propagation of the front can also be beneficial. The RTM-based mould presented in Appendix A can provide a good starting point for designing a test setup that can be utilized in FP research. Based on some of the proposed solutions, it is recommended to further optimize the design to make it modular and cost-effective.

Bibliography

[1] R.A. Witik, F. Gaille, R. Teuscher, H. Ringwald, V. Michaud, and Jan-Anders Månson, "Assessing the economic and environmental potential of out of autoclave processing," *ICCM 18*, 6 2012.

[2] A. Quilter, "Composites in Aerospace Applications," *IHS White Paper*, vol. 444, pp. 1–264, 2001.

[3] T. J. Reinhart, "Overview of Composite Materials," in *Handbook of Composites*, pp. 21–33, Boston, MA: Springer US, 1998.

[4] P. Mallick, *Fiber-Reinforced Composites.* CRC Press, 11 2007.

[5] A. J. Timmis, A. Hodzic, L. Koh, M. Bonner, C. Soutis, A. W. Schäfer, and L. Dray, "Environmental impact assessment of aviation emission reduction through the implementation of composite materials," *The International Journal of Life Cycle Assessment*, vol. 20, pp. 233–243, 2 2015.

[6] NM Chechilo, RJ Khvilivitskii, and NS Enikolopyan, "Propagation of the polymerization reaction," *Dokl. Akad. Nauk SSSR*, vol. 204, pp. 1180–1181, 1972.

[7] J. A. Pojman, V. M. Ilyashenko, and A. M. Khan, "Free-radical frontal polymerization: self-propagating thermal reaction waves," *Journal of the Chemical Society, Faraday Transactions*, vol. 92, no. 16, p. 2825, 1996.

[8] K. A. Arutyunyan, S. P. Davtyan, B. A. Rozenberg, and N. S. Yenikolopyan, "Kinetics of adiabatic thermal setting of oligo-epoxydianes in the presence of m-phenylenediamine," *Polymer Science U.S.S.R.*, vol. 17, pp. 333–338, 1 1975.

[9] D. Bomze, P. Knaack, and R. Liska, "Successful radical induced cationic frontal polymerization of epoxy-based monomers by C–C labile compounds," *Polymer Chemistry*, vol. 6, no. 47, pp. 8161–8167, 2015.

[10] M. Sangermano, A. D'Anna, C. Marro, N. Klikovits, and R. Liska, "UV-activated frontal polymerization of glass fibre reinforced epoxy composites," *Composites Part B: Engineering*, vol. 143, pp. 168–171, 6 2018.

[11] M. Sangermano, I. Antonazzo, L. Sisca, and M. Carello, "Photoinduced cationic frontal polymerization of epoxy–carbon fibre composites," *Polymer International*, vol. 68, pp. 1662–1665, 10 2019.

[12] S. Vyas, X. Zhang, E. Goli, and P. H. Geubelle, "Frontal vs. bulk polymerization of fiber-reinforced polymer-matrix composites," *Composites Science and Technology*, vol. 198, p. 108303, 9 2020.

[13] I. D. Robertson, M. Yourdkhani, P. J. Centellas, J. E. Aw, D. G. Ivanoff, E. Goli, E. M. Lloyd, L. M. Dean, N. R. Sottos, P. H. Geubelle, J. S. Moore, and S. R. White, "Rapid energy-efficient manufacturing of polymers and composites via frontal polymerization.," *Nature*, vol. 557, pp. 223–227, 5 2018.

[14] B. Suslick, J. Hemmer, B. Groce, K. Stawiasz, P. Geubelle, G. Malucelli, A. Mariani, J. Moore, J. Pojman, and N. Sottos, "Frontal Polymerizations: From Chemical Perspectives to Macroscopic Properties and Applications," 2022.

[15] C. Nason, T. Roper, C. Hoyle, and J. A. Pojman, "UV-Induced Frontal Polymerization of Multifunctional (Meth)acrylates," *Macromolecules*, vol. 38, pp. 5506–5512, 6 2005.

[16] Q.-Z. Yan, W.-F. Zhang, G.-D. Lu, X.-T. Su, and C.-C. Ge, "Frontal Polymerization Synthesis of Starch-Grafted Hydrogels: Effect of Temperature and Tube Size on Propagating Front and Properties of Hydrogels," *Chemistry - A European Journal*, vol. 12, pp. 3303–3309, 4 2006.

[17] Y. A. Chekanov and J. A. Pojman, "Preparation of functionally gradient materials via frontal polymerization," *Journal of Applied Polymer Science*, vol. 78, pp. 2398–2404, 12 2000.

[18] D. Nuvoli, V. Alzari, J. A. Pojman, V. Sanna, A. Ruiu, D. Sanna, G. Malucelli, and A. Mariani, "Synthesis and Characterization of Functionally Gradient Materials Obtained by Frontal Polymerization," *ACS Applied Materials & Interfaces*, vol. 7, pp. 3600–3606, 2 2015.

[19] S. Chen, J. Sui, L. Chen, and J. A. Pojman, "Polyurethane-nanosilica hybrid nanocomposites synthesized by frontal polymerization," *Journal of Polymer Science Part A: Polymer Chemistry*, vol. 43, pp. 1670–1680, 4 2005.

[20] C. Kim, H. Teng, C. L. Tucker, and S. R. White, "The Continuous Cuing Process for Thermoset Polymer Composites. Part 1: Modeling and Demonstration," *Journal of Composite Materials*, vol. 29, pp. 1222–1253, 6 1995.

[21] I. P. Nagy, L. Sike, and J. A. Pojman, "Thermochromic Composite Prepared via a Propagating Polymerization Front," *Journal of the American Chemical Society*, vol. 117, pp. 3611–3612, 3 1995.

[22] X. Guo, C.-F. Wang, Y. Fang, L. Chen, and S. Chen, "Fast synthesis of versatile nanocrystal-embedded hydrogels toward the sensing of heavy metal ions and organoamines," *J. Mater. Chem.*, vol. 21, no. 4, pp. 1124–1129, 2011.

[23] O. Nuyken and S. Pask, "Ring-Opening Polymerization—An Introductory Review," *Polymers*, vol. 5, pp. 361–403, 4 2013.

[24] J. Zhou, S. Jia, W. Fu, Z. Liu, and Z. Tan, "Fast curing of thick components of epoxy via modified UV-triggered frontal polymerization propagating horizontally," *Materials Letters*, vol. 176, pp. 228–231, 8 2016.

[25] S. Scognamillo, C. Bounds, M. Luger, A. Mariani, and J. A. Pojman, "Frontal cationic curing of epoxy resins," *Journal of Polymer Science Part A: Polymer Chemistry*, vol. 48, pp. 2000–2005, 5 2010.

[26] A. Mariani, V. Alzari, O. Monticelli, J. A. Pojman, and G. Caria, "Polymeric nanocomposites containing polyhedral oligomeric silsesquioxanes prepared via frontal polymerization," *Journal of Polymer Science Part A: Polymer Chemistry*, vol. 45, pp. 4514–4521, 10 2007.

[27] S. Scognamillo, V. Alzari, D. Nuvoli, and A. Mariani, "Hybrid organic/inorganic epoxy resins prepared by frontal polymerization," *Journal of Polymer Science Part A: Polymer Chemistry*, vol. 48, pp. 4721–4725, 9 2010.

[28] D. Bomze, P. Knaack, T. Koch, H. Jin, and R. Liska, "Radical induced cationic frontal polymerization as a versatile tool for epoxy curing and composite production," *Journal of Polymer Science Part A: Polymer Chemistry*, vol. 54, pp. 3751–3759, 12 2016.

[29] A. Mariani, S. Bidali, S. Fiori, M. Sangermano, G. Malucelli, R. Bongiovanni, and A. Priola, "UV-ignited frontal polymerization of an epoxy resin," *Journal of Polymer Science Part A: Polymer Chemistry*, vol. 42, pp. 2066–2072, 5 2004.

[30] P. Chabanne, L. Tighzert, J.-P. Pascault, and B. Bonnetot, "Epoxy polymerization initiated by BF3–amine complexes. I. Synthesis and characterization of BF3–amine complexes and BF3–amine complexes dissolved in γ–butyrolactone," *Journal of Applied Polymer Science*, vol. 49, pp. 685–699, 7 1993.

[31] B. J. Stovall and T. E. Long, "Recent advances in halogen-free, additive-free polymers with inherent flame-retardant properties," *Synthesis and Characterization of Wholly Aromatic, Water-Soluble Polyimides and Poly (amic acid) s Towards Fire Suppression Foams*, pp. 1–47, 2021.

[32] Y. Liao, "Design and Applications of Metastable-State Photoacids," *Accounts of Chemical Research*, vol. 50, pp. 1956–1964, 8 2017.

[33] B. Gachet, M. Lecompère, C. Croutxé-Barghorn, D. Burr, G. L'Hostis, and X. Allonas, "Highly reactive photothermal initiating system based on sulfonium salts for the photoinduced thermal frontal cationic polymerization of epoxides: a way to create carbon-fiber reinforced polymers," *RSC Advances*, vol. 10, no. 68, pp. 41915–41920, 2020.

[34] J. V. Crivello, "Investigation of the photoactivated frontal polymerization of oxetanes using optical pyrometry," *Polymer*, vol. 46, pp. 12109–12117, 12 2005.

[35] F. A. Abdul-Rasoul, A. Ledwith, and Y. Yagci, "Photochemical and thermal cationic polymerizations promoted by free radical initiators," *Polymer*, vol. 19, pp. 1219–1222, 10 1978.

[36] A. Ledwith, "FORMATION AND REACTIVITIES OF FREE IONS IN CATIONIC POLYMERISATION," *Ions and Ion Pairs and their Role in Chemical Reactions*, pp. 159–171, 1 1979.

[37] A. Ledwith, "Possibilities for promoting cationic polymerization by common sources of free radicals," *Polymer*, vol. 19, pp. 1217–1219, 10 1978.

[38] D. Braun and K. H. Becker, "Aromatic pinacols as polymerization initiators," *Industrial \& Engineering Chemistry Product Research and Development*, vol. 10, no. 4, pp. 386–388, 1971.

[39] A. D. Tran, T. Koch, R. Liska, and P. Knaack, "Radical-induced cationic frontal polymerisation for prepreg technology," *Monatshefte für Chemie - Chemical Monthly*, vol. 152, pp. 151–165, 1 2021.

[40] A. D. Tran, T. Koch, P. Knaack, and R. Liska, "Radical induced cationic frontal polymerization for preparation of epoxy composites," *Composites Part A: Applied Science and Manufacturing*, vol. 132, p. 105855, 5 2020.

[41] M. Shirai and M. Tsunooka, "Photoacid and photobase generators: chemistry and applications to polymeric materials," *Progress in polymer science*, vol. 21, no. 1, pp. 1–45, 1996.

[42] R. Taschner, P. Knaack, and R. Liska, "Bismuthonium□ and pyrylium□based radical induced cationic frontal polymerization of epoxides," *Journal of Polymer Science*, vol. 59, pp. 1841–1854, 8 2021.

[43] J. Pojman, "Frontal Polymerization," in *Polymer Science: A Comprehensive Reference*, pp. 957–980, Elsevier, 2012.

[44] B. V. Novozhilov, "Propagation rate of the front of an exothermic reaction in condensed phase," vol. 141, no. 1, pp. 151–153, 1961.

[45] E. Goli, S. R. Peterson, and P. H. Geubelle, "Instabilities driven by frontal polymerization in thermosetting polymers and composites," *Composites Part B: Engineering*, vol. 199, p. 108306, 10 2020.

[46] M. Birkner, A. Seifert, and S. Spange, "Radical induced cationic frontal twin polymerization of Sispiro compound in combination with bisphenol-A-diglycidylether," *Polymer*, vol. 160, pp. 19–23, 1 2019.

[47] E. Goli, I. D. Robertson, H. Agarwal, E. L. Pruitt, J. M. Grolman, P. H. Geubelle, and J. S. Moore, "Frontal polymerization accelerated by continuous conductive elements," *Journal of Applied Polymer Science*, vol. 136, p. 47418, 5 2019.

[48] N. Klikovits, R. Liska, A. D'Anna, and M. Sangermano, "Successful UV-Induced RICFP of Epoxy-Composites," *Macromolecular Chemistry and Physics*, vol. 218, p. 1700313, 9 2017.

[49] E. Goli, T. Gai, and P. H. Geubelle, "Impact of Boundary Heat Losses on Frontal Polymerization," *The Journal of Physical Chemistry B*, vol. 124, pp. 6404–6411, 7 2020.

[50] P. Knaack, N. Klikovits, A. D. Tran, D. Bomze, and R. Liska, "Radical induced cationic frontal polymerization in thin layers," *Journal of Polymer Science Part A: Polymer Chemistry*, vol. 57, pp. 1155–1159, 6 2019.

[51] J. Staal, E. Smit, B. Caglar, and V. Michaud, "Thermal management in radical induced cationic frontal polymerisation for optimised processing of fibre reinforced polymers," *Composites Science and Technology*, vol. 237, p. 110009, 5 2023.

[52] G. Hhne, J. McNaughton, W. Hemminger, and H.-J. Flammersheim, *Differential scanning calorimetry*. Springer Science \& Business Media, 2003.

[53] Dow Chemicals corporation, "SILASTIC™ RTV-4250-S Kit Green Technical Data Sheet," 2017.

[54] M. MInus and S. Kumar, "The processing, properties, and structure of carbon fibers," *JOM*, vol. 57, pp. 52–58, 2 2005.

[55] X. Cai, Z. Jiang, X. Zhang, T. Gao, K. Yue, and X. Zhang, "Thermal property improvement of polytetrafluoroethylene nanocomposites with graphene nanoplatelets," *RSC Advances*, vol. 8, no. 21, pp. 11367–11374, 2018.

[56] E. Sozer, P. Simacek, and S. Advani, "Resin transfer molding (RTM) in polymer matrix composites," *Manufacturing Techniques for Polymer Matrix Composites (PMCs)*, pp. 245–309, 1 2012.

[57] P. J. Centellas, M. Yourdkhani, S. Vyas, B. Koohbor, P. H. Geubelle, and N. R. Sottos, "Rapid multiple-front polymerization of fiber-reinforced polymer composites," *Composites Part A: Applied Science and Manufacturing*, vol. 158, p. 106931, 7 2022.

A
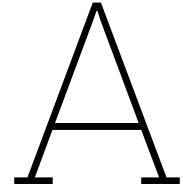
RTM Concept

The RTM mould test setup, which could be used to manufacture composite samples cured via Frontal Polymerization, was conceptualized as part of this thesis and is presented here. This setup could serve as a reference for the future design of test setups tailored for FP.

A.1. Introduction

The composite laminates manufactured as a part of the various experimental trials throughout the duration of the thesis have demonstrated the feasibility of utilizing FP as a viable curing strategy. The experiments performed have also ventured into new domains, such as the variation of V_f and the introduction of geometrical complexities. The results of these experiments have further enhanced the understanding of the physical phenomena governing FP.

Given the results of the various experimental trials presented in chapter 5, it is evident that several challenges were faced, particularly due to the inefficiencies in the manufacturing process. However, through repeated optimization, the quality of the laminates and the repeatability of the process were improved. It is quite difficult to estimate if the same acquired know-how would be applicable in dealing with inconsistencies of similar nature that might arise as and when the scale and complexity of the samples are increased.

Furthermore, if frontal polymerization has to become a viable alternative to the traditional methods of curing composites, a more holistic view is needed in the research surrounding frontal processes. This all-encompassing view would only be complete when FP is complemented by an appropriate composite manufacturing technique that finds widespread industrial application. One such manufacturing technique that is most compatible with FP is a type of liquid composite moulding (LCM) known as resin transfer moulding (RTM). As eluded to in the literature review in chapter 2, VARTM, a variation of the RTM, has already been used to manufacture FRCs cured via FP.

A.2. Overview of the Literature

A.2.1. Working Principle

As represented in Figure A.1, the RTM process begins with the preparation of the moulds (See Figure A.1 1). The mould cavities are coated with a release agent to prevent the cured resin from sticking to them. Next, the fabric layers (such as dry continuous strand mats, woven roving or fabrics) are draped into the mould cavity to give the part its required net shape (See Figure A.1 2,3 & 4). These mould cavities are usually shaped according to the final part to be manufactured. In the case of complex mould geometries, the fabric layers are held together by a tackifier or by being stitched together to prevent any movement during the resin injection process. Once the fabric layers have been placed in the cavity, the molds are closed and clamped (See Figure A.1 5). The next step is the injection of resin under pressure through one or more gates designed into the mould (See Figure A.1 6). The resin injection points are usually at the lowest point of the mould cavity. Meanwhile, as the resin flows through the cavity, it displaces the entrapped air through the exit vents and impregnated the fabric. The resin injection stops once the resin is seen exiting from the vents. After this point, the resin injection is discontinued, and the vent ports are closed. The resin is then allowed to cure through heating or the addition of initiators to the resin. The part is removed only after it has sufficiently hardened, which is often referred to as green strength (See Figure A.1 7 & 8) [4] [56].
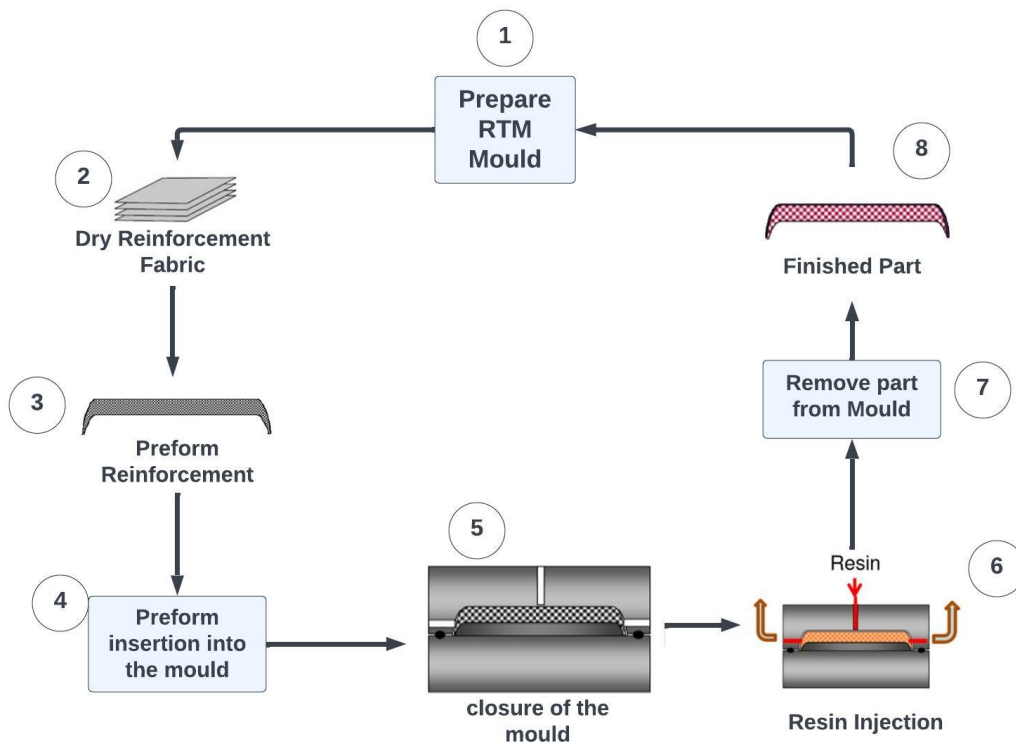
Figure A.1: Schematic overview of the RTM process

A.2.2. Use of RTM in FP

The RTM tool design that has been implemented so far in RICFP applications has primarily focused on achieving a uniform 1D flow (a linear flow) [39]. This design approach is justifiable as the samples that are to be manufactured typically have very small thicknesses when compared to their in-plane dimensions. While there have been many variations in the moulds, the general principles have been found to remain the same across a wide range of literature.

As already mentioned, Dung Tran et al.[39] successfully demonstrated the use of VARTM as a composite manufacturing technique with FP as a complimentary curing technique. As shown in Figure A.2, they utilized a simple setup with a frame manufactured out of a polydimethylsiloxane (PDMS) sheet sandwiched between two glass plates to form a mould. On the upper mould half, two holes were drilled, each connecting to the formulation container and a vacuum system through a PVC pipe. The preform was then placed in the silicon mould and closed on both sides with the glass plates. The entire setup was held together by simple metal clamps, which helped maintain the dimensions of the setup. The use of glass plates was an optimal choice for initiation via UV/vis.
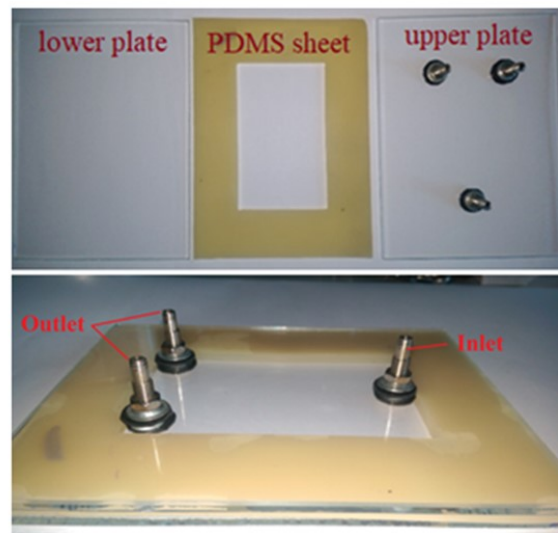
Figure A.2: VARTM setup used for the manufacturing of composites cured via FP.[39].

Furthermore, the utilization of VARTM as a resin infusion technique coupled with FP was also demonstrated by Centellias et al. [57] and Robertson et al. [13]. Centellias et al. used a double bag VARTM setup to infuse resin into the fabric preforms. The fabric layers were prepared on a flat tool plate, and a vacuum was applied to the inner bag, which infused the resin into the dry carbon fibres. A stronger vacuum was then pulled on the outer bag to compact the laminate and produce composite parts with a V_f of 50%. In contrast to the moulds used in the literature, a closed mould RTM test setup with a modular design was considered more appropriate to ensure cost-effectiveness while increasing the scope of FP research. Therefore, building on the experiences acquired through the manufacturing of composites and the inspiration gained from literature, a conceptual RTM test mould was designed.

A.3. RTM Mould Design

As shown in Figure A.3, the conceptual mould design consists of four major elements: a frame, upper mould plates, lower mould plates and a press plate. The mould design is intended for a linear flow RTM test setup, which consists of matched moulds with two rigid moulds halves (male and female moulds). In this design, each of the upper and lower mould halves is comprised of two individual plates, which are held together with eight M6 countersunk bolts.
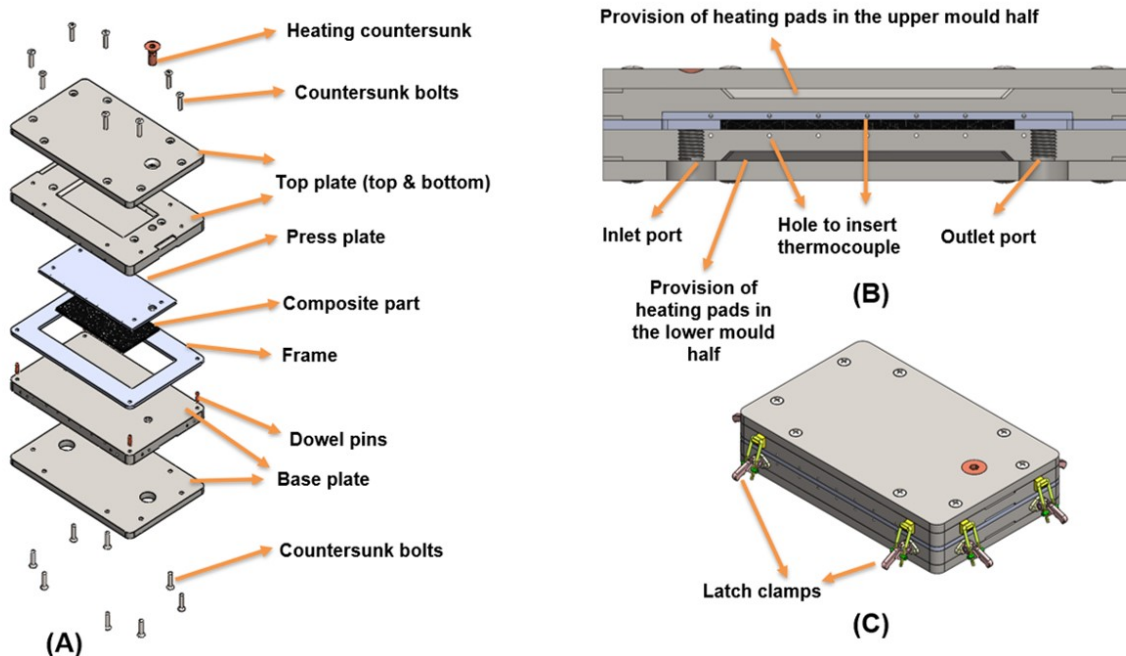
Figure A.3: Exploded view of the conceptual mould

The mould was designed to be manufactured entirely with Chromium-plated tool steel, which is commonly used in high-volume RTM manufacturing due to its high hardness and resistance to wear. However, since the design was conducted in parallel to the experiments, it did not incorporate practical learnings from the experiments. If this mould were to be designed again, Chromium-plated tool steel would still be the material of choice, but the faces of the mould that come in contact with the layup would be coated with an additional layer of insulation. Insulation films made of Teflon, fibreglass, or any foam material with low thermal conductivity would be most appropriate.

As discussed in chapter 2, for the successful propagation of the front, the heat generated by the exothermic reaction of the resin system must be in equilibrium with the heat consumed by the propagating front. However, this thermal equilibrium is affected by the heat loss from the system to the surrounding. The mould used to manufacture composite laminates in this thesis utilized elements such as a silicone joint and Teflon plates to contain the heat within the system. While the presence of these elements successfully allowed for the manufacturing of a variety of laminates, it was observed that the front would quench at the initiation pool when the V_f was increased beyond a certain value. To tackle this challenge, an external heating method was devised, which involved the use of heating elements to supplement the heat loss (see Figure A.3 A). These heating elements would artificially counter the effects of heat loss and maintain the equilibrium required for the propagation of the front.

Thin Film Polyimide Adhesive Heater was the chosen heating element for this purpose. The individual mould plates in contact with the layup (Top plate (bottom) and base plate (top)) were provided with a housing pit for placing these heating elements (See Figure A.4 B & D). These pits were also designed with outlet ports for directing the wires of the heating elements outside the mould. Furthermore, the heating elements would be held in place with thermally conductive adhesive tape that had very high operating temperatures.
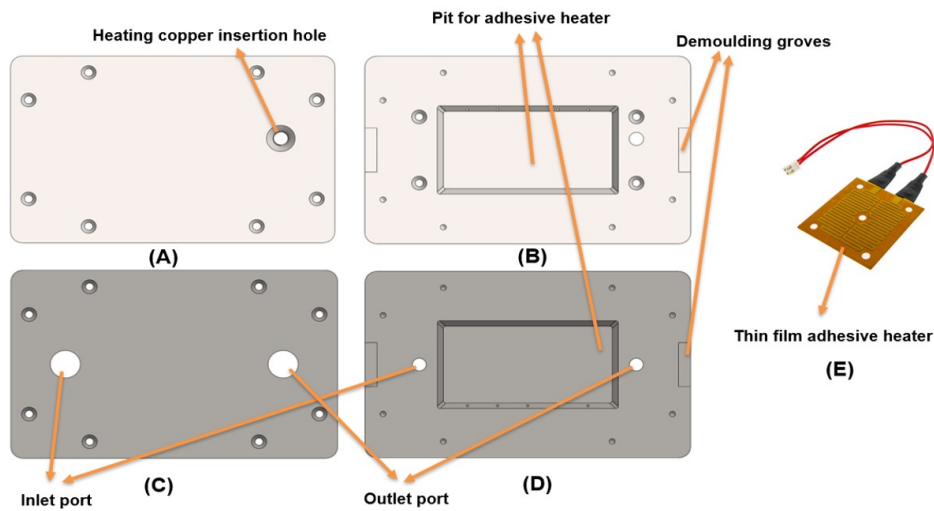
Figure A.4: Upper and Lower rigid mould plates. **A:** Upper mould plate (top), **B:** Upper mould plate (bottom), **C:** Base mould plate (bottom), **D:** Base mould plate (top).**E:** This film adhesive heater

This RTM mould setup is a pressure-controlled system where the resin is injected at constant pressure. This method relies on over-pressure and is hence mostly used with 2 rigid moulds with proper sealing to prevent any leakage of resin from the periphery of the mould. Simple metal-to-metal contact is utilized for sealing the mould periphery. Additionally, further sealing is provided by a silicone joint that surrounds the laminate and runs along the inner walls of the frame. In this method, the pressure can be steadily increased if needed, to prevent washout or displacement of the fabrics due to the initial rush of resin into the mould cavity.

The mould boundary conditions (inlet and outlet ports) can be based on the a simple end-to-end placement, with the injection of the resin being carried out from the bottom of the mould (See Figure A.4 C & D). As the dimensions of the part being manufactured are small, the location of the ports ensures that the preform is well impregnated by the resin, preventing the formation of dry spots [56].

To initiate the front, a copper heating element in the form of a countersunk was also incorporated into the design. This eliminates the need for an initiation hole in the mould setup, which can create a pressure imbalance. The use of a copper countersunk would create an air-tight seal while providing a mechanism to initiate the front. Furthermore, the laminates can be compacted using a press plate, which is an element attached to the top plate (bottom) via four countersunk screws. This modular design is necessary to allow for a multipurpose mould. To achieve variation in the thickness of the laminate or to vary the V_f within the samples the taper of the press plate could be changed (See Figure A.5).
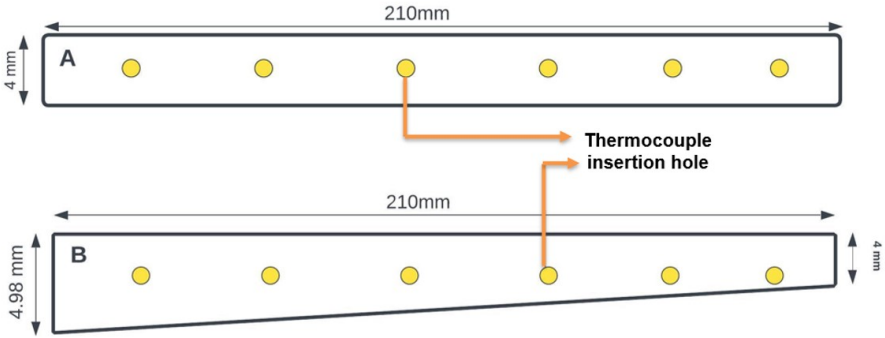
Figure A.5: Modular Press plates. **A:** Flat press plate. **B:** tapered press plate

The upper and the lower mould halves are held together using horizontal latch clamps, which can facilitate fast and easy assembly of the mould setup. To balance the internal pressure created by the injection of resin, 8 latch clamps were incorporated into the design. The thickness of the composite sample could be varied by using a frame of different thicknesses, for which adjustable latch clamps were utilized. Additionally, templates based on the required shape could be used to alter the geometry of the samples. However, it is important to ensure that the resin is allowed to flow smoothly from the inlet to the outlet.

Manufacturing

B.1. Casting Silicone Moulds

The RTV Silicone rubber used for casting moulds is a two-part liquid silicone consisting of a silicone base and a catalyst that cures at room temperature when mixed. Mould-making liquid silicone is convenient for making moulds via the "pour-on method". The mould-making process involves mixing the two parts together and subsequently pouring them into a box cavity that contains the pattern that has to be cast. As the liquid silicone is soft and flexible, every detail of the pattern is captured. After curing, silicone moulds exhibit excellent tear strength and chemical resistance. SILASTIC^{TM} RTV- 4136-M Liquid Silicone Rubber base and catalyst were chosen to cast all the silicon moulds for the initial set of experiments. The silicone mixture would expand to 3 to 4 times its volume under vacuum, and once the froth collapsed, it would recede back to its original volume. After sufficient time under vacuum, the vacuum pump was turned off, and the air was let into the chamber after 1 or 2 minutes (see Figure B.1 L). Then the mixture was poured into the cavity with the pattern as soon as possible to avoid any air entrapment.
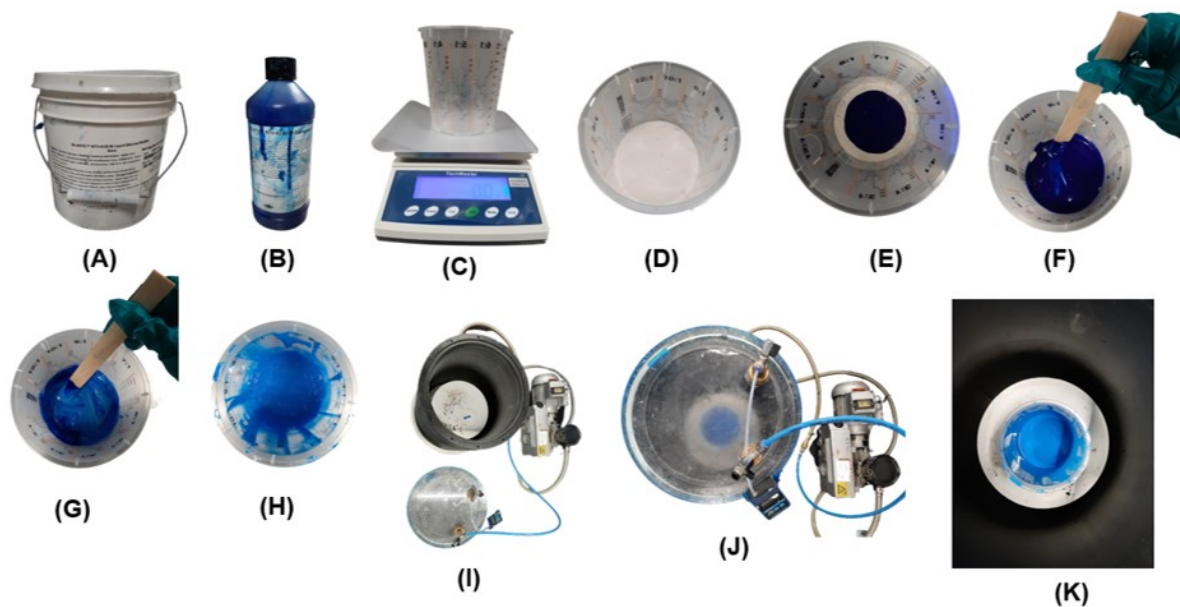
Figure B.1: Silicone components mixing and degassing. **A & B:** SILASTIC^{TM} RTV- 4136-M base and curing agent. **C,D,E,F,G & H:** Mixing of base and curing agent. **I,J & K:** Degassing of the liquid silicone mixture. **L:** Degassed silicone mixture.

Before the pattern was used, Care had to be taken to ensure that it was free of any contaminants and dirt. To do so, the pattern was thoroughly cleaned and blown over with compressed air (see Figure B.2 D,E & F). The pattern was then thoroughly fixed to the base of the box cavity to prevent it from floating

when the silicone was poured into the cavity (see Figure B.2 G). Additionally, a good release agent had to be coated over the pattern (preferably wax) to ensure easy release after curing(see Figure B.2 H & I).
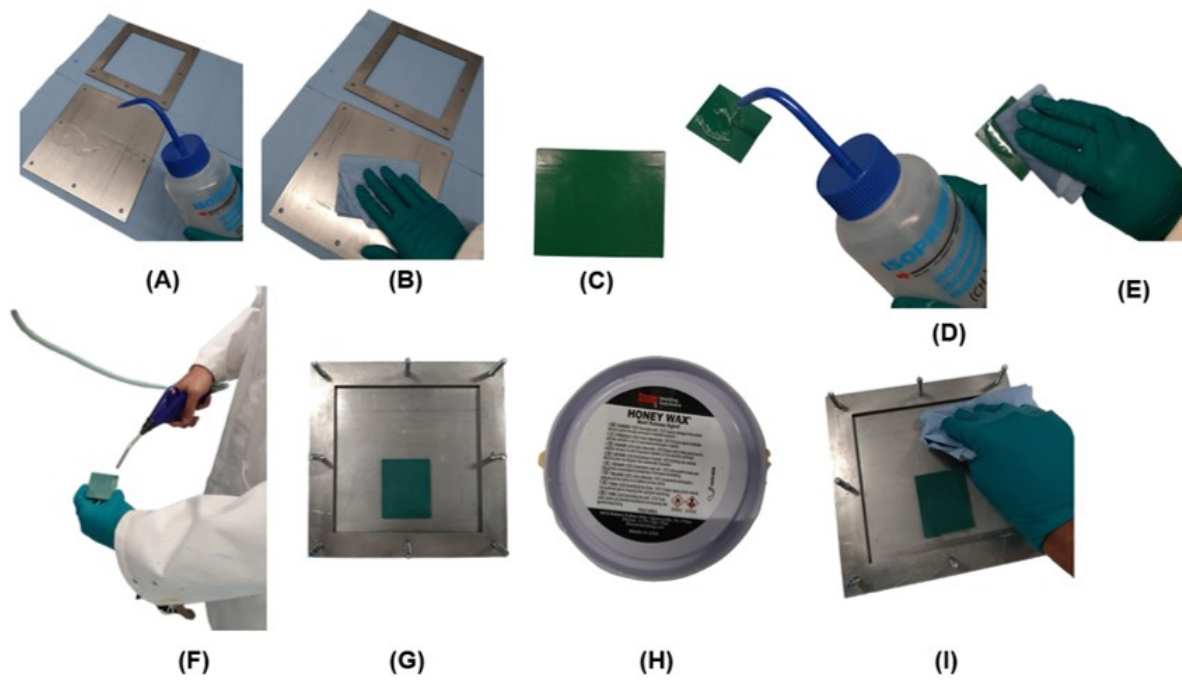
Figure B.2: Preparation of mould for casting. **A,B,C,D,E** & **F:** Cleaning the mould and the pattern. **G:** Fixing the pattern into the box cavity. **I:** Applying the release agent

B.2. DSC Characterization

The various steps involved in the DSC measurement are shown in Figure B.3. The DSC measurements began with the preparation of the sample and the reference crucibles. Standard aluminium pans and lids with an operating temperature range from -180 °C to 600 °C were used for the preparation of the crucible (see Figure B.3 A & B). These pans and lids enclosed the materials in the crimp seal mode. First, an empty standard pan was weighed on a Mettler Toledo weighing balance (see Figure B.3 H). Then, the scale was zeroed, and the pan was filled with the required amount of liquid sample using a disposable syringe (see Figure B.3 G). A standard die set and T-zero press from TA instruments were used for crimping the standard pans and lids (see Figure B.3 C, D & E). The standard pan was then transferred into the standard die, and the lid was then placed on top, enclosing the pan (see Figure B.3 I & J). Subsequently, the die was transferred to the die holder in the T-zero press (see Figure B.3 K). Once the sample lid was closed, the sample was ready for use. The preparation of the reference crucible was similar to the sample crucible, except the pan and lids were closed without any liquid sample. The sample and the reference crucible were transferred to the DSC machine. The DSC 250 from TA instruments was used to perform the DSC trails (see Figure B.3 F). Before use, the DSC instrument tank was filled with nitrogen, which was necessary to provide an inert atmosphere for the DSC trials. Once the tank was filled, a temperature program was preloaded into the operating software. After these steps were performed, DSC data could be obtained and processed according to the experimental requirements.
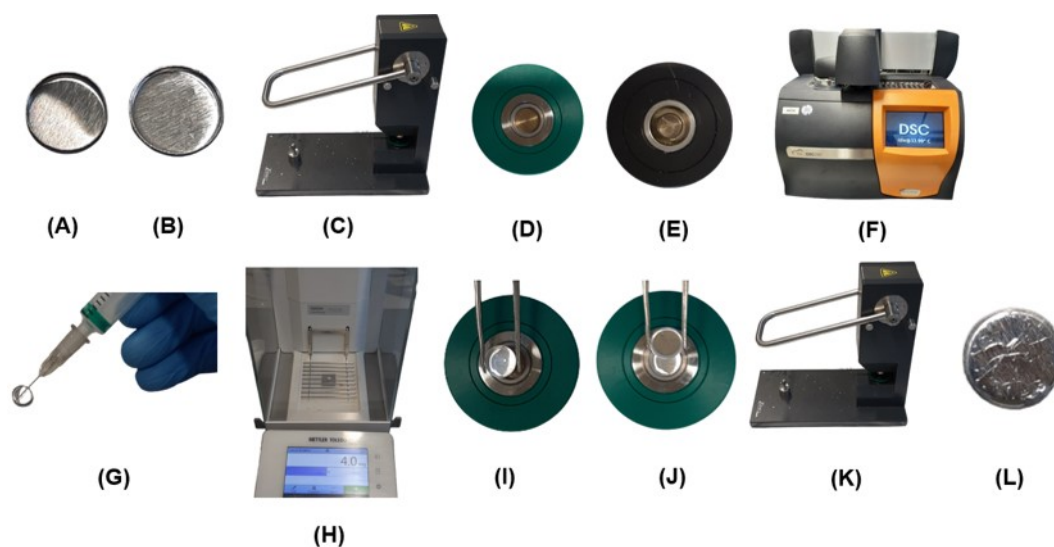
Figure B.3: Various steps in a DSC measurement.**A:** Standard aluminium pan. **B:** Standard aluminium lid. **C:** Tzero press. **D & E** Standard die set. **F:** DSC 250 from TA Instruments. **G, H, I, J & K:** Preparation of the sample crucible. **L:** Sample crucible.

B.3. Manufacturing by FP

1. Manufacturing composite samples in an open mould

Steps that were followed to manufacture composite samples using an open silicone mould have been presented in order.
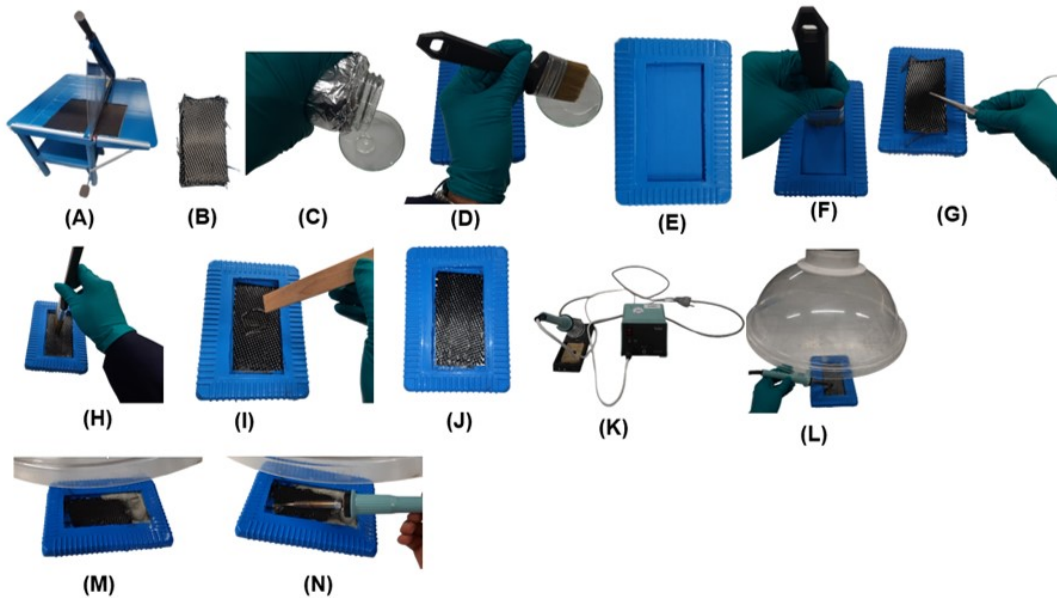
Figure B.4: Manufacturing composite samples in an open mould. **A:** Guillotine shear USED to cut fabric layers. **B:** Cut fabric layers. **C,D** & **E:** A brush used to wet the mould cavity. **F,G,H,I** & **J** Layup of the fabric and resin spreading. **K:** Soldering iron used for initiation. **L:** Initiation of the front. **M:** propagating front. **N:** Re-initiation of front.

2. Measuring the weight of a fabric cut out for the calculation of area weight
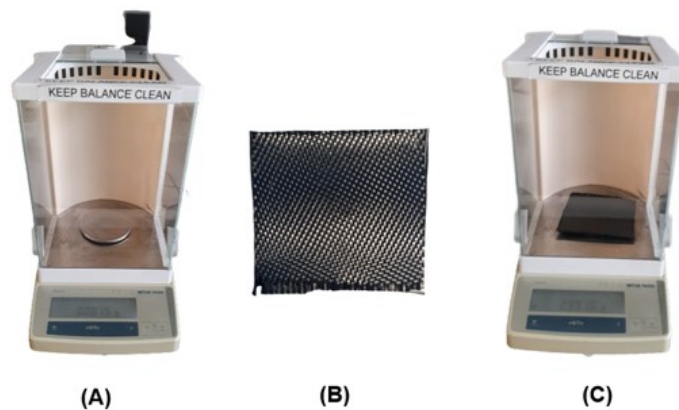
Figure B.5: Measuring the weight of a fabric cut out for the calculation of area weight. **A:** Weighing balance. **B:** Fabric cut out. **C:** Weighing the fabric cut out.

3. Manufacturing composites samples with a Teflon covered silicone mould

Steps that were followed to manufacture composite samples using a Teflon-covered silicone mould have been presented in order
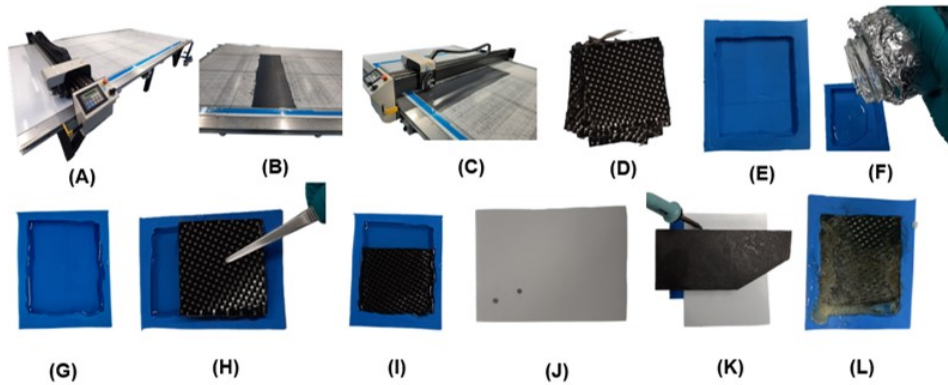
Figure B.6: Manufacturing composites samples with a Teflon cover. **A,B** & **C:** Gerber cutting machine. **D:** Cut plies. **E,F,G,H**& **I:** Hand layup. **J:** $3mm$ thick Teflon cover with an initiation hole. **K:** Placing the weights and initiating the front using a soldering iron. **L:** Cured samples.

4. Components and assembly of the closed mould test setup

The various components that make up the closed mould test setup and the sequence of assembly of these components have been presented
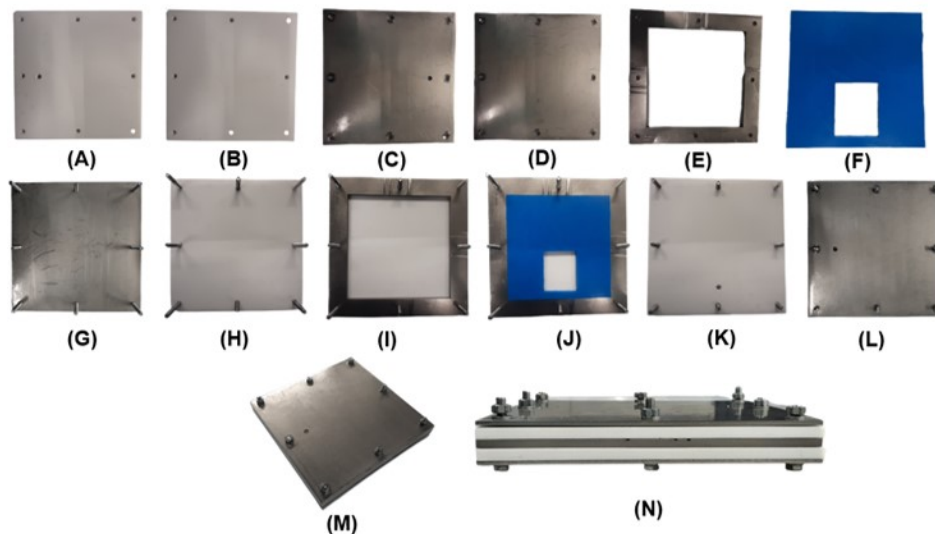
Figure B.7: Components of the closed mould setup and their sequential assembly. **A:** Upper teflon plate. **B:** lower teflon plate. **C:** Upper Stainless steel plate. **D:** Lower Stainless steel plate. **E:** Stainless steel frame. **F:** Silicone joint. **G,H,I,J,K** & **L:** Assembly of the various components in sequence. **M:** Isometric view of the mould assembly. **N:** Front view of the mould assembly.

5. Manufacturing composites samples with a closed mould testup

Steps that were followed to manufacture composite samples with uniform V_f in a closed mould test setup have been presented in order
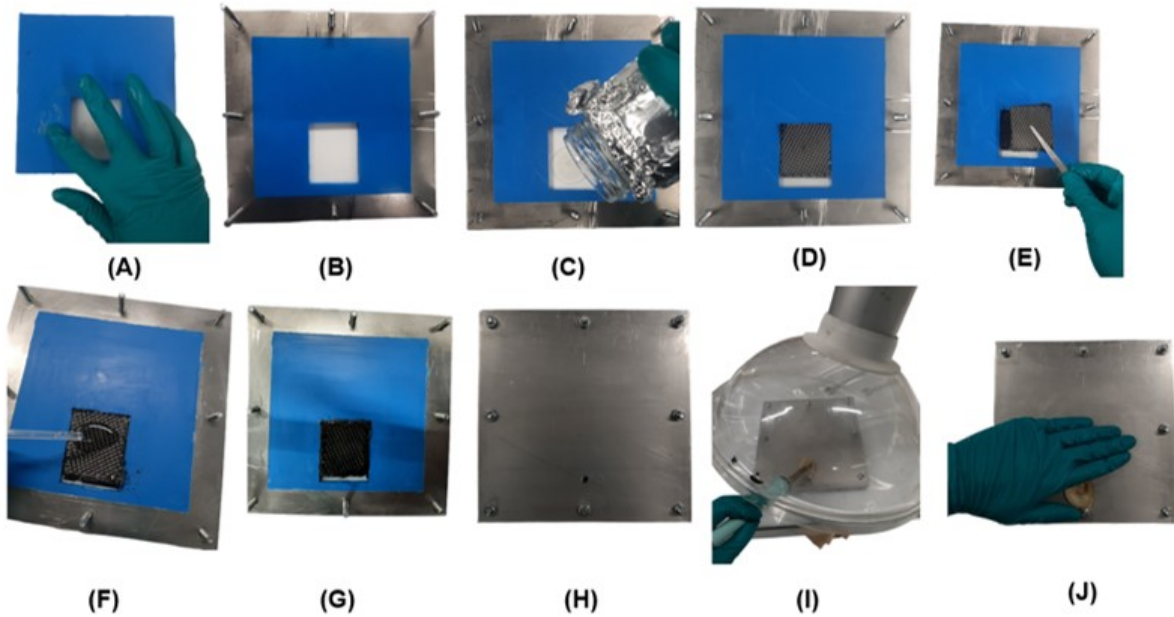
Figure B.8: Manufacturing of a composite sample with the closed mould setup. **A:** Applying grease lubricant onto the silicone joint. **B:** Bottom mould assembly. **C:** Pouring the resin into the cavity. **D,E,F & G:** Hand layup. **H:** Mould closure. **I:** Initiation of the front via a soldering iron. **J:** Checking for heating of the steel plate over the sample to check the progression of the front.

6. Cutting of fabric layers manually via a roller cutter and a template.

Steps that were followed to manually cut fabric layers required to build regions of higher and lower V_fs
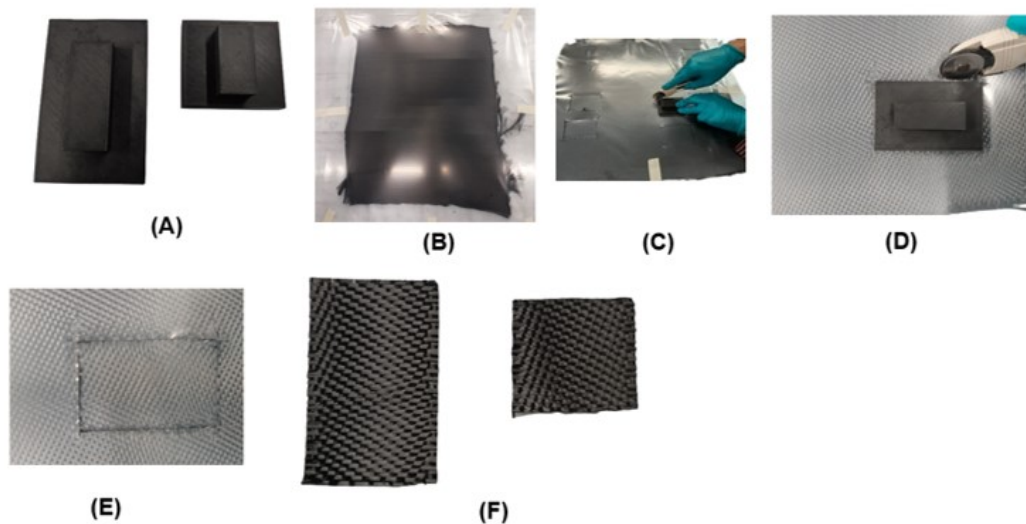
Figure B.9: Cutting of fabric layers manually via a roller cutter and a template. **A:** Templates. **B:** fabric cutout sandwiched between two plastic films and stuck to a cutting table with masking tapes. **C & D:** Cutting. **E & F:** Cut laminae layers.

7. Manufacturing composites samples with varying V_fs within the sample

Steps that were followed to manufacture composite samples with varying V_f within the sample have been presented
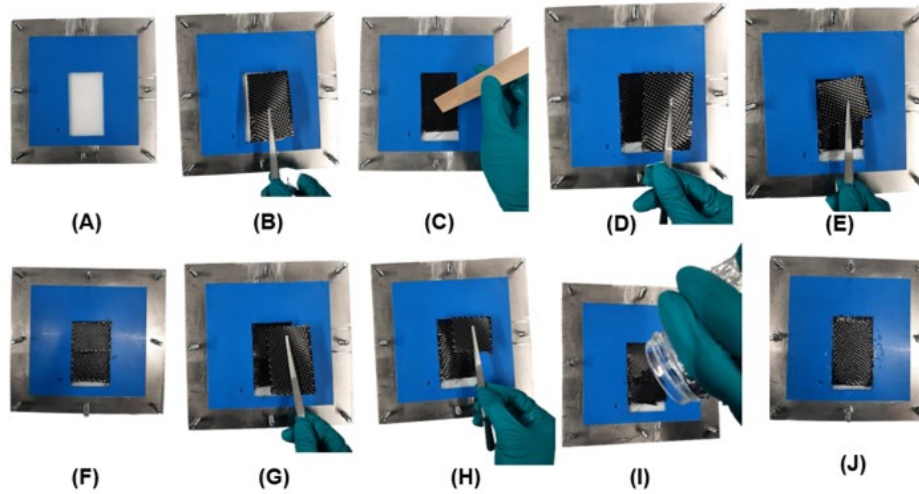
Figure B.10: Manufacturing composite sample with the variation of V_f within the sample. **A:** Creating a resin pool for the initial layup. **B:** Layup of the first layer. **C:** Compaction of the layer. **E,F,G** & **H :** The layup of the smaller fabric layer creates the region of higher V_f. **I:** Pouring additional resin as and when needed. **J:** Final layup.

8. Manufacturing of L shaped composite samples with uniform V_f

Steps that were followed to manufacture L shaped composites samples with uniform V_f have been presented
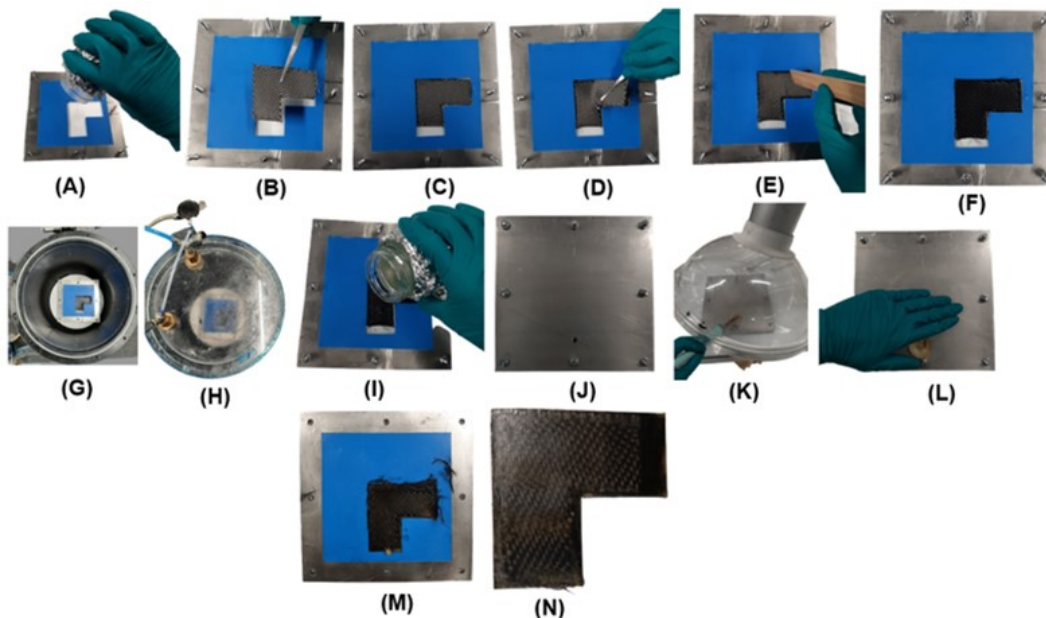
Figure B.11: [Manufacturing of L shaped composite samples with uniform V_f. **A:** Pouring resin into the cavity. **B,C,D,E** & **F:** Hand Layup. **G** & **H:** Degassing of the entire layup. **I:** Pouring resin to fill up the initiation pool and create a thin resin film on top of the layup. **J** & **K:** Initiation of the front. **L:** Checking for the progress of the front. **M** & **N:** Cured sample

9. Manufacturing L-shaped composites samples with variation of V_fs within the sample

Steps that were followed to manufacture L-shaped composite parts with a variation of V_f within the sample have been presented.
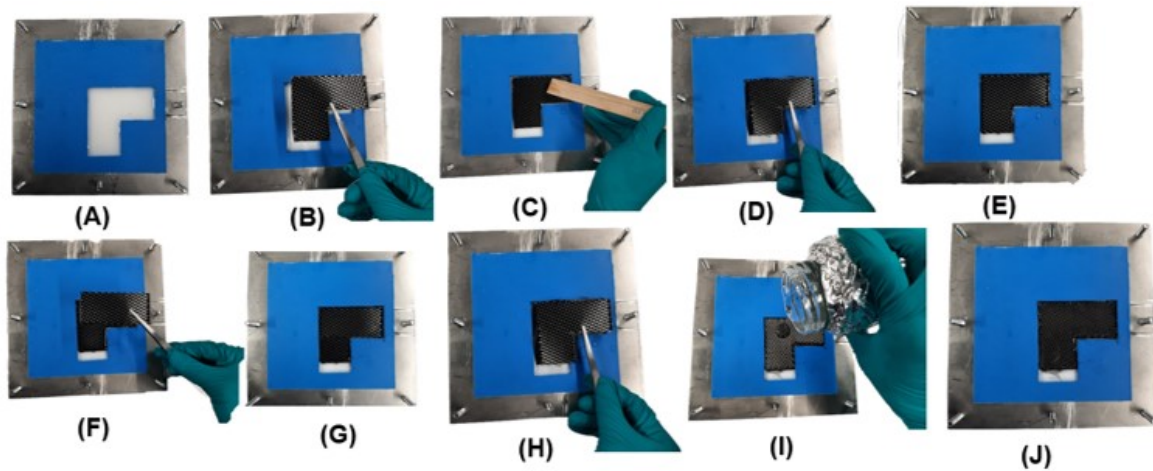
Figure B.12: Blended hand layup of the fabric layers to create regions of different V_f's. **A:** Pouring of resin to create an initial pool for the layup. **B:** Layup of the first fabric layer. **C:** Compaction of the fabric layer. **D & E:** Layup of the 3rd continuous "L" shaped fabric layer. **F & G:** Layup of the rectangular fabric layer between the 3rd & 4th continuous "L" layers to create a region of higher V_f. **H:** Layup of the 4th continuous laminae layer. **I:** Adding resin between the layers as and when required. **J:** Fully laid laminae stack.